A Thermo-Mechanical, Viscoelasto-Plastic Model for Semi-Crystalline Polymers Exhibiting One-Way and Two-Way Shape Memory Effects Under Phase Change

Hasan Gülaşik[a], Maxime Houbben[b], Clara Pereira Sànchez[c], Juan Manuel Calleja Vázquez[a], Philippe Vanderbemden[c], Christine Jérôme[b], Ludovic Noels[a,*]

[a] *University of Liege, Department of Mechanical and Aerospace Engineering, Computational & Multiscale Mechanics of Materials (CM3), Allée de la découverte 9, B-4000 Liège, Belgium*
[b] *University of Liege, Center for Education and Research on Macromolecules (CERM UR CESAM), Allée du six août, B-4000 Liège, Belgium*
[c] *University of Liege, Department of Electrical Engineering and Computer Science, Allée de la découverte 10, B-4000 Liège, Belgium*

Abstract

A finite strain phenomenological model is developed to simulate the shape memory behavior of semi-crystalline polymers under thermo-mechanical loading. The polymer is considered to be a composite of crystalline and amorphous phases with constant volume fractions. While the amorphous phase is stable, the crystalline phase is considered to change phase with temperature. Therefore, the crystalline phase is considered further to be composed of two phases, whose volume fractions are controlled by a temperature and strain dependent function: the melted phase which is soft, and the crystallized phase which is stiff.

A pressure dependent viscoelasto-plastic behavior is considered for the constitutive model of the different phases. In addition to pressure dependent plasticity, additional deformation measures are applied to the crystalline phase to model temporary (imperfect shape fixity) and permanent (imperfect shape recovery) deformations in a thermo-mechanical loading cycle. Formulating a compressible plastic flow during the phase changes yields the possibility to capture both one-way and two-way shape memory effects. As a consequence, the load-dependent and anisotropic thermal expansion observed experimentally in semi-crystalline polymers during phase change is naturally captured.

The model is validated within a test campaign performed on nano-composite having a semi-crystalline polymer as a base material. It is shown that the model gives close results with the tests and it is able to capture the shape fixity and shape recovery behaviors of the polymer, for both one-way and two-way shape memory effects.

Preprint submitted to International Journal of Solids and Structures (C) 2024; Licensed under the Creative Commons (CC-BY-NC-ND); formal publication on: 10.1016/j.ijsolstr.2024.112814

Keywords: Shape Memory Polymers (SMP), thermo-viscoelasto-plastic coupling, phase transition, one-way shape memory effect, two-way shape memory effect

1. Introduction

The shape of a polymer specimen can be shifted through some permanent and temporary configurations by an external stimulus, such as temperature (Srivastava et al., 2010, Boatti et al., 2016), light (Lendlein et al., 2005), electromagnetism (Buckley et al., 2006, Niyonzima et al., 2019) etc. This phenomenon is known as the *shape memory behavior*. Because of this behavior, the shape memory polymers (SMP) are utilized in various engineering areas: artificial muscles (Maksimkin et al., 2018), biomedical applications (Srivastava et al., 2010, Reese et al., 2010), self healing (Xu and Li, 2010), composites (Ge et al., 2012), microelectronics (Lee et al., 2015). Liu et al. (2007), Mu et al. (2018), and Pereira Sanchez et al. (02 November 2022) can be referred to for reviews.

Temperature is the most widely used method to trigger the shape memory effect, and a typical shape change is basically obtained by a thermo-mechanical loading-unloading cycle around the transition temperatures (T_t) of the considered polymer whose material properties change in order of magnitudes (Srivastava et al., 2010) during the process. SM behavior can be observed in both *amorphous* (Nguyen et al., 2008) and *semi-crystalline* (Defize et al., 2012) polymers. The main difference between them resides in their T_t nature. For amorphous polymers, there is only one transition temperature, the glass transition temperature T_g. On the other hand, for semi-crystalline polymers, there are two transition temperatures. The first one is the glass transition temperature (T_g) for the amorphous phase and the second one is the crystallization/melting ($T_\mathrm{c}/T_\mathrm{m}$) temperature for the crystalline phase. In the crystalline phase, the transition temperature is generally different during crystallization and melting (Defize et al., 2012). Therefore, $T_\mathrm{t} = T_\mathrm{c}$, when temperature is decreasing, and $T_\mathrm{t} = T_\mathrm{m}$ when temperature is increasing. Volk et al. (2011) and Defize et al. (2012) provided experimental studies on amorphous and semi-crystalline SMPs, respectively.

Figure 1(a) shows an idealized one-way shape memory (1W-SM) cycle which consists of 4 steps: step 1- deformation is applied to the specimen at a high temperature above the transition temperature ($T > T_\mathrm{t}$); step 2- the applied deformation is maintained and the specimen is cooled down to a temperature below the transition temperature ($T < T_\mathrm{t}$) to fix the shape; step 3- the specimen is released at the low temperature; step 4- the specimen is heated back to the initial high temperature to recover the original shape. The procedure is also shown on a temperature-deformation graph in Fig. 1(a). From the figure, it can be seen that the specimen geometry cannot be completely fixed (point B) and some amount of spring back (point C) is observed when the specimen is released at low temperature. When the specimen is heated back to the initial temperature, the initial configuration (point A) cannot be recovered completely (point D). It can also be seen that, with the increase in temperature, the shape recovery happens gradually around T_t ($T_\mathrm{t} - \Delta T < T_\mathrm{t} < T_\mathrm{t} + \Delta T$), rather than as a sudden change at T_t. Some polymers can also exhibit two-way shape memory (2W-SM) effect, in particular semi-crystalline polymers which exhibit an elongation during the crystallization phase under constant applied stress (Defize et al., 2012; Pereira Sanchez et al., 20 July 2022), as depicted in Fig. 1(b). In that case reheating the sample under the same applied stress allows getting back the initial deformation state (point B) at high temperature, while a

*Corresponding author
Email address: L.Noels@ulg.ac.be (Ludovic Noels)

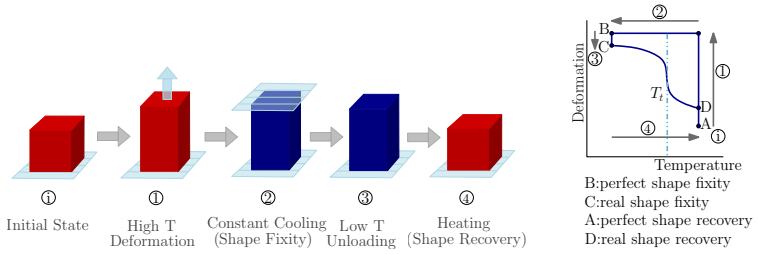

(a) 1W-shape memory

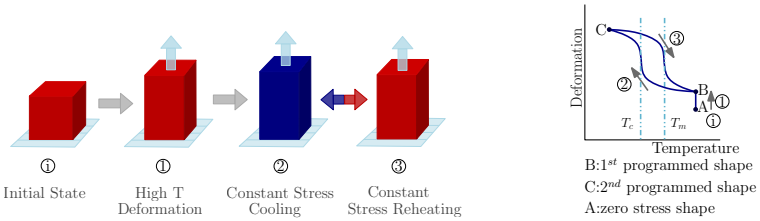

(b) 2W-shape memory

Figure 1: One-Way (1W) and Two-Way (2W) shape memory (SM) effects: (a) 1W-SM temperature-deformation cycle; and (b) 2W-SM temperature-deformation cycle.

subsequent cooling at constant stress allows recovering the low-temperature deformation state (point C), as schematically illustrated in Fig. 1(b).

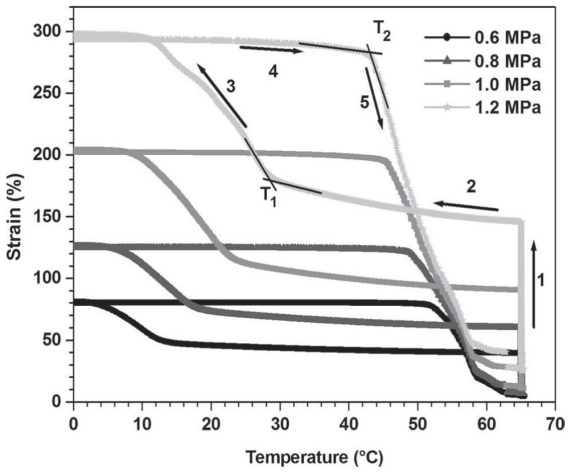

Figure 2: Evolution of strain under thermomechanical cycling loading with increasing load level (Defize et al., 2012). Note the evolution of T_c ($\approx T_1$), T_m ($\approx T_2$), w_c (slope of curve 3), w_m (slope of curve 5), α^c (slope of curve 4), α^m (slope of curve 2), and the distance between curves 2 and 4 characterizing the 2W-SM effect.

In the case of semi-crystalline polymers, from Figure 2, which represents the thermo-

mechanical responses of a semi-crystalline polymer under constant applied stress, two unusual behaviors can be observed: an additional expansion/contraction during the phase transition (distance between curves 2 and 4), which is responsible for the existance of the 2W-SM effect, and the negative thermal expansion coefficients during cooling/heating (slopes of curves 2 and 4). Li et al. (2011) observed the same sudden deformation during phase transition and name it as *crystallization induced elongation* and *melting induced contraction*. Choy et al. (1981) showed that under deformation, negative anisotropic thermal expansion can be observed, i.e. expansion in the loading direction, contraction in lateral directions in a tensile test when cooling. These behaviors get more pronounced with the increase in the load level and are absent when no external load is applied as shown by Pereira Sanchez et al. (20 July 2022), i.e. at zero load the thermal expansion is isotropic and positive. Both Li et al. (2011) and Choy et al. (1981) argued that these behaviors arise from the formation of the liquid crystalline structure anisotropically aligned in the stress direction. In particular, the extension during crystallization is responsible for the 2W-SM observed for these polymers (Pereira Sanchez et al., 20 July 2022).

In the literature, there has been an interest for the numerical modeling of SMPs in the recent years. In addition to micromechanics models (Srivastava et al., 2010, Yang and Li, 2016), many phenomenological models have also been developed for SMPs. Nguyen et al. (2008) developed a viscoelastic constitutive model for amorphous SMPs with softening viscoplastic behavior. They used time and temperature dependent material properties to model the SM behavior. Diani et al. (2012) developed a finite strain viscoelastic model for amorphous polymers. They showed that the SM behavior can be captured by material viscoelasticity with several viscous branches. Ge et al. (2012) studied a composite material with an elastomeric matrix reinforced by a semi-crystalline polymer fiber network which is utilized as the SM mechanism. Their model includes a kinetic description such that a gradual phase change and deformation of the polymer fractions can be taken into account. Boatti et al. (2016) considered an amorphous SMP as a mixture of glassy (stiff) and rubbery (soft) phases. The volume fractions of the phases were considered to change with a temperature dependent function. They achieved the imperfect shape-fixity and shape-recovery by introducing internal tensor variables. Considering a viscoelastic material model embedding phase transition, Guo et al. (2016) proposed a normal distribution model, which is physically motivated, to evaluate the variation in the volume fraction of the frozen and active phases.

In this study, a phenomenological viscoelasto-plastic constitutive model is developed for the modeling of semi-crystalline SMPs under thermo-mechanical loading conditions, with the aim of reproducing both 1W-SM and 2W-SM effects. A 1D analogy of the model is given in Fig. 3. It considers that the semi-crystalline polymer is a two-phase composite material made of the semi-crystalline (CR) and amorphous (a) phases. The polymer is considered to operate above the T_{g} of the amorphous phase. Therefore, it is assumed that the amorphous phase does not change phase with temperature and has a constant volume fraction (z^{a}). Additionally, the operating temperature range includes T_{c} and T_{m}, therefore, the SM behavior is obtained by the phase transition of the crystalline phase. The crystalline phase is further considered to be composed of two phases: the crystallized phase (c) and the melted phase (m). The crystallized phase is active at low temperatures, while the melted phase is active at high temperatures and both phases are active during the phase transition. The volume fractions of the phases are considered

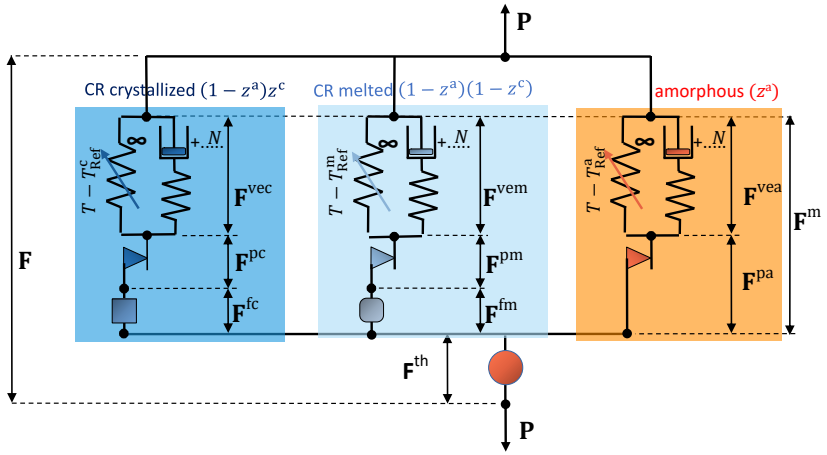

Figure 3: 1D analogy of the SMP constitutive model. $\mathbf{F} = \mathbf{F}^{\mathrm{vec}} \cdot \mathbf{F}^{\mathrm{pc}} \cdot \mathbf{F}^{\mathrm{fc}} \cdot \mathbf{F}^{\mathrm{th}} = \mathbf{F}^{\mathrm{vem}} \cdot \mathbf{F}^{\mathrm{pm}} \cdot \mathbf{F}^{\mathrm{fm}} \cdot \mathbf{F}^{\mathrm{th}} = \mathbf{F}^{\mathrm{vea}} \cdot \mathbf{F}^{\mathrm{pa}} \cdot \mathbf{F}^{\mathrm{th}} = \mathbf{F}^{\mathrm{m}} \cdot \mathbf{F}^{\mathrm{th}}$; $\mathbf{F}$: deformation gradient; $\mathbf{F}^{\mathrm{ve}i}$: viscoelastic deformation gradient of branch i; $\mathbf{F}^{\mathrm{p}i}$: plastic deformation gradient of branch i; $\mathbf{F}^{\mathrm{f}i}$: frozen deformation gradient of branch i; $\mathbf{F}^{\mathrm{th}}$: thermal deformation gradient; $\mathbf{F}^{\mathrm{m}}$: purely mechanical deformation gradient, CR: crystalline phase; $\mathbf{F}^{x\mathrm{c}}$: x-part of crystallized-branch deformation gradient; $\mathbf{F}^{x\mathrm{m}}$: x-part of melted-branch deformation gradient; $\mathbf{F}^{x\mathrm{a}}$: x-part of amorphous-branch deformation gradient; z^{c}: volume fraction of the crystallized phase; z^{a}: volume fraction of the amorphous phase, $\mathbf{P}$: load; ∞: non-linear (as denoted by the arrow) elastic spring at equilibrium, in which the thermal difference $T - T^{i}_{\mathrm{Ref}}$ in branch i induces an anisotropic thermal deformation; N: number of dashpots.

to change with a temperature and strain dependent function (z^{c}) which represents the volume fraction of the glassy phase. Eventually, the volume fractions of each phase, with respect to the reference volume, are given as:

$$v^{\mathrm{c}} = (1 - z^{\mathrm{a}})(z^{\mathrm{c}})\,; \tag{1}$$

$$v^{\mathrm{m}} = (1 - z^{\mathrm{a}})(1 - z^{\mathrm{c}})\,; \tag{2}$$

$$v^{\mathrm{a}} = (z^{\mathrm{a}})\,. \tag{3}$$

As shown in Fig. 3, for both crystallized and melted phases, a viscoelasto-plastic behavior is assumed with the respective deformation gradient decompositions, $\mathbf{F}^{\mathrm{vec}} \cdot \mathbf{F}^{\mathrm{pc}}$, $\mathbf{F}^{\mathrm{vem}} \cdot \mathbf{F}^{\mathrm{pm}}$. The viscoelastic branches include $N + 1$ springs and N dashpots. Since the change of phase does not occur at zero strain, history deformation gradients, $\mathbf{F}^{\mathrm{fc}}$ and $\mathbf{F}^{\mathrm{fm}}$ are considered in the crystallized and melted phases, respectively. The amorphous phase is modeled by another viscoelasto-plastic branch with the deformation gradient decomposition $\mathbf{F}^{\mathrm{vea}} \cdot \mathbf{F}^{\mathrm{pa}}$. For the sake of generality, the model is developed by considering a possible plastic flow in the different branches, although the identification procedure will show that only the melted crystalline branch require to account for a plastic flow in order to capture the two-way shape memory effect, while no plasticity model is required in the other branches in the considered strain ranges. Thermal deformation is composed of an isotropic volumetric part $\mathbf{F}^{\mathrm{th}}$, and of anisotropic parts. Experiments (Choy et al., 1981, Defize et al., 2012, Jones et al., 2013) show the existence of anisotropic thermal deformation with a negative thermal expansion along the loading direction. Assuming these anisotropic (here assumed deviatoric) thermal deformations are due to the mismatch be-

tween phases, they are modeled in the different phases by considering non-linear springs whose stiffness depends on the temperature difference with respect to the phases reference temperatures T^{c}_{Ref}, T^{m}_{Ref} and T^{a}_{Ref}.

The developed model is phenomenological and requires less parameters and therefore experiments compared to corresponding micromechanics models. The developed model is able to capture the permanent and temporary deformations of the polymer in the considered temperature range by using viscoelastic-plastic and additional deformation measures in order to capture the additional expansion/contraction observed during the phase change occuring under stress (Defize et al., 2012), which makes it possible to represent both 1W-SM and 2W-SM effects of semi-crystalline SMP. It also considers the anisotropic thermal deformation of polymers under load. Although the current model is developed to model the semi-crystalline SMPs, it can also be used to model the composite materials as in the work of Ge et al. (2012).

The article is organized as follows. In Section 2, the kinematics of the SMP model and evolution equations of the internal variables are given. In Section 3, the thermodynamic problem is solved for the considered model. The energy balance and heat dissipation formulations are given. In Section 4, the details of the viscoelastic-plastic formulation are given. In Section 5, the incremental form of the model is presented in view of its numerical implementation. In Section 6, the model parameters are identified from experimental test results. In Section 7, the conclusions are provided and some possible future works are pointed out. All the details of the formulations are provided in Appendices.

2. Model Ingredients

2.1. Basic Kinematics

In a homogeneous body, let $\mathbf{X}$ denote an arbitrary point in the reference configuration (Ω_0), $\mathbf{x} = \mathbf{x}(\mathbf{X}, t)$ denotes the position of $\mathbf{X}$ in the current configuration (Ω) that is defined by a smooth one-to-one mapping as:

$$\mathbf{F} = \boldsymbol{\nabla}_0 \mathbf{x} = \frac{\partial \mathbf{x}}{\partial \mathbf{X}}, \tag{4}$$

where $\mathbf{F}$ is the deformation gradient and $\boldsymbol{\nabla}_0$ is the gradient operator in the reference configuration. The deformation gradient $\mathbf{F}$ can be decomposed into the product of an orthogonal matrix $\mathbf{R}$ (i.e. rigid body rotation, $\mathbf{R}^{T} \cdot \mathbf{R} = \mathbf{I}$, $\det \mathbf{R} = 1$, ^{T} is the transpose), and a symmetric positive definite matrix $\mathbf{U}$ (i.e. pure stretch) as:

$$\mathbf{F} = \mathbf{R} \cdot \mathbf{U}. \tag{5}$$

Based on the calculated deformation gradient, the right Cauchy-Green tensor $\mathbf{C}$ and the logarithmic strain tensor $\mathbf{E}$ are defined, respectively, as:

$$\mathbf{C} = \mathbf{F}^{T} \cdot \mathbf{F} = \mathbf{U} \cdot \mathbf{R}^{T} \cdot \mathbf{R} \cdot \mathbf{U} = \mathbf{U}^2, \text{ and} \tag{6}$$

$$\mathbf{E} = \ln \mathbf{U} = \ln\left(\sqrt{\mathbf{C}}\right) = \frac{1}{2} \ln \mathbf{C}, \tag{7}$$

where $\mathbf{E}$ is calculated following a polar decomposition. The polar decomposition of $\mathbf{E}$ is given as:

$$\mathbf{E} = \sum_{\ell=1}^{3} \frac{1}{2} \ln(\xi_\ell^C)\, \mathbf{N}_\ell \otimes \mathbf{N}_\ell = \sum_{\ell=1}^{3} \xi_\ell^E\, \mathbf{N}_\ell \otimes \mathbf{N}_\ell \,, \tag{8}$$

where ξ_ℓ^C are the eigenvalues of $\mathbf{C}$, ξ_ℓ^E are the eigenvalues of $\mathbf{E}$, and $\mathbf{N}_\ell$ are the eigenvectors (of both $\mathbf{C}$ and $\mathbf{E}$).

The velocity gradient $\mathbf{L}$ is defined as:

$$\mathbf{L} = \dot{\mathbf{F}} \cdot \mathbf{F}^{-1} \,, \tag{9}$$

which can further be decomposed as $\mathbf{L} = \mathbf{D} + \mathbf{W}$ with:

$$\mathbf{D} = \frac{1}{2} \left(\mathbf{L} + \mathbf{L}^{\mathrm{T}} \right) \,, \text{ and } \mathbf{W} = \frac{1}{2} \left(\mathbf{L} - \mathbf{L}^{\mathrm{T}} \right) \,, \tag{10}$$

where $\mathbf{D}$ is the symmetrical deformation rate tensor and $\mathbf{W}$ is the asymmetrical spin rate tensor. If it is assumed that the deformation is irrotational, $\mathbf{W} = \mathbf{0}$, it is obtained that $\mathbf{L}$ is symmetric with:

$$\mathbf{L} = \mathbf{D} \,. \tag{11}$$

*2.2. Deformation gradient, **F**, decomposition*

As it can be seen from Figure 3, it is assumed that the total deformation gradient $\mathbf{F}$ ($J = \det \mathbf{F} > 0$) is the same for all phases and multiplicatively decomposed into an isotropic thermal ($\mathbf{F}^{\mathrm{th}}$) and a mechanical deformation gradients ($\mathbf{F}^{\mathrm{m}}$) as:

$$\mathbf{F} = \mathbf{F}^{\mathrm{m}} \cdot \mathbf{F}^{\mathrm{th}} \,. \tag{12}$$

All branches experience the same mechanical $\mathbf{F}^{\mathrm{m}}$ and isotropic thermal $\mathbf{F}^{\mathrm{th}}$ deformation gradients. In the presented model, the isotropic thermal deformation gradient, $\mathbf{F}^{\mathrm{th}}$, captures the elastic strain-independent volume change of the material resulting from a change in the temperature or from the change of rubbery to glassy, or glassy to rubbery, phase in the crystalline part. The anisotropic and elastic-strain dependent change of volume is modeled in the material branches through internal variables as explained here below.

2.2.1. Crystallized phase

In the crystallized phase, a viscoelasto-plastic behavior is considered and $\mathbf{F}^{\mathrm{m}}$ is further decomposed as:

$$\mathbf{F}^{\mathrm{m}} = \mathbf{F}^{\mathrm{vec}} \cdot \mathbf{F}^{\mathrm{pc}} \cdot \mathbf{F}^{\mathrm{fc}} \,, \tag{13}$$

where $\mathbf{F}^{\mathrm{fc}}$ ($J^{\mathrm{fc}} = \det \mathbf{F}^{\mathrm{fc}} > 0$) is the *frozen* deformation gradient representing the amount of temporary deformation stored in the crystallized phase during the crystallization –this choice being motivated by the fact that the deformation induced at high-temperatures acts as a temporary residual deformation (i.e. "frozen") at low temperatures, $\mathbf{F}^{\mathrm{pc}}$ ($J^{\mathrm{pc}} = \det \mathbf{F}^{\mathrm{pc}} > 0$) is the *plastic* part of the deformation gradient arising during the plastic flow of the crystallized phase[1], and $\mathbf{F}^{\mathrm{vec}}$ ($J^{\mathrm{vec}} = \det \mathbf{F}^{\mathrm{vec}} > 0$) is the *viscoelastic* part.

[1] For polymers, the plastic Poisson's ratio is not necessarily 0.5, which can be captured by considering pressure-dependent yield surfaces with a non-associated plastic flow, and hence J^{pc} is not necessarily equal to the unity.

2.2.2. Melted phase

A similar decomposition is also considered for the melted phase. Then, $\mathbf{F}^{\mathrm{m}}$ and $\mathbf{F}$ are obtained as:

$$\mathbf{F}^{\mathrm{m}} = \mathbf{F}^{\mathrm{vem}} \cdot \mathbf{F}^{\mathrm{pm}} \cdot \mathbf{F}^{\mathrm{fm}} , \tag{14}$$

where $\mathbf{F}^{\mathrm{fm}}$ ($J^{fm} = \det \mathbf{F}^{fm} > 0$) is the *residual frozen*, $\mathbf{F}^{\mathrm{pm}}$ ($J^{\mathrm{pm}} = \det \mathbf{F}^{\mathrm{pm}} > 0$) is the *plastic* and $\mathbf{F}^{\mathrm{vem}}$ ($J^{\mathrm{vem}} = \det \mathbf{F}^{\mathrm{vem}} > 0$) is the *viscoelastic* deformation gradients. The residual frozen term $\mathbf{F}^{\mathrm{fm}}$ is introduced by similarity to the crystallized phase but we will see that this term can actually be set to the identity tensor.

2.2.3. Amorphous phase

The amorphous phase does not change phase within the temperature range. Therefore, an additional residual deformation gradient is not considered, and a viscoelasto-plastic behavior is adopted only for the amorphous phase. Then, $\mathbf{F}^{\mathrm{m}}$ and $\mathbf{F}$ are obtained as:

$$\mathbf{F}^{\mathrm{m}} = \mathbf{F}^{\mathrm{vea}} \cdot \mathbf{F}^{\mathrm{pa}} , \tag{15}$$

where $\mathbf{F}^{\mathrm{pa}}$ ($J^{\mathrm{pa}} = \det \mathbf{F}^{\mathrm{pa}} > 0$) is the *plastic* deformation gradient, and $\mathbf{F}^{\mathrm{vea}}$ ($J^{\mathrm{vea}} = \det \mathbf{F}^{\mathrm{vea}} > 0$) is the *viscoelastic* deformation gradient.

In the remaining of the paper, the superscripts $\bullet^{\mathrm{c}}$, $\bullet^{\mathrm{m}}$ and $\bullet^{\mathrm{a}}$ are used to refer to the crystallized, melted and amorphous branches, respectively.

2.3. Evolution of the volume fraction of the crystallized phase, z^c

As suggested by Boatti et al. (2016), the crystallization process is assumed to be driven by the temperature evolution, with the transition temperatures dependent on the strain level. In other words, a change of strain at constant temperature does not trigger the phase transition, but it will modify the transition rate with respect to the temperature. We assume that the driving strain is

$$|\mathbf{E}^{\mathrm{vem}}| = (\mathbf{E}^{\mathrm{vem}} : \mathbf{E}^{\mathrm{vem}})^{1/2} , \tag{16}$$

the magnitude of the viscoelastic strain tensor in the melted phase, $\mathbf{E}^{\mathrm{vem}}$, calculated by using $\mathbf{F}^{\mathrm{vem}}$ in Eqs. (6) and (7).

The evolution of the crystallized volume fraction z^{c} of the crystalline phase (CR), is thus defined in the rate form as:

$$\dot{z}^{\mathrm{c}} = -f\left(T, |\mathbf{E}^{\mathrm{vem}}|\right) \dot{T} , \text{ with } z^{\mathrm{c}} \in [0, 1] . \tag{17}$$

In order to characterize the rate function $f\left(T, |\mathbf{E}^{\mathrm{vem}}|\right)$, Fig. 4 reports the Differential Scanning Calorimetry (DSC) curve of a 3% weight reinforced PCL764MAL/FUR polymer obtained following the protocol further explained in Section 6. One can observe a melting peak temperature around $T_{\mathrm{m}} = 43°\mathrm{C}$ during heating, and a peak crystallization temperature around $T_{\mathrm{c}} = 27°\mathrm{C}$ during cooling. The presence of such peaks during the changes of phase motivates the approximation of the rate function $f\left(T, |\mathbf{E}^{\mathrm{vem}}|\right)$ with a Gaussian probability density function:

$$f\left(T, |\mathbf{E}^{\mathrm{vem}}|\right) = \frac{1}{w_{\mathrm{t}}\left(|\mathbf{E}^{\mathrm{vem}}|\right)\sqrt{2\pi}} \exp\left[-\frac{1}{2}\left(\frac{T - T_{\mathrm{t}}\left(|\mathbf{E}^{\mathrm{vem}}|\right)}{w_{\mathrm{t}}\left(|\mathbf{E}^{\mathrm{vem}}|\right)}\right)^2\right] , \tag{18}$$

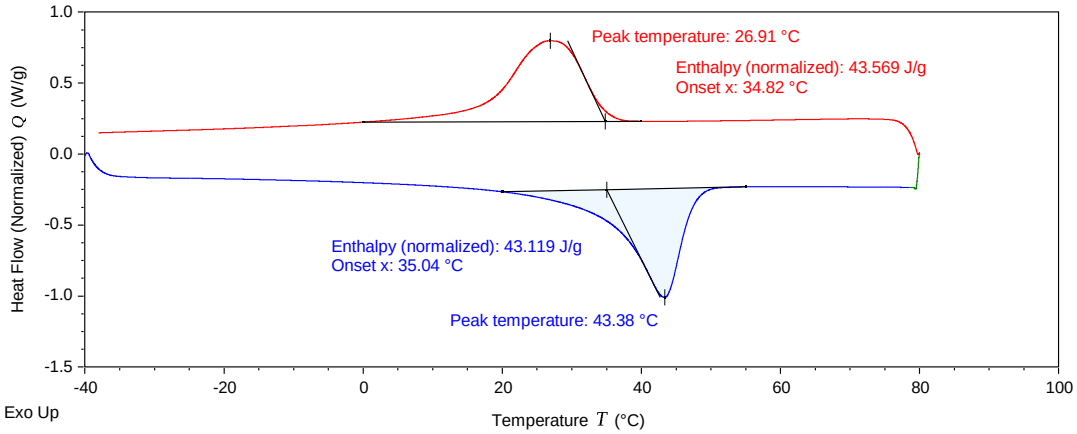

Figure 4: Differential Scanning Calorimetry (DSC) performed on an unloaded PCL76-4MAL/FUR 3 wt%CNT sample.

where $T_\mathrm{t}\left(|\mathbf{E}^\mathrm{vem}|\right)$ is the transition temperature and $w_\mathrm{t}\left(|\mathbf{E}^\mathrm{vem}|\right)$ (>0) defines the smoothness of the transition as further explained. We also use the error function with mean $T_\mathrm{t}\left(|\mathbf{E}^\mathrm{vem}|\right)$ and standard deviation $w_\mathrm{t}\left(|\mathbf{E}^\mathrm{vem}|\right)$:

$$\mathrm{erf}\left(\frac{T-T_\mathrm{t}\left(|\mathbf{E}^\mathrm{vem}|\right)}{\sqrt{2}w_\mathrm{t}\left(|\mathbf{E}^\mathrm{vem}|\right)}\right)=2\int_0^T f\left(T',\,|\mathbf{E}^\mathrm{vem}|\right)dT'\,, \tag{19}$$

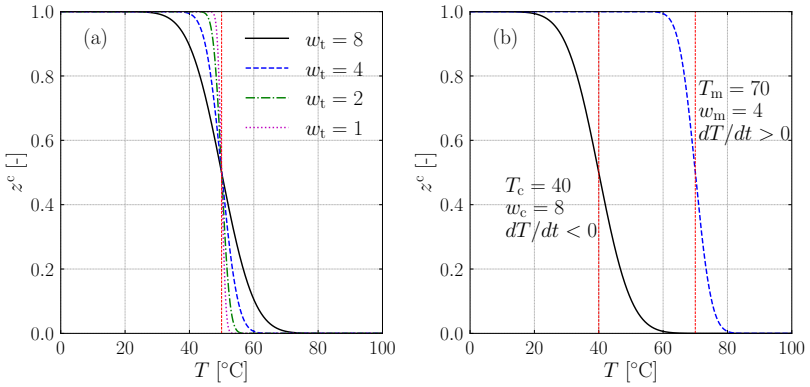

Figure 5: (a) evolution of z^c for $T_\mathrm{t}=50$°C for different values of w_t. (b) evolution of z^c for decreasing temperature, $T_\mathrm{t}=T_\mathrm{c}=40$°C and $w_\mathrm{t}=w_\mathrm{c}=8$, and for increasing temperature, $T_\mathrm{t}=T_\mathrm{m}=70$°C and $w_\mathrm{t}=w_\mathrm{c}=4$.

Figure 5 shows the behavior of z^c on w_t and T_t. As it can be seen from Fig. 5(a), if w_t is increased, a smoother transition centered on T_t is obtained.

For a semi-crystalline polymer, Fig. 2 shows that under cyclic thermomechanical loading, T_t and w_t take different values during crystallization and melting (Defize et al., 2012): T_c and w_c are the values during crystallization, whereas, T_m and w_m are the

values during melting, Fig. 5(b). It can also be observed that with the increase in load level, the gap between $T_{\mathrm{c}}(\approx T_1)$ and $T_{\mathrm{m}}(\approx T_2)$ gets smaller, w_{c} (slope of curve 3) and w_{m} (slope of curve 5) increase and the transitions become less smooth. Therefore, it is written that:

$$T_{\mathrm{t}}\left(|\mathbf{E}^{\mathrm{vem}}|\right),\, w_{\mathrm{t}}\left(|\mathbf{E}^{\mathrm{vem}}|\right) = \begin{cases} T_{\mathrm{c}}\left(|\mathbf{E}^{\mathrm{vem}}|\right),\, w_{\mathrm{c}}\left(|\mathbf{E}^{\mathrm{vem}}|\right) & \text{if} \quad \dot{T} < 0 \text{ (during cooling)}\,; \\ T_{\mathrm{m}}\left(|\mathbf{E}^{\mathrm{vem}}|\right),\, w_{\mathrm{m}}\left(|\mathbf{E}^{\mathrm{vem}}|\right) & \text{if} \quad \dot{T} > 0 \text{ (during heating)}\,. \end{cases} \tag{20}$$

Besides, in order to capture the dependency on the strain, T_{c}, T_{m}, w_{c} and w_{m} are assumed to be functions of the melted phase elastic strain as:

$$T_{\mathrm{c}}\left(|\mathbf{E}^{\mathrm{vem}}|\right) = A_{Tc}\tanh(\alpha_{Tc}\left|\mathbf{E}^{\mathrm{vem}}|\right) + T_{c0}\,; \tag{21}$$

$$T_{\mathrm{m}}\left(|\mathbf{E}^{\mathrm{vem}}|\right) = A_{Tm}\tanh(\alpha_{Tm}\left|\mathbf{E}^{\mathrm{vem}}|\right) + T_{m0}\,; \tag{22}$$

$$w_{\mathrm{c}}\left(|\mathbf{E}^{\mathrm{vem}}|\right) = A_{wc}\tanh(\alpha_{wc}\left|\mathbf{E}^{\mathrm{vem}}|\right) + w_{c0}\,; \tag{23}$$

$$w_{\mathrm{m}}\left(|\mathbf{E}^{\mathrm{vem}}|\right) = A_{wm}\tanh(\alpha_{wm}\left|\mathbf{E}^{\mathrm{vem}}|\right) + w_{m0}\,; \tag{24}$$

where T_{c0}, T_{m0}, w_{c0} and w_{m0} are the related isotropic values in undeformed configuration, $A_{Tc}, A_{Tm}, A_{wc}, A_{wm}$, α_{Tc}, α_{Tm}, α_{wc}, α_{wm} are the coefficients to be obtained from test results in terms of the magnitude of the viscoelastic strain tensor $\mathbf{E}^{\mathrm{vem}}$. In Eqs. (21-24), the tanh functions are chosen for the evolution of the parameters based on the test campaign that will be provided in Section 6.

2.4. Thermal deformation gradient, F^{th}

The rate of the isotropic thermal deformation gradient is expressed as

$$\dot{\mathbf{F}}^{\mathrm{th}} \cdot \mathbf{F}^{\mathrm{th}^{-1}} = \dot{\lambda}^{\mathrm{th}}\mathbf{I}\,, \tag{25}$$

and with

$$\begin{aligned} \dot{\lambda}^{\mathrm{th}} = {} & \left(1-z^{\mathrm{a}}\right) z^{\mathrm{c}}\alpha_0^{\mathrm{c}}\dot{T} + \left(1-z^{\mathrm{a}}\right)\left(1-z^{\mathrm{c}}\right)\alpha_0^{\mathrm{m}}\dot{T} + z^{\mathrm{a}}\alpha_0^{\mathrm{a}}\dot{T} + \\ & \left(1-z^{\mathrm{a}}\right)\dot{z}^{\mathrm{c}}\left[\alpha_0^{\mathrm{tr}} + \alpha^{\mathrm{cr}}\left(z^{\mathrm{c}}\right)\right]\,, \end{aligned} \tag{26}$$

where α_0^{c}, α_0^{m} are the isotropic thermal expansion coefficients of each phase in the undeformed state, α_0^{tr} is the transition term defined to have a continuous deformation cycle as explained below, and where $\alpha^{\mathrm{cr}} \leq 0$ is the crystallization change of volume associated to the phase change. This change of volume associated to the phase change is written:

$$\alpha^{\mathrm{cr}}\left(z^{\mathrm{c}}\right) = \alpha_0^{\mathrm{cr}} \times \begin{cases} \frac{2}{\left(z_0^{\mathrm{cr}}\right)^2}\left(z_0^{\mathrm{cr}} - z^{\mathrm{c}}\right) & \text{if} \quad z^{\mathrm{c}} \leq z_0^{\mathrm{cr}}\,; \\ 0 & \text{if} \quad z^{\mathrm{c}} \geq z_0^{\mathrm{cr}}\,; \end{cases} \tag{27}$$

where $\alpha_0^{\mathrm{cr}} \leq 0$ controls the amplitude of the change of volume during the change of phase, and is negative since the melted phase takes more volume than the crystallized one, and where $0 \leq z_0^{\mathrm{cr}} \leq 1$ controls the crystallinity level around which the change of volume arises.

An example of thermal deformation of a generic SMP in a thermal cycle is given in Fig. 6. Figure 6(a) shows that, if $T_c = T_m$, $w_c = w_m$ and $\alpha_0^{\mathrm{cr}} = 0$, deformation follows the same path during cooling and heating. If $T_c \neq T_m$, because of the difference in α_0^{c}

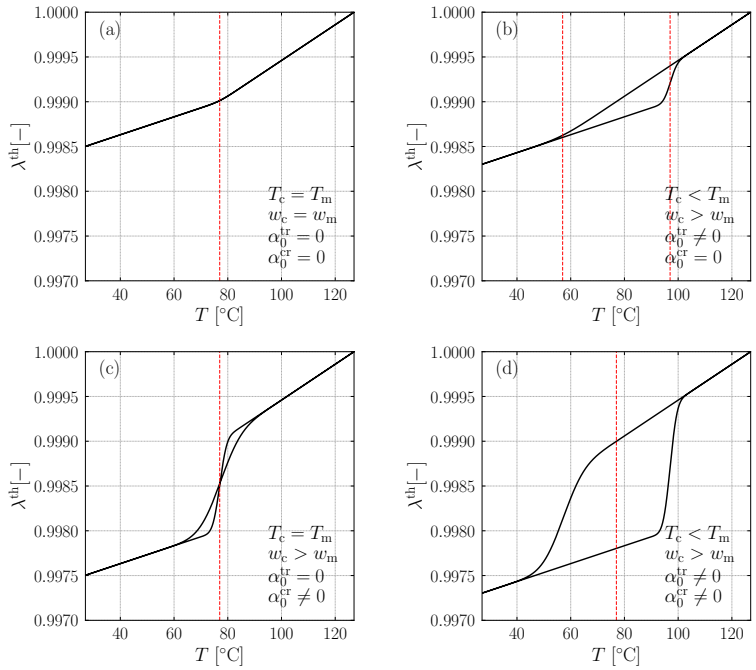

Figure 6: Evolution of the isotropic thermal deformation for different thermal parameters combinations: (a) $T_c = T_m$, $w_c = w_m$, $\alpha_0^{tr} = 0$, $\alpha_0^{cr} = 0$; (b) $T_c < T_m$, $w_c > w_m$, $\alpha_0^{tr} \neq 0$, $\alpha_0^{cr} = 0$; (c) $T_c = T_m$, $w_c > w_m$, $\alpha_0^{tr} = 0$, $\alpha_0^{cr} \neq 0$; and (d) $T_c < T_m$, $w_c > w_m$, $\alpha_0^{tr} \neq 0$, $\alpha_0^{cr} \neq 0$.

and α_0^m, a strain difference is automatically created during the thermal cycle, Fig. 6(b). The term α_0^{tr} in Eq. (113) is used to control this transition strain difference:

$$\alpha_0^{tr} = (\alpha_0^m - \alpha_0^c)(T_c - T_m)\,. \tag{28}$$

This accumulated temporary strain difference during cooling has to be added during melting to have a closed loop in a thermal cycle:

$$\begin{cases} \alpha_0^{tr} = 0 & \text{if} \quad \dot{T} \leqslant 0\,; \\ \alpha_0^{tr} = (\alpha_0^m - \alpha_0^c)(T_c - T_m) & \text{if} \quad \dot{T} > 0\,. \end{cases} \tag{29}$$

Fig. 6(c) shows the case where $T_c = T_m$ and $\alpha_0^{cr} \neq 0$. It can be seen that the deformation gradient does not follow the same path because $w_c \neq w_m$. Fig. 6(d) shows the most general case where $T_c \neq T_m$, $w_c \neq w_m$, $\alpha_0^{tr} \neq 0$ and $\alpha_0^{cr} \neq 0$.

2.5. Evolution of the state deformation gradients and temperatures

In the model formulation, it is considered that the total deformation gradient, $\mathbf{F}$, and temperature, T, are the driving kinematic quantities. Then, some evolution rules have to be defined for the state deformation gradients $\mathbf{F}^{fc}$, $\mathbf{F}^{fm}$, $\mathbf{F}^{pc}$, $\mathbf{F}^{pm}$ and $\mathbf{F}^{pa}$. Besides, the anisotropic and elastic-strain-dependent thermal deformations, responsible for the (elastic-strain-dependent) negative slope of curve 2 in Fig. 2 are modeled by considering in the different phases non-linear springs, see Fig. 3, whose stiffness depends on the

temperature difference with respect to the phases reference temperature $T^{\mathrm{c}}_{\mathrm{Ref}}$, $T^{\mathrm{m}}_{\mathrm{Ref}}$ and $T^{\mathrm{a}}_{\mathrm{Ref}}$, which are thus also state variables.

2.5.1. Frozen deformation, $\boldsymbol{F}^{fc}$, and reference temperature, T^{c}_{Ref}, in the crystallized phase

The frozen deformation, $\mathbf{F}^{\mathrm{fc}}$, represents the temporary deformation stored in the crystallized phase during the crystallization resulting from the deformation induced at high-temperatures which acts as a temporary residual deformation (i.e. "frozen") at low temperatures, yielding the evolution law

$$\mathbf{F}^{\mathrm{fc}} = \begin{cases} \mathbf{F}^{\mathrm{m}} & \text{if fully melted}\,; \\ \text{constant} & \text{otherwise}\,, \end{cases} \tag{30}$$

in which $\mathbf{F}^{\mathrm{m}}$ is the mechanical deformation gradient defined in Eq. (12). Theoretically, the wording fully melted refers to $z^c = 0$, while fully crystallized refers to $z^c = 1$. These values being not reachable in the incremental form of the implementation, these definitions will be refined in Section 5. We note that Boatti et al. (2016) defined a similar evolution of $\mathbf{F}^{\mathrm{fc}}$, in which they introduced a parameter $c^{\mathrm{fc}} \in [0, 1]$ determining the amount of the shape-fixity at the end of the crystallization. In this study, the amorphous phase is considered to be an additional phase which is responsible for the non-perfect shape fixity (real shape fixity in Fig. 1(a)) at low temperature. Therefore, it is assumed that the melted phase freezes completely to the crystallized phase.

The reference temperature governing the elastic-strain-dependent thermal deformation in the crystallized phase is evaluated similarly in order for the reference temperature to be the crystallization point:

$$T^{\mathrm{c}}_{\mathrm{Ref}} = \begin{cases} T & \text{if fully melted}\,; \\ \text{constant} & \text{otherwise}\,. \end{cases} \tag{31}$$

2.5.2. Residual frozen deformation, $\boldsymbol{F}^{fm}$, and reference temperature, T^{m}_{Ref}, in the melted phase

In this model we assume that upon melting, the melted phase does not store a deformation, yielding

$$\mathbf{F}^{\mathrm{fm}} = \mathbf{I}\,. \tag{32}$$

Once more, we note that Boatti et al. (2016) considered a similar relation in which they introduced some deformation gradient in order to model the imperfect shape recovery, while the imperfect shape recovery in the developed approach is obtained because of the presence of the amorphous phase.

The reference temperature governing the elastic-strain-dependent thermal deformation in the melted phase is evaluated similarly to Eq. (31), but using the melting point as the reference temperature:

$$T^{\mathrm{m}}_{\mathrm{Ref}} = \begin{cases} T & \text{if fully crystallized}\,; \\ \text{constant} & \text{otherwise}\,. \end{cases} \tag{33}$$

2.5.3. Reference temperature, T^{a}_{Ref}, in the amorphous phase

The reference temperature governing the elastic-strain-dependent thermal deformation in the amorphous phase is simply the initial temperature since there is no change of phase:

$$T^{\mathrm{a}}_{\mathrm{Ref}} = \text{constant}\,. \tag{34}$$

2.5.4. Plastic deformation in the crystallized phase, $\boldsymbol{F}^{pc}$

The flow rule of the plastic deformation gradient is provided in Section 4. Additionally, because of phase change (melting), a further evolution law is defined for $\mathbf{F}^{\mathrm{pc}}$ as:

$$\mathbf{F}^{\mathrm{pc}} = \begin{cases} \text{evolves according to the assigned flow rule in Section 4} & \text{if not fully melted}\,; \\ \mathbf{I} & \text{otherwise}\,. \end{cases} \tag{35}$$

The above equation states that there is no plastic deformation left in the crystallized phase after melting.

2.5.5. Plastic deformation in the melted phase, $\boldsymbol{F}^{pm}$

As in the crystallized phase, in addition to the flow rule provided in Section 4, a further law is defined for the evolution of $\mathbf{F}^{\mathrm{pm}}$ as:

$$\mathbf{F}^{\mathrm{pm}} = \begin{cases} \text{evolves according to the assigned flow rule in Section 4} & \text{if not fully crystallized}\,; \\ \mathbf{I} & \text{otherwise}\,. \end{cases} \tag{36}$$

The above equation states that there is no plastic deformation left in the melted phase after freezing.

2.5.6. Plastic deformation in the amorphous phase, $\boldsymbol{F}^{pa}$

Since, the amorphous phase does not change phase, $\mathbf{F}^{\mathrm{pa}}$ directly results from the flow rule provided in Section 4.

3. Thermodynamics Considerations

3.1. Helmholtz Free Energy and Stress Decomposition

According to the considered model in Figure 3, the total free energy per unit reference volume, Ψ, is calculated as the summation of the free energies per unit reference volume of each phase:

$$\begin{aligned} \Psi =& \Psi^{\mathrm{c}}\left(T, \mathbf{C}^{\mathrm{vec}}, \widetilde{\mathbf{q}}^{\mathrm{c}}_j, \xi^{\mathrm{pc}}_i, z^{\mathrm{c}}; \mathbf{F}^{\mathrm{pc}}, T^{\mathrm{c}}_{\mathrm{Ref}}, \mathbf{F}^{\mathrm{fc}}\right) + \Psi^{\mathrm{m}}\left(T, \mathbf{C}^{\mathrm{vem}}, \widetilde{\mathbf{q}}^{\mathrm{m}}_j, \xi^{\mathrm{pm}}_i, z^{\mathrm{c}}; \mathbf{F}^{\mathrm{pm}}, T^{\mathrm{m}}_{\mathrm{Ref}}, \mathbf{F}^{\mathrm{fm}}\right) \\ &+ \Psi^{\mathrm{a}}\left(T, \mathbf{C}^{\mathrm{vea}}, \widetilde{\mathbf{q}}^{\mathrm{a}}_j, \xi^{\mathrm{pa}}_i; \mathbf{F}^{\mathrm{pa}}, T^{\mathrm{a}}_{\mathrm{Ref}}\right)\,, \end{aligned} \tag{37}$$

which is also written as:

$$\begin{aligned} \Psi =& v^{\mathrm{c}}\left(T, |\mathbf{E}^{\mathrm{vem}}|\right) \widetilde{\Psi}^{\mathrm{c}}\left(T, \mathbf{E}^{\mathrm{vec}}, \widetilde{\mathbf{q}}^{\mathrm{c}}_j, \xi^{\mathrm{pc}}_i, z^{\mathrm{c}}; \mathbf{F}^{\mathrm{pc}}, T^{\mathrm{c}}_{\mathrm{Ref}}, \mathbf{F}^{\mathrm{fc}}\right) + \\ & v^{\mathrm{m}}\left(T, |\mathbf{E}^{\mathrm{vem}}|\right) \widetilde{\Psi}^{\mathrm{m}}\left(T, \mathbf{E}^{\mathrm{vem}}, \widetilde{\mathbf{q}}^{\mathrm{m}}_j, \xi^{\mathrm{pm}}_i, z^{\mathrm{c}}; \mathbf{F}^{\mathrm{pm}}, T^{\mathrm{m}}_{\mathrm{Ref}}, \mathbf{F}^{\mathrm{fm}}\right) + \\ & v^{\mathrm{a}}\widetilde{\Psi}^{\mathrm{a}}\left(T, \mathbf{E}^{\mathrm{vea}}, \widetilde{\mathbf{q}}^{\mathrm{a}}_j, \xi^{\mathrm{pa}}_i; \mathbf{F}^{\mathrm{pa}}, T^{\mathrm{a}}_{\mathrm{Ref}}\right) + \Psi^{\mathrm{th}}\left(T, v^{\mathrm{c}}\left(T, |\mathbf{E}^{\mathrm{vem}}|\right)\right)\,, \end{aligned} \tag{38}$$

where the crystallized and melted phase volume fractions v^{c} and v^{m} are functions of T and $|\mathbf{E}^{\mathrm{vem}}|$[2] through Eqs. (1), (2), (17) and (18), Ψ^{c}, Ψ^{m} and Ψ^{a} are the weighted

[2]Although for algorithmic reasons we use $|\mathbf{E}^{\mathrm{vem}}_n|$ in the incremental form, see Section 5, we keep the explicit dependence to derive the thermodynamic consistency.

free energy functions of each phase, $\widetilde{\Psi}^{\mathrm{c}}$, $\widetilde{\Psi}^{\mathrm{m}}$ and $\widetilde{\Psi}^{\mathrm{a}}$ are the free energy functions per unit reference volume of each phase, hereafter, $(\widetilde{\bullet})$ will be used for the variables when the volume fractions are not considered, i.e. for values per unit reference volume of the related phase, Ψ^{th} is the thermal energy function, $\widetilde{\mathbf{q}}_j$ is the stress like internal variable related to a dashpot and j is the dashpot number, ξ_i is the state variable i that defines the elasto-plastic behavior, $\mathbf{C}^{\mathrm{vec}}$, $\mathbf{C}^{\mathrm{vem}}$ and $\mathbf{C}^{\mathrm{vea}}$ are the elastic Cauchy-Green tensors and $\mathbf{E}^{\mathrm{vec}}$, $\mathbf{E}^{\mathrm{vem}}$, $\mathbf{E}^{\mathrm{vea}}$ are the logarithmic strains obtained from the elastic Cauchy-Green tensors and which are considered for the viscoelasto-plastic branches. In this last expression, $T^{\mathrm{c}}_{\mathrm{Ref}}$, $T^{\mathrm{m}}_{\mathrm{Ref}}$ and $T^{\mathrm{a}}_{\mathrm{Ref}}$, the reference temperatures governing the non-linear phases responses, as well as $\mathbf{F}^{\mathrm{fc}}$ and $\mathbf{F}^{\mathrm{fm}}$, the frozen deformation gradients are constant when the branch is active, i.e. when their corresponding volume fraction is positive. As a consequence they do not yield to conjugate forces, *i.e.* $v^{\mathrm{c}}\dot{T}^{\mathrm{c}}_{\mathrm{Ref}} = 0$, $v^{\mathrm{m}}\dot{T}^{\mathrm{c}}_{\mathrm{Ref}} = 0$, $v^{\mathrm{a}}\dot{T}^{\mathrm{a}}_{\mathrm{Ref}} = 0$, and $v^{\mathrm{c}}\dot{\mathbf{F}}^{\mathrm{fc}} = 0$ and $v^{\mathrm{m}}\dot{\mathbf{F}}^{\mathrm{fm}} = 0$. Each free energy function $\widetilde{\Psi}^{i}$, $i = \mathrm{c}, \mathrm{m}, \mathrm{a}$, is further decomposed into a viscoelastic part $\widetilde{\Psi}^{\mathrm{ve}i}$ and a plastic part $\widetilde{\Psi}^{\mathrm{p}i}$, resulting into, where we omit the dependencies with $\mathbf{F}^{\mathrm{p}i}$, T^{i}_{Ref}, $\mathbf{F}^{\mathrm{f}i}$ for conciseness

$$
\begin{aligned}
\Psi =& v^{\mathrm{c}}\left(T, |\mathbf{E}^{\mathrm{vem}}|\right)\left[\widetilde{\Psi}^{\mathrm{vec}}\left(T, \mathbf{E}^{\mathrm{vec}}, \widetilde{\mathbf{q}}^{\mathrm{c}}_j, z^{\mathrm{c}}\right) + \widetilde{\Psi}^{\mathrm{pc}}\left(\mathbf{E}^{\mathrm{vec}}, \xi^{\mathrm{pc}}_i, z^{\mathrm{c}}\right)\right] + \\
& v^{\mathrm{m}}\left(T, |\mathbf{E}^{\mathrm{vem}}|\right)\left[\widetilde{\Psi}^{\mathrm{vem}}\left(T, \mathbf{E}^{\mathrm{vem}}, \widetilde{\mathbf{q}}^{\mathrm{m}}_j, z^{\mathrm{c}}\right) + \widetilde{\Psi}^{\mathrm{pm}}\left(\mathbf{E}^{\mathrm{vem}}, \xi^{\mathrm{pm}}_i, z^{\mathrm{c}}\right)\right] + \\
& v^{\mathrm{a}}\left[\widetilde{\Psi}^{\mathrm{vea}}\left(T, \mathbf{E}^{\mathrm{vea}}, \widetilde{\mathbf{q}}^{\mathrm{a}}_j\right) + \widetilde{\Psi}^{\mathrm{pa}}\left(\mathbf{E}^{\mathrm{vea}}, \xi^{\mathrm{pa}}_i\right)\right] + \Psi^{\mathrm{th}}\left(T, v^{\mathrm{c}}\left(T, |\mathbf{E}^{\mathrm{vem}}|\right)\right) .
\end{aligned}
\tag{39}
$$

Similar to the free energy, the total first Piola-Kirchhoff stress tensor, $\mathbf{P}$, is calculated as the summation of phase stresses:

$$
\mathbf{P} = \mathbf{P}^{\mathrm{c}} + \mathbf{P}^{\mathrm{m}} + \mathbf{P}^{\mathrm{a}} = v^{\mathrm{c}}\widetilde{\mathbf{P}}^{\mathrm{c}} + v^{\mathrm{m}}\widetilde{\mathbf{P}}^{\mathrm{m}} + v^{\mathrm{a}}\widetilde{\mathbf{P}}^{\mathrm{a}} ,
\tag{40}
$$

where $\mathbf{P}^{\mathrm{c}}$, $\mathbf{P}^{\mathrm{m}}$, and $\mathbf{P}^{\mathrm{a}}$ are the weighted stresses of the different phases, $\widetilde{\mathbf{P}}^{\mathrm{c}}$, $\widetilde{\mathbf{P}}^{\mathrm{m}}$, and $\widetilde{\mathbf{P}}^{\mathrm{a}}$ are the stresses evaluated from the branches free energy functions. We also define in the relaxed configuration the (visco)elastic second Piola-Kirchhoff stress tensors $\widetilde{\mathbf{S}}^{\mathrm{vec}}$, $\widetilde{\mathbf{S}}^{\mathrm{vem}}$, and $\widetilde{\mathbf{S}}^{\mathrm{vea}}$, following:

$$
\widetilde{\mathbf{S}}^{\mathrm{vec}} = \mathbf{F}^{\mathrm{vec}^{-1}} \cdot \widetilde{\mathbf{P}}^{\mathrm{c}} \cdot \mathbf{F}^{\mathrm{th}^{\mathrm{T}}} \cdot \mathbf{F}^{\mathrm{fc}^{\mathrm{T}}} \cdot \mathbf{F}^{\mathrm{pc}^{\mathrm{T}}} ;
\tag{41}
$$

$$
\widetilde{\mathbf{S}}^{\mathrm{vem}} = \mathbf{F}^{\mathrm{vem}^{-1}} \cdot \widetilde{\mathbf{P}}^{\mathrm{m}} \cdot \mathbf{F}^{\mathrm{th}^{\mathrm{T}}} \cdot \mathbf{F}^{\mathrm{fm}^{\mathrm{T}}} \cdot \mathbf{F}^{\mathrm{pm}^{\mathrm{T}}} ; \text{ and}
\tag{42}
$$

$$
\widetilde{\mathbf{S}}^{\mathrm{vea}} = \mathbf{F}^{\mathrm{vea}^{-1}} \cdot \widetilde{\mathbf{P}}^{\mathrm{a}} \cdot \mathbf{F}^{\mathrm{th}^{\mathrm{T}}} \cdot \mathbf{F}^{\mathrm{pa}^{\mathrm{T}}} .
\tag{43}
$$

Their expressions in terms of the free energies $\widetilde{\Psi}^{\mathrm{ve}i}$ defined in Eq. (38) will arise from the Clausius-Duhem Inequality in Section 3.2.

Eventually, the (visco)elastic Mandel stresses[3] $\widetilde{\mathbf{M}}^{\mathrm{vec}}$, $\widetilde{\mathbf{M}}^{\mathrm{vem}}$, and $\widetilde{\mathbf{M}}^{\mathrm{vec}}$ are defined in the relaxed configuration as:

$$
\widetilde{\mathbf{M}}^{\mathrm{ve}i} = \mathbf{C}^{\mathrm{ve}i} \cdot \widetilde{\mathbf{S}}^{\mathrm{ve}i} \qquad i = \mathrm{c}, \mathrm{m}, \mathrm{a} .
\tag{44}
$$

[3] We will discuss the nature of this stress tensor later in this Section 3.2.

3.2. Clausius-Duhem Inequality

The second law of thermodynamics in the Clausius-Duhem form is written as:

$$\mathfrak{D} = \mathbf{P} : \dot{\mathbf{F}} - \dot{\Psi} - \eta\,\dot{T} - \frac{1}{T}\,\mathbf{Q}\cdot \mathrm{Grad}\; T \geq 0\,, \tag{45}$$

where $\mathfrak{D}$ is the dissipation per unit reference volume, η is the entropy per unit reference volume, $\mathbf{Q}$ is the heat flux per unit reference area, $\mathrm{Grad}(\bullet)(=\boldsymbol{\nabla}_0(\bullet))$ is the gradient operator in the reference configuration.

Introducing the expression (39) in the Clausius-Duhem Inequality, following Appendix A, yields

$$\begin{aligned}
0 \leq & \mathfrak{D}_{\mathrm{loc}} + \mathfrak{D}_{\mathrm{conv}} + v^{\mathrm{c}}\left[\frac{1}{2}\widetilde{\mathbf{S}}^{\mathrm{vec}} - \frac{\partial\widetilde{\Psi}^{\mathrm{vec}}}{\partial\mathbf{C}^{\mathrm{vec}}}\right] : \dot{\mathbf{C}}^{\mathrm{vec}} + v^{\mathrm{m}}\left[\frac{1}{2}\widetilde{\mathbf{S}}^{\mathrm{vem}} - \frac{\partial\widetilde{\Psi}^{\mathrm{vem}}}{\partial\mathbf{C}^{\mathrm{vem}}}\right] : \dot{\mathbf{C}}^{\mathrm{vem}} + \\
& v^{\mathrm{a}}\left[\widetilde{\frac{1}{2}\mathbf{S}^{\mathrm{vea}}} - \frac{\partial\widetilde{\Psi}^{\mathrm{vea}}}{\partial\mathbf{C}^{\mathrm{vea}}}\right] : \dot{\mathbf{C}}^{\mathrm{vea}} + \mathbf{M}^{\mathrm{m}} : \left(\left.\frac{\partial\mathbf{F}^{\mathrm{th}}}{\partial T}\right|_{\mathbf{C}^{\mathrm{vem}}} \cdot \mathbf{F}^{\mathrm{th}^{-1}}\right)\dot{T} - \eta\dot{T} - \\
& \left[v^{\mathrm{c}}\frac{\partial\widetilde{\Psi}^{\mathrm{vec}}}{\partial T} + v^{\mathrm{m}}\frac{\partial\widetilde{\Psi}^{\mathrm{vem}}}{\partial T} + v^{\mathrm{a}}\frac{\partial\widetilde{\Psi}^{\mathrm{vea}}}{\partial T}\right]\dot{T} - \\
& \left[(1-v^{\mathrm{a}})\left(\widetilde{\Psi}^{\mathrm{vec}} + \widetilde{\Psi}^{\mathrm{pc}}\right) - (1-v^{\mathrm{a}})\left(\widetilde{\Psi}^{\mathrm{vem}} + \widetilde{\Psi}^{\mathrm{pm}}\right)\right]\frac{\partial z^{\mathrm{c}}}{\partial T}\dot{T} - \left[\frac{\partial\Psi^{\mathrm{th}}}{\partial T} + \frac{\partial\Psi^{\mathrm{th}}}{\partial z^{\mathrm{c}}}\frac{\partial z^{\mathrm{c}}}{\partial T}\right]\dot{T}\,.
\end{aligned} \tag{46}$$

In Eq. (46), the local dissipation $\mathfrak{D}_{\mathrm{loc}}$ results from the viscous contribution $\mathfrak{D}^{\mathrm{ve}}_{\mathrm{loc}} \geq 0$ and from the plastic contribution $\mathfrak{D}^{\mathrm{p}}_{\mathrm{loc}} \geq 0$ following $\mathfrak{D}_{\mathrm{loc}} = \mathfrak{D}^{\mathrm{ve}}_{\mathrm{loc}} + \mathfrak{D}^{\mathrm{p}}_{\mathrm{loc}}$ with

$$\mathfrak{D}^{\mathrm{ve}}_{\mathrm{loc}} = -v^{\mathrm{c}}\sum_{j}^{N}\frac{\partial\widetilde{\Psi}^{\mathrm{vec}}}{\partial\widetilde{\mathbf{q}}^{\mathrm{vec}}_j} : \dot{\widetilde{\mathbf{q}}}^{\mathrm{vec}}_j - v^{\mathrm{vem}}\sum_{j}^{N}\frac{\partial\widetilde{\Psi}^{\mathrm{vem}}}{\partial\widetilde{\mathbf{q}}^{\mathrm{vem}}_j} : \dot{\widetilde{\mathbf{q}}}^{\mathrm{vem}}_j - v^{\mathrm{a}}\sum_{j}^{N}\frac{\partial\widetilde{\Psi}^{\mathrm{vea}}}{\partial\widetilde{\mathbf{q}}^{\mathrm{a}}_j} : \dot{\widetilde{\mathbf{q}}}^{\mathrm{a}}_j \geq 0\,, \tag{47}$$

and

$$\mathfrak{D}^{\mathrm{p}}_{\mathrm{loc}} \simeq \beta_{\mathrm{TQ}}\left[v^{\mathrm{c}}\widetilde{\mathbf{M}}^{\mathrm{vec}} : \mathbf{L}^{\mathrm{pc}} + v^{\mathrm{m}}\widetilde{\mathbf{M}}^{\mathrm{vem}} : \mathbf{L}^{\mathrm{pm}} + v^{\mathrm{a}}\widetilde{\mathbf{M}}^{\mathrm{vea}} : \mathbf{L}^{\mathrm{pa}}\right] \geq 0\,, \tag{48}$$

where we consider the Taylor-Quinney coefficient β_{TQ}, and where $\mathbf{L}^{\mathrm{p}i} = \dot{\mathbf{F}}^{\mathrm{p}i}\cdot\mathbf{F}^{\mathrm{p}i^{-1}}$ are the plastic velocity gradients of the different phases, $i = \mathrm{c}, \mathrm{m}, \mathrm{a}$. Besides, the convective dissipation $\mathfrak{D}_{\mathrm{conv}}$ reads

$$\mathfrak{D}_{\mathrm{conv}} = -\frac{1}{T}\,\mathbf{Q}\cdot\mathrm{Grad}\; T \geq 0\,. \tag{49}$$

Eventually, the stress $\mathbf{M}^{\mathrm{m}}$ in Eq. (46) reads, see Appendix A,

$$\begin{aligned}
\mathbf{M}^{\mathrm{m}} = \; & v^{\mathrm{c}}\mathbf{F}^{\mathrm{fc}^{\mathrm{T}}}\cdot\mathbf{F}^{\mathrm{pc}^{\mathrm{T}}}\cdot\widetilde{\mathbf{M}}^{\mathrm{vec}}\cdot\mathbf{F}^{\mathrm{pc}^{-\mathrm{T}}}\cdot\mathbf{F}^{\mathrm{fc}^{-\mathrm{T}}} + v^{\mathrm{m}}\mathbf{F}^{\mathrm{fm}^{\mathrm{T}}}\cdot\mathbf{F}^{\mathrm{pm}^{\mathrm{T}}}\cdot\widetilde{\mathbf{M}}^{\mathrm{vem}}\cdot\mathbf{F}^{\mathrm{pm}^{-\mathrm{T}}}\cdot\mathbf{F}^{\mathrm{fm}^{-\mathrm{T}}} + \\
& v^{\mathrm{a}}\left(\mathbf{F}^{\mathrm{pa}^{\mathrm{T}}}\cdot\widetilde{\mathbf{M}}^{\mathrm{vea}}\cdot\mathbf{F}^{\mathrm{pa}^{-\mathrm{T}}}\right)\,.
\end{aligned} \tag{50}$$

Considering that Eq. (46) must hold for any arbitrary variations of strain and temperature, the (visco)elastic second Piola-Kirchhoff stress tensors are defined in the relaxed

configuration by[4]:

$$\widetilde{\mathbf{S}}^{\mathrm{vei}} = 2\frac{\partial\widetilde{\Psi}^{\mathrm{vei}}}{\partial\mathbf{C}^{\mathrm{vei}}} \qquad i = \mathrm{c},\ \mathrm{m},\ \mathrm{a}\,. \tag{51}$$

From the expressions (51), assuming that the (visco)elastic second Piola-Kirchhoff stress tensors $\widetilde{\mathbf{S}}^{\mathrm{vei}}$, $i = \mathrm{c}, \mathrm{m}, \mathrm{a}$, permute with their respective Cauchy strain tensors, then the (visco)elastic stresses $\widetilde{\mathbf{M}}^{\mathrm{vei}}$, $i = \mathrm{c}, \mathrm{m}, \mathrm{a}$, defined in Eqs. (44) are the symmetric (visco)elastic Mandel stress tensors. As it will be further discusssed, in case of no viscous contribution, if the energy functions $\widetilde{\Psi}^{\mathrm{vei}}$, $i = \mathrm{c}, \mathrm{m}, \mathrm{a}$, are defined as functions of the eigenvalues of their respective Cauchy strain tensors $\mathbf{C}^{\mathrm{vei}}$, $i = \mathrm{c}, \mathrm{m}, \mathrm{a}$, the permutation is ensured; in case of viscous contribution, we will postulate this assumption.

Considering arbitrary variations of strain and temperature in Eq. (46), the total entropy, η, is defined as

$$\begin{aligned}\eta = &-\left[\frac{\partial\Psi^{\mathrm{th}}}{\partial T} + \frac{\partial\Psi^{\mathrm{th}}}{\partial z^{\mathrm{c}}}\frac{\partial z^{\mathrm{c}}}{\partial T}\right] - \left[(1-v^{\mathrm{a}})\left(\widetilde{\Psi}^{\mathrm{vec}} + \widetilde{\Psi}^{\mathrm{pc}}\right) - (1-v^{\mathrm{a}})\left(\widetilde{\Psi}^{\mathrm{vem}} + \widetilde{\Psi}^{\mathrm{pm}}\right)\right]\frac{\partial z^{\mathrm{c}}}{\partial T} + \\ &\mathbf{M}^{\mathrm{m}} : \left(\left.\frac{\partial\mathbf{F}^{\mathrm{th}}}{\partial T}\right|_{\mathbf{C}^{\mathrm{vem}}} \cdot \mathbf{F}^{\mathrm{th}^{-1}}\right) - \left[v^{\mathrm{c}}\frac{\partial\widetilde{\Psi}^{\mathrm{vec}}}{\partial T} + v^{\mathrm{m}}\frac{\partial\widetilde{\Psi}^{\mathrm{vem}}}{\partial T} + v^{\mathrm{a}}\frac{\partial\widetilde{\Psi}^{\mathrm{vea}}}{\partial T}\right].\end{aligned} \tag{52}$$

In Eq. (46), the terms $\mathbf{M}^{\mathrm{m}} : \left(\left.\frac{\partial\mathbf{F}^{\mathrm{th}}}{\partial T}\right|_{\mathbf{C}^{\mathrm{vem}}} \cdot \mathbf{F}^{\mathrm{th}^{-1}}\right)\dot{T}$ and $-\left[v^{\mathrm{c}}\frac{\partial\widetilde{\Psi}^{\mathrm{c}}}{\partial T} + v^{\mathrm{m}}\frac{\partial\widetilde{\Psi}^{\mathrm{m}}}{\partial T} + v^{\mathrm{a}}\frac{\partial\widetilde{\Psi}^{\mathrm{a}}}{\partial T}\right]\dot{T}$, and hence the corresponding terms in Eq. (52), are responsible for the thermo-elastic damping and are neglected in this work. The term

$$\left[(1-v^{\mathrm{a}})\left(\widetilde{\Psi}^{\mathrm{vec}} + \widetilde{\Psi}^{\mathrm{pc}}\right) - (1-v^{\mathrm{a}})\left(\widetilde{\Psi}^{\mathrm{vem}} + \widetilde{\Psi}^{\mathrm{pm}}\right)\right]\frac{\partial z^{\mathrm{c}}}{\partial T}\dot{T}$$

corresponds to the elastic energy which is stored in a phase and lost upon phase transition. It is assumed that this contribution is small compared to the latent energy and is therefore neglected. Eventually, the entropy is defined as:

$$\eta = -\left[\frac{\partial\Psi^{\mathrm{th}}}{\partial T} + \frac{\partial\Psi^{\mathrm{th}}}{\partial z^{\mathrm{c}}}\frac{\partial z^{\mathrm{c}}}{\partial T}\right]. \tag{53}$$

3.3. First law of thermodynamics

The balance of energy equation can be given as:

$$\dot{e} = \mathbf{P} : \dot{\mathbf{F}} + Q_{\mathrm{m}} - \mathrm{Div}\,\mathbf{Q}\,, \tag{54}$$

---

[4] The second Piola-Kirchhoff stress tensor in the reference configuration reads $\tilde{\mathbf{S}}^{i} = 2\frac{\partial\widetilde{\Psi}^{\mathrm{vei}}}{\partial\mathbf{C}} = 2\frac{\partial\widetilde{\Psi}^{\mathrm{vei}}}{\partial\mathbf{C}^{\mathrm{vei}}} : \frac{\partial\mathbf{C}^{\mathrm{vei}}}{\partial\mathbf{C}} = \tilde{\mathbf{S}}^{\mathrm{vei}} : \frac{\partial\mathbf{C}^{\mathrm{vei}}}{\partial\mathbf{C}}$. Using the relations (12-15), this last relation becomes

$$\tilde{\mathbf{S}}^{i} \quad = \quad \mathbf{F}^{\mathrm{th}^{-1}}\left(\cdot\mathbf{F}^{fi^{-1}}\right)\cdot\mathbf{F}^{\mathrm{p}i^{-1}}\cdot\tilde{\mathbf{S}}^{\mathrm{vei}}\cdot\mathbf{F}^{\mathrm{p}i^{-T}}\cdot\left(\mathbf{F}^{fi^{-T}}\cdot\right)\mathbf{F}^{\mathrm{th}^{-T}}\,,$$

while expressing the first Piola-Kirchhoff stress tensors following $\tilde{\mathbf{P}}^{i} = \mathbf{F}\cdot\tilde{\mathbf{S}}^{i}$ allows recovering Eqs. (41-43).

where Q_{m} is the internal sources of heat generation per unit reference volume, $\mathrm{Div}(\bullet)(=\boldsymbol{\nabla}_0 \cdot (\bullet))$ is the divergence operator in the reference configuration, and e is the internal energy per unit mass:

$$e = \Psi + \eta T \,. \tag{55}$$

Then, $\dot{e}$ can be obtained:

$$\dot{e} = \dot{\Psi} + \dot{\eta} T + \eta \dot{T} \,. \tag{56}$$

By considering the local dissipation in Eq. (45) and using Eq. (56) in Eq. (54), the energy balance can be rewritten as:

$$\dot{\eta} T = \mathfrak{D}_{\mathrm{loc}} + Q_{\mathrm{m}} - \mathrm{Div}\, \mathbf{Q} \,. \tag{57}$$

We consider the thermal energy

$$\Psi^{\mathrm{th}} = \begin{cases} \left[v^{\mathrm{a}} c_p^{\mathrm{a}} + (1 - v^{\mathrm{a}})\, c_p^{\mathrm{c}}\right] \left[(T - T_0) - T \ln\left(\frac{T}{T_0}\right)\right] & \text{if fully crystallized} \;; \\ -C_1 (T - T_0) + C_3 + & \\ \rho_0 \,(1 - v^{\mathrm{a}})\, \Delta H^{\text{g-r}} \int_{T_0}^{T} \int_{T_0}^{T'} \frac{f\left(T'', |\mathbf{E}^{\mathrm{vem}}|\right)}{T''} dT'' dT' & \text{during the phase transition} \;; \\ -C_2 (T - T_0) + C_4 + & \\ \left[v^{\mathrm{a}} c_p^{\mathrm{a}} + (1 - v^{\mathrm{a}})\, c_p^{\mathrm{m}}\right] \left[(T - T_0) - T \ln\left(\frac{T}{T_0}\right)\right] & \text{if fully melted} \;; \end{cases} \tag{58}$$

where the crystallization rate function $f\,(T, |\mathbf{E}^{\mathrm{vem}}|)$ is approximated with the Gaussian probability density function (18), $\Delta H^{\text{g-r}} < 0$ is the latent heat of the crystallized to melted phase transformation in the crystalline phase per unit reference mass, $T_0 = \frac{T_{\mathrm{c}} + T_{\mathrm{m}}}{2}$ is the reference change of phase temperature, C_1 and C_2 are reference entropies, C_3 and C_4 are reference energies, and

$$c_p = -T \frac{\partial^2 \Psi^{\mathrm{th}}}{\partial T^2} = \begin{cases} \left[v^{\mathrm{a}} c_p^{\mathrm{a}} + (1 - v^{\mathrm{a}})\, c_p^{\mathrm{c}}\right] & \text{if fully crystallized} \,, \\ \left[v^{\mathrm{a}} c_p^{\mathrm{a}} + (1 - v^{\mathrm{a}})\, c_p^{\mathrm{m}}\right] & \text{if fully melted} \,, \end{cases} \tag{59}$$

is the heat capacity per unit reference volume. From Eq. (53), η can be written as:

$$\eta = -\frac{\partial \Psi^{\mathrm{th}}}{\partial T} = \begin{cases} \left[v^{\mathrm{a}} c_p^{\mathrm{a}} + (1 - v^{\mathrm{a}})\, c_p^{\mathrm{c}}\right] \ln\left(\frac{T}{T_0}\right) & \text{if fully crystallized} \;; \\ C_1 - \rho_0 \,(1 - v^{\mathrm{a}})\, \Delta H^{\text{g-r}} \int_{T_0}^{T} \frac{f\left(T', |\mathbf{E}^{\mathrm{vem}}|\right)}{T'} dT' & \text{during phase transition} \;; \\ C_2 + \left[v^{\mathrm{a}} c_p^{\mathrm{a}} + (1 - v^{\mathrm{a}})\, c_p^{\mathrm{m}}\right] \ln\left(\frac{T}{T_0}\right) & \text{if fully melted} \,; \end{cases} \tag{60}$$

From Eq. (60), $\dot{\eta} T$ can be written as:

$$\dot{\eta} = \frac{\partial \eta}{\partial T} \dot{T} = \begin{cases} \left[v^{\mathrm{a}} c_p^{\mathrm{a}} + (1 - v^{\mathrm{a}})\, c_p^{\mathrm{c}}\right] \frac{\dot{T}}{T} & \text{if fully crystallized} \,; \\ -\rho_0 \,(1 - v^{\mathrm{a}})\, \Delta H^{\text{g-r}} \frac{f(T, |\mathbf{E}^{\mathrm{vem}}|)}{T} \dot{T} & \text{during phase transition} \;; \\ \left[v^{\mathrm{a}} c_p^{\mathrm{a}} + (1 - v^{\mathrm{a}})\, c_p^{\mathrm{c}}\right] \frac{\dot{T}}{T} & \text{if fully melted} \,. \end{cases} \tag{61}$$

Therefore, using Eq. (17), the balance of energy equation, Eq. (57), can be obtained as:

$$\text{Div}\,\mathbf{Q} = -c_p\dot{T} - (1-v^{\text{a}})\,\rho_0\Delta H^{\text{g-r}}\dot{z}^{\text{c}} + \mathfrak{D}_{\text{loc}} + Q_{\text{m}}\,. \tag{62}$$

4. Constitutive Equations

4.1. Viscoelastic-plastic branches

4.1.1. Viscoelasticity

For each viscoelastic branch in Fig. 3, the generalized Maxwell model is considered with $N+1$ springs and N dashpots. The energy of a phase consists of elastic and dissipation potentials (Nguyen et al., 2016):

$$\begin{aligned}\widetilde{\Psi}^{\text{vei}}(\mathbf{E}^{\text{vei}},\,T;\widetilde{\mathbf{q}}^i_1...\widetilde{\mathbf{q}}^i_N,\,T^i_{\text{Ref}}) =& \widetilde{\Psi}^{\text{vei}}_{\infty}(\mathbf{E}^{\text{vei}},\,T;\,T^i_{\text{Ref}}) + \\ &\sum_{j=1}^{N}\left[\widetilde{\Psi}^{\text{vei}}_j(\mathbf{E}^{\text{vei}}) + \widetilde{\Upsilon}^i_j(\mathbf{E}^{\text{vei}},\widetilde{\mathbf{q}}^i_j)\right]\,,\quad i=\text{c},\text{m},\text{a}\,;\end{aligned} \tag{63}$$

where $\widetilde{\Psi}^{\text{vei}}_{\infty}$ is the energy in the relaxed condition, which is the energy of the spring ∞, the dependency of $\widetilde{\Psi}^{\text{vei}}_{\infty}$ on the temperature difference with respect to the phases reference temperature T^i_{Ref} is responsible for the anisotropic thermal deformations due to the mismatch of the phases, $\widetilde{\Psi}^{\text{vei}}_j$ is the elastic potential of the other springs, and $\widetilde{\Upsilon}^i_j$ is the dissipating potential of the dashpots. These potentials are expressed in terms of the viscoelastic logarithmic strain tensor, $\mathbf{E}^{\text{vei}} = \frac{1}{2}\ln\left(\mathbf{F}^{\text{vei}^T}\cdot\mathbf{F}^{\text{vei}}\right)$, and in terms of $\widetilde{\mathbf{q}}^i_j$, the internal variables governing the viscoelastic process.

The following bi-logarithmic potentials are considered for the elastic springs[5]:

$$\widetilde{\Psi}^{\text{vei}}_j(\mathbf{E}^{\text{vei}}) = \frac{K^i_j}{2}\left[\text{tr}\,\mathbf{E}^{\text{vei}}\right]^2 + G^i_j\text{dev}\,\mathbf{E}^{\text{vei}} : \text{dev}\,\mathbf{E}^{\text{vei}}\,,\quad i=\text{c},\text{m},\text{a}\,,\quad j=1..N\,;\ \text{and} \tag{64}$$

$$\begin{aligned}\widetilde{\Psi}^{\text{vei}}_{\infty}(\mathbf{E}^{\text{vei}}) =& \int_0^{\text{tr}\,\mathbf{E}^{\text{vei}}} K^i_{\infty}\left(\text{tr}\,\mathbf{E}^{\text{vei}'},\,T;\,T^i_{\text{Ref}}\right)\text{tr}\,\mathbf{E}^{\text{vei}'}\,d\,\text{tr}\,\mathbf{E}^{\text{vei}'} + \\ &\int_0^{\text{dev}\ \mathbf{E}^{\text{vei}}} 2G^i_{\infty}\left(\left|\mathbf{E}^{\text{vei}'}\right|,\,T;\,T^i_{\text{Ref}}\right)\text{dev}\,\mathbf{E}^{\text{vei}'} : d\,\text{dev}\,\mathbf{E}^{\text{vei}'}\,,\quad i=\text{c},\text{m},\text{a}\,,\end{aligned} \tag{65}$$

where $\text{tr}(\bullet)$ is the trace operator, $\text{dev}(\bullet)$ is the deviatoric operator, K^i_j and G^i_j for $j=1..N$ are the bulk and shear moduli, respectively, of the viscoelastic branches, and $K^i_{\infty}\left(\text{tr}\,\mathbf{E}^{\text{vei}},\,T;\,T^i_{\text{Ref}}\right)$ and $G^i_{\infty}\left(\left|\mathbf{E}^{\text{vei}}\right|,\,T;\,T^i_{\text{Ref}}\right)$ are non-linear bulk and shear moduli, respectively, of the elastic branch. The non-linearity is introduced since the polymer exhibits a hyper-elastic response, which cannot be captured by considering a bi-logarithmic potential with constant material moduli. Indeed, when the polymeric sample is under tension, the logarithmic strain tensor is increasing less than required with the engineering

[5] We note the algebraic identity $\ln(\det\mathbf{A}) = \text{tr}(\ln\mathbf{A})$, where $\mathbf{A}$ is a symmetric second-order tensor.

strain to be able to capture the polymer stress response with constant material moduli. We thus need to introduce a stiffening effect with the strain measure in the material response. These non-linear expressions for K^i_∞ and G^i_∞ write:

$$K^i_\infty = \hat{K}^i_\infty\left(T;T^i_{\text{Ref}}\right)\left(1+\underbrace{V^i_K\left[\tanh\left(\frac{\vartheta^i_K}{3}\left(\text{tr }\mathbf{E}^{\text{ve}i}\right)^2-\zeta^i_K\right)+\tanh\left(\zeta^i_K\right)\right]}_{f^i_K(\text{tr }\mathbf{E}^{\text{ve}i})}\right), \text{ and} \tag{66}$$

$$G^i_\infty = \hat{G}^i_\infty\left(T;T^i_{\text{Ref}}\right)\left(1+\underbrace{V^i_G\left[\tanh\left(\vartheta^i_G\text{dev }\mathbf{E}^{\text{ve}i}:\text{dev }\mathbf{E}^{\text{ve}i}-\zeta^i_G\right)+\tanh\left(\zeta^i_G\right)\right]}_{f^i_G(\text{dev }\mathbf{E}^{\text{ve}i})}\right), \tag{67}$$

where V^i_K, ϑ^i_K and ζ^i_K, respectively V^i_G, ϑ^i_G and ζ^i_G, are material parameters that control the stiffening in the bulk, respectively shear, behavior of branch $i=$ c, m, a. This elastic hardening of the polymer at high deformations was also observed by Srivastava et al. (2010).

The anisotropic thermal deformation is captured by the temperature dependency of the elastic moduli

$$\hat{K}^i_\infty\left(T;T^i_{\text{Ref}}\right) = \bar{K}^i_\infty\left[1+A_{f^{\text{ve}i}_K}\tanh\left(\alpha_{f^{\text{ve}i}_K}\left(T-T^{\text{i}}_{\text{Ref}}\right)\right)\right], \text{ and} \tag{68}$$

$$\hat{G}^i_\infty\left(T;T^i_{\text{Ref}}\right) = \bar{G}^i_\infty\left[1+A_{f^{\text{ve}i}_G}\tanh\left(\alpha_{f^{\text{ve}i}_G}\left(T-T^{\text{i}}_{\text{Ref}}\right)\right)\right], \tag{69}$$

where $A_{f^{\text{ve}i}_K}$, $\alpha_{f^{\text{ve}i}_K}$, respectively $A_{f^{\text{ve}i}_G}$, $\alpha_{f^{\text{ve}i}_G}$, control the temperature difference effects on the negative and isotropic, respectively anisotropic, expansion coefficient.

A quadratic dissipating potential is considered for the dashpots as in the work by Nguyen et al. (2016):

$$\widetilde{\Upsilon}^i_j(\mathbf{E}^{\text{ve}i},\widetilde{\mathbf{q}}^i_j) = -\widetilde{\mathbf{q}}^i_j:\mathbf{E}^{\text{ve}i}+\frac{1}{18K^i_j}(\text{tr }\widetilde{\mathbf{q}}^i_j)^2+\frac{1}{4G^i_j}\text{dev }\widetilde{\mathbf{q}}^i_j:\text{dev }\widetilde{\mathbf{q}}^i_j\,,\ i=\text{c, m, a},\ j=1..N\,. \tag{70}$$

In the remaining of this section, $i=\text{c},\text{m},\text{a}$ and $j=1..N$ will be assumed in the equations, unless otherwise specified.

The viscoelastic behavior is considered in both deviatoric and volumetric deformations and the evolution of $\widetilde{\mathbf{q}}^i_j$ is characterized by a retardation action as (Simo, 1987; Nguyen et al., 2016):

$$\text{dev }\dot{\widetilde{\mathbf{q}}}^i_j = \frac{2G^i_j}{g^i_j}\text{dev }\mathbf{E}^{\text{ve}i}-\frac{1}{g^i_j}\text{dev }\widetilde{\mathbf{q}}^i_j\,; \tag{71}$$

$$\text{tr }\dot{\widetilde{\mathbf{q}}}^i_j = \frac{3K^i_j}{k^i_j}\text{tr }\mathbf{E}^{\text{ve}i}-\frac{1}{k^i_j}\text{tr }\widetilde{\mathbf{q}}^i_j\,; \tag{72}$$

where g_j^i and k_j^i are the characteristic relaxation times for the deviatoric and volumetric parts, respectively. The current values can be given in the form of the convolution integrals by the integration of the above rate equations up to the current time:

$$\text{dev}\ \widetilde{\mathbf{q}}_j^i = \frac{2G_j^i}{g_j^i}\int_{-\infty}^{t} \exp\left(-\frac{t-s}{g_j^i}\right) \text{dev}\ \mathbf{E}^{\text{vei}}(s)ds\,; \tag{73}$$

$$\widetilde{p}_{\text{q}j}^i = \frac{1}{3}\text{tr}\ \widetilde{\mathbf{q}}_j^i = \frac{K_j^i}{k_j^i}\int_{-\infty}^{t} \exp\left(-\frac{t-s}{k_j^i}\right) \text{tr}\ \mathbf{E}^{\text{vei}}(s)ds\,; \tag{74}$$

with $\widetilde{\mathbf{q}}_j^i$ given as:

$$\widetilde{\mathbf{q}}_j^i = \text{dev}\ \widetilde{\mathbf{q}}_j^i + \widetilde{p}_{\text{q}j}^i\,\mathbf{I}\,. \tag{75}$$

The stress tensor $\widetilde{\mathbf{S}}^{\text{vei}}$ defined following Eq. (51) can further be expanded as:

$$\widetilde{\mathbf{S}}^{\text{vei}} = \widetilde{\boldsymbol{\tau}}^{\text{vei}} : \boldsymbol{\mathcal{L}}^{\text{vei}}\,; \tag{76}$$

where:

$$\widetilde{\boldsymbol{\tau}}^{\text{vei}} = \rho_0 \frac{\partial \widetilde{\Psi}^{\text{vei}}}{\partial \mathbf{E}^{\text{vei}}}\,; \quad \text{and} \quad \boldsymbol{\mathcal{L}}^{\text{vei}} = 2\,\frac{\partial \mathbf{E}^{\text{vei}}}{\partial \mathbf{C}^{\text{vei}}} = \frac{\partial \ln \mathbf{C}^{\text{vei}}}{\partial \mathbf{C}^{\text{vei}}}\,; \tag{77}$$

where the co-rotational Kirchoff stress $\widetilde{\boldsymbol{\tau}}^{\text{vei}}$ is defined as the work conjugate of $\mathbf{E}^{\text{vei}}$, $\boldsymbol{\mathcal{L}}^{\text{vei}} = \boldsymbol{\mathcal{I}}^2 \cdot \mathbf{C}^{\text{vei}^{-1}}$ with $\boldsymbol{\mathcal{I}}$ the 4th order identity tensor and the symbol ${}^2\cdot$ refers to a single contraction on its second index, and assuming $\mathbf{C}^{\text{vei}^{-1}}$ permutes with $\widetilde{\boldsymbol{\tau}}^{\text{vei}}$, $\widetilde{\boldsymbol{\tau}}^{\text{vei}}$ corresponds to the Mandel stress (44).

Then, by using Eq. (63), the deviatoric and volumetric parts of $\widetilde{\boldsymbol{\tau}}^{\text{vei}}$ can be written in the form of convolution integrals as:

$$\text{dev}\ \widetilde{\boldsymbol{\tau}}^{\text{vei}}(t) = 2G_\infty^i\ \text{dev}\ \mathbf{E}^{\text{vei}}(t) + \int_{-\infty}^{t} 2G^i(t-s)\frac{d}{ds}\text{dev}\ \mathbf{E}^{\text{vei}}(s)ds\,; \tag{78}$$

$$\widetilde{p}^{\text{vei}}(t) = \frac{1}{3}\text{tr}\ \widetilde{\boldsymbol{\tau}}^{\text{vei}}(t) = K_\infty^i \text{tr}\ \mathbf{E}^{\text{vei}}(t) + \int_{-\infty}^{t} K^i(t-s)\frac{d}{ds}\text{tr}\ \mathbf{E}^{\text{vei}}(s)ds\,; \tag{79}$$

where $\widetilde{p}^{\text{vei}}$ is the pressure and:

$$G^i(t) = \sum_{j=1}^{N} G_j^i \exp\left(-\frac{t}{g_j^i}\right)\ ; \text{ and} \tag{80}$$

$$K^i(t) = \sum_{j=1}^{N} K_j^i \exp\left(-\frac{t}{k_j^i}\right)\ . \tag{81}$$

Finally, $\widetilde{\boldsymbol{\tau}}^{\text{vei}}$ of each phase in Eq. (77) is given as:

$$\widetilde{\boldsymbol{\tau}}^{\text{vei}} = \text{dev}\left(\widetilde{\boldsymbol{\tau}}^{\text{vei}}\right) + \widetilde{p}^{\text{vei}}\mathbf{I}\,. \tag{82}$$

We note that following Eq. (78), because of the integral terms, it cannot be demonstrated that $\widetilde{\boldsymbol{\tau}}^{\mathrm{vei}}$ permutes with either $\mathbf{E}^{\mathrm{vei}}$ or $\mathbf{E}^{\mathrm{vei}}$ in the general elasto-plastic case. This results from the fact that the terms are defined in the relaxed configuration which might change with the plastic flow. As a result, as explained in Section 3.2, the (visco)elastic stresses $\widetilde{\mathbf{M}}^{\mathrm{vei}}$, i = c, m, a, defined in Eqs. (44), are not formally the symmetric (visco)elastic Mandel stress tensors when viscous terms and plastic flows are involved; we however make the assumption that they are.

In this model, the material parameters dependency on the temperature is only accounted for in Eqs. (68-69) in order to capture the negative and anisotropic thermal expansion. Although the polymer viscoelastic response depends on the temperature, in particular for the amorphous branch, in this study, the temperature variation is restricted in a range around the transition temperature. In that case, below the crystallization temperature, the material response is mainly governed by the crystallized phase, while above the melting temperature it is governed by both the melted and amorphous phases, whose parameters will thus have to be identified altogether. Besides, the parameters of the amorphous branch also have to be selected in order to capture the two-way shape memory effect as well as the imperfect shape fixity/recovery. The studied temperature ranges considered in this paper above the melting temperature and below the crystallization temperature are too small in order to identify the parameters dependency on the temperature, which is the reason why we do not introduce it, but this is not a limitation of the model.

4.1.2. Plasticity

The viscoelastic region is limited by a pressure-sensitive yield function F expressed in terms of the corotational Kirchhoff stress $\widetilde{\boldsymbol{\tau}}^{\mathrm{vei}}$ and the back-stress $\widetilde{\mathbf{b}}^{i}$, allowing to define the combined stress tensor $\widetilde{\boldsymbol{\phi}}^{i}$

$$\widetilde{\boldsymbol{\phi}}^{i} = \widetilde{\boldsymbol{\tau}}^{\mathrm{vei}} - \widetilde{\mathbf{b}}^{i}\,, \tag{83}$$

and the yield surface $F^{i}\left(\widetilde{\boldsymbol{\phi}}^{i}\right)$, as

$$F^{i}\left(\widetilde{\boldsymbol{\phi}}^{i}\right) = a_2^{i}\left(\widetilde{\phi}_{\mathrm{e}}^{i}\right)^{\alpha^{i}} - a_1^{i}\widetilde{\phi}_{\mathrm{v}}^{i} - a_0^{i} \leq 0\,, \tag{84}$$

with the combined pressure and equivalent terms

$$\widetilde{\phi}_{\mathrm{v}}^{i} = \frac{1}{3}\mathrm{tr}\,\widetilde{\boldsymbol{\phi}}^{i} = \widetilde{p}^{\mathrm{vei}} - \frac{1}{3}\mathrm{tr}\,\widetilde{\mathbf{b}}^{i}\,,\ \text{and}\ \tilde{\phi}_{\mathrm{e}}^{i} = \sqrt{\frac{3}{2}\mathrm{dev}\left(\widetilde{\boldsymbol{\phi}}^{i}\right) : \mathrm{dev}\left(\widetilde{\boldsymbol{\phi}}^{i}\right)}\,, \tag{85}$$

where $\widetilde{p}^{\mathrm{vei}}$ is given in Eq. (79), and the material parameter α^{i} enhances the Drucker-Prager pressure-dependency description of branch i.

The coefficients a_0^{i}, a_1^{i} and a_2^{i} introduced in the yield surface (84) are functions of the equivalent plastic strain γ^{i} of branch i through the isotropic hardening description of the yield surface. Considering successively uni-axial compressive and tensile loading conditions, at the onset of plastic flow, one has

$$\begin{cases} a_2^{i}(\sigma_{\mathrm{c}}^{i})^{\alpha^{i}} - a_1^{i}\frac{-\sigma_{\mathrm{c}}^{i}}{3} - a_0^{i} = 0 \\ a_2^{i}(\sigma_{\mathrm{t}}^{i})^{\alpha^{i}} - a_1^{i}\frac{\sigma_{\mathrm{t}}^{i}}{3} - a_0^{i} = 0 \end{cases} \tag{86}$$

where σ_{c}^i and σ_{t}^i are the immediate compressive and tensile yield stress, respectively. Therefore, the coefficients a_0^i, a_1^i and a_2^i are expressed in terms of the yield stresses σ_{c}^i and σ_{t}^i as

$$a_2^i = \frac{1}{\left(\sigma_{\mathrm{c}}^i\right)^{\alpha^i}}\,, \quad a_1^i = 3\frac{\left(\sigma_{\mathrm{t}}^i\right)^{\alpha^i} - \left(\sigma_{\mathrm{c}}^i\right)^{\alpha^i}}{\sigma_{\mathrm{t}}^i + \sigma_{\mathrm{c}}^i} a_2^i\,, \text{ and } \; a_0^i = \frac{\left(\sigma_{\mathrm{t}}^i\right)^{\alpha^i} \sigma_{\mathrm{c}}^i + \left(\sigma_{\mathrm{c}}\right)^{\alpha^i} \sigma_{\mathrm{t}}^i}{\sigma_{\mathrm{t}}^i + \sigma_{\mathrm{c}}^i} a_2^i\,, \tag{87}$$

or, by introducing a tension-compression flow asymmetry parameter $m^i = \frac{\sigma_{\mathrm{t}}^i}{\sigma_{\mathrm{c}}^i}$,

$$a_2^i = \frac{1}{\left(\sigma_{\mathrm{c}}^i\right)^{\alpha^i}},\; a_1^i = 3\frac{\left(m^i\right)^{\alpha^i} - 1}{m^i + 1}\frac{1}{\sigma_{\mathrm{c}}^i} \text{ and } \; a_0^i = \frac{\left(m^i\right)^{\alpha^i} + m^i}{m^i + 1}\,. \tag{88}$$

Considering a non-associated flow rule, with a quadratic function used as the plastic flow potential as suggested by Nguyen et al. (2016), the latter reads

$$P^i = \left(\widetilde{\phi}_{\mathrm{e}}^i\right)^2 + \beta^i \left(\widetilde{\phi}_{\mathrm{v}}^i\right)^2\,, \tag{89}$$

where β^i is a material parameter governing the volumetric plastic deformation, e.g. $\beta^i = 0$ indicates a zero volumetric plastic deformation. The plastic velocity gradient defined in Eqs. (9) and (10):

$$\mathbf{D}^{\mathrm{p}i} = \dot{\mathbf{F}}^{\mathrm{p}i}\,\mathbf{F}^{\mathrm{p}i^{-1}} = \dot{\Gamma}^i\,\mathbf{N}^i\,, \tag{90}$$

where $\dot{\Gamma}^i$ is the plastic multiplier and where

$$\mathbf{N}^i = \frac{\partial P^i}{\partial \widetilde{\boldsymbol{\tau}}^{\mathrm{ve}i}} = 3\;\mathrm{dev}\;\widetilde{\boldsymbol{\phi}}^i + \frac{2\beta^i}{3}\widetilde{\phi}_{\mathrm{v}}^i\mathbf{I}\,, \tag{91}$$

is the normal to the plastic flow. The equivalent plastic strain rate $\dot{\gamma}^i$ is then defined from the plastic strain rate tensor following

$$\dot{\gamma}^i = k^i\sqrt{\mathbf{D}^{\mathrm{p}i} : \mathbf{D}^{\mathrm{p}i}}\,, \tag{92}$$

where

$$k^i = \frac{1}{\sqrt{1 + 2\left(\nu_{\mathrm{p}}^i\right)^2}}\,, \tag{93}$$

with ν_{p}^i being the plastic Poisson's ratio. This plastic Poisson's ratio is assumed to be constant and is related to β^i at the plastic flow onset (Melro et al., 2013) by

$$\nu_{\mathrm{p}}^i = \frac{9 - 2\beta^i}{18 + 2\beta^i}\,. \tag{94}$$

Finally, the Kuhn-Tucker condition for the evolution of the plastic flow is written as:

$$\dot{\gamma}^i F^i\left(\widetilde{\boldsymbol{\phi}}^i\right) = 0, \quad \dot{\gamma}^i \geqslant 0, \quad F^i\left(\widetilde{\boldsymbol{\phi}}^i\right) \leqslant 0\,. \tag{95}$$

The isotropic hardening functions define distinctive tensile and compressive yield stress evolutions following

$$\begin{aligned}\sigma_{\mathrm{t}}^{i}\left(\gamma^{i}\right) &= h^{i}\left(z^{\mathrm{c}}\right)\left[\sigma_{\mathrm{t}}^{0i}+\int H_{\mathrm{t}}^{i}\left(\gamma^{i}\right)d\gamma^{i}\right],\\ \sigma_{\mathrm{c}}^{i}\left(\gamma^{i}\right) &= h^{i}\left(z^{\mathrm{c}}\right)\left[\sigma_{\mathrm{c}}^{0i}+\int H_{\mathrm{c}}^{i}\left(\gamma^{i}\right)d\gamma^{i}\right],\end{aligned} \tag{96}$$

where σ_{t}^{0i} and σ_{c}^{0i} are the initial tensile and compressive yield stresses, respectively. For simplicity, in this work we keep the hardening moduli H_{t}^{i} and H_{c}^{i} constant. The function $h^{i}\left(v^{i}\right)$ is introduced in Eq. (96) in order to capture the two-way shape memory effect by allowing the amorphous phase to act as a spring during the phase transition, which is achieved by allowing for plastic flow during the early stage of the crystallization. To this end, we decrease the initial yield stress, $\sigma_{\mathrm{t}}^{0\mathrm{c}}$ or $\sigma_{\mathrm{c}}^{0\mathrm{c}}$, of the crystallized phase during the early stage of crystallization, yielding

$$\begin{aligned}h^{\mathrm{c}}\left(z^{\mathrm{c}}\right) &= \begin{cases} h_{0}^{\mathrm{c}} & \text{if } z^{\mathrm{c}} \leq z_{0}^{\mathrm{c}} \\ h_{0}^{\mathrm{c}}+\left(1-h_{0}^{\mathrm{c}}\right)\frac{z^{\mathrm{c}}-z_{0}^{\mathrm{c}}}{1-z_{0}^{\mathrm{c}}} & \text{if } z^{\mathrm{c}} > z_{0}^{\mathrm{c}} \end{cases},\\ h^{\mathrm{m}}\left(z^{\mathrm{c}}\right)=h^{\mathrm{c}}\left(z^{\mathrm{c}}\right) &= 1\,.\end{aligned} \tag{97}$$

The kinematic hardening law reads:

$$\overset{\sim}{\dot{\mathbf{b}}}^{i}=kH_{\mathrm{k}}^{i}\left(\gamma^{i}\right)\mathbf{D}^{\mathrm{p}i},\ \text{with}\ \overset{\sim}{\mathbf{b}}^{i}\left(\gamma^{i}=0\right)=0\,, \tag{98}$$

or using Eq. (92) as

$$\sqrt{\overset{\sim}{\dot{\mathbf{b}}}^{i}:\overset{\sim}{\dot{\mathbf{b}}}^{i}}=H_{\mathrm{k}}^{i}\left(\gamma^{i}\right)\dot{\gamma}^{i}\,, \tag{99}$$

with the polynomial law

$$H_{\mathrm{k}}^{i}\left(\gamma^{i}\right)=\sum_{j=0}^{M_{k}}H_{\mathrm{k},j}^{i}\left(\gamma^{i}\right)^{j}\,. \tag{100}$$

4.2. Heat Equation

The balance of energy equation is given in Eq. (54), in which the different terms have to be specified.

The heat flux $\mathbf{Q}$ is calculated by the Fourier's law of heat conduction as:

$$\mathbf{Q}=-\mathbf{K}\cdot\boldsymbol{\nabla}_{0}T=-J\left(\mathbf{F}^{-1}\cdot\mathbf{k}\cdot\mathbf{F}^{-\mathrm{T}}\right)\cdot\boldsymbol{\nabla}_{0}T\,, \tag{101}$$

where $\mathbf{K}$ is the heat conductivity tensor in the reference configuration, $\mathbf{k}$ is the heat conductivity tensor in the current configuration that can be defined by the rule of mixtures as:

$$\mathbf{k}=v^{\mathrm{c}}\mathbf{k}^{\mathrm{c}}+v^{\mathrm{m}}\mathbf{k}^{\mathrm{m}}+v^{\mathrm{a}}\mathbf{k}^{\mathrm{a}}\,, \tag{102}$$

with $\mathbf{k}^{\mathrm{c}}$, $\mathbf{k}^{\mathrm{m}}$ and $\mathbf{k}^{\mathrm{a}}$ being the thermal conductivities of each phase, whose positive definite nature ensures satisfying Eq. (49). Similarly, the heat capacity per unit reference volume follows:

$$c_{p}=v^{\mathrm{c}}c_{p}^{\mathrm{c}}+v^{\mathrm{m}}c_{p}^{\mathrm{m}}+v^{\mathrm{a}}c_{p}^{\mathrm{a}}\,. \tag{103}$$

The local dissipation $\mathfrak{D}_{loc}$ detailed in Eq. (A.16), is also separated into a viscous part $\mathfrak{D}^{\rm ve}_{\rm loc} \geq 0$ and a plastic part $\mathfrak{D}^{\rm p}_{\rm loc} \geq 0$ following Eqs. (A.18-48). Assuming that $\mathbf{D}^{pi} = \mathbf{L}^{pi}$ and that $\widetilde{\boldsymbol{\tau}}^{\rm vei}$ and $\mathbf{C}^{\rm vei}$ permute –see discussion in Section 4.1.1– and using Eq. (90), Eq. (104) is rewritten:

$$\begin{aligned}\mathfrak{D}^{\rm p}_{\rm loc} &\simeq \beta_{\rm TQ}\left[v^{\rm c}\widetilde{\mathbf{M}}^{\rm vec} : \mathbf{L}^{\rm pc} + v^{\rm m}\widetilde{\mathbf{M}}^{\rm vem} : \mathbf{L}^{\rm pm} + v^{\rm a}\widetilde{\mathbf{M}}^{\rm vea} : \mathbf{L}^{\rm pa}\right] \\ &\simeq \beta_{\rm TQ}\left[v^{\rm c}\dot{\Gamma}^{\rm c}\,\widetilde{\boldsymbol{\tau}}^{\rm vec} : \mathbf{N}^{\rm c} + v^{\rm m}\dot{\Gamma}^{\rm m}\,\widetilde{\boldsymbol{\tau}}^{\rm vem} : \mathbf{N}^{\rm m} + v^{\rm a}\dot{\Gamma}^{\rm a}\,\widetilde{\boldsymbol{\tau}}^{\rm vea} : \mathbf{N}^{\rm a}\right] \geq 0\,. \end{aligned} \tag{104}$$

The term $\mathfrak{D}^{\rm ve}_{\rm loc}$ in Eq. (47) can be rewritten:

$$\mathfrak{D}^{\rm ve}_{\rm loc} = v^{\rm c}\widetilde{\mathfrak{D}}^{\rm vec}_{\rm loc} + v^{\rm m}\widetilde{\mathfrak{D}}^{\rm vem}_{\rm loc} + v^{\rm a}\widetilde{\mathfrak{D}}^{\rm vea}_{\rm loc} \geq 0\,, \tag{105}$$

where, using Eqs. (63) and (70), it comes:

$$\begin{aligned}\widetilde{\mathfrak{D}}^{\rm vei}_{\rm loc} &= -\sum_{j=1}^{N}\frac{\partial\left[\widetilde{\Upsilon}_j\left(\mathbf{E}^{\rm vei},\widetilde{\mathbf{q}}^i_j\right)\right]}{\partial\widetilde{\mathbf{q}}^i_j} : \dot{\widetilde{\mathbf{q}}}^i_j \\ &= \left[\mathbf{E}^{\rm vei} - \frac{1}{9K^i_j}(\mathrm{tr}\;\widetilde{\mathbf{q}}^i_j)\,\mathbf{I} - \frac{1}{2G^i_j}\mathrm{dev}\;\widetilde{\mathbf{q}}^i_j\right] : \dot{\widetilde{\mathbf{q}}}^i_j \qquad i = \mathrm{c},\mathrm{m},\mathrm{a}\,. \end{aligned} \tag{106}$$

4.3. Model Parameters Summary

Table 1: Constitutive model inputs and identified parameters for PCL76-4MAL/FUR 3%wtCNT following Section 6. No values are given for parameters not effective in the model.

property	**unit**	**c**	**m**	**a**	**ref. Eq.**
volume fraction	[-]	$z^{\rm c}\,v^{\rm a}$	$(1-z^{\rm c})v^{\rm a}$	$v^{\rm a} = 0.685$	(1, 2, 3)
bulk modulus	[MPa]	$\bar{K}^{\rm c}_\infty = 868.1$, $K^{\rm c}_1 = K^{\rm c}_2 = 10^{-6}$	$\bar{K}^{\rm m}_\infty = 6.74$, $K^{\rm m}_1 = K^{\rm m}_2 = 10^{-6}$	$\bar{K}^{\rm a}_\infty = 0.0694$, $K^{\rm a}_1 = K^{\rm a}_2 = 10^{-8}$	(64, 65, 70, 73)
bulk modulus stiffening	[-]	$V^{\rm c}_K = 0$, $\vartheta^{\rm c}_K$, $\zeta^{\rm c}_K$	$V^{\rm m}_K = 8$, $\vartheta^{\rm m}_K = 1$, $\zeta^{\rm m}_K = 1.65$	$V^{\rm a}_K = 2$, $\vartheta^{\rm a}_K = 1$, $\zeta^{\rm a}_K = 1.2$	(66)
shear modulus	[MPa]	$\bar{G}^{\rm c}_\infty = 496$, $G^{\rm c}_1 = 40$, $G^{\rm c}_2 = 50$	$\bar{G}^{\rm m}_\infty = 3.85$, $G^{\rm m}_1 = G^{\rm m}_2 = 0.2$	$\bar{G}^{\rm a}_\infty = 0.0397$, $G^{\rm a}_1 = G^{\rm a}_2 = 0.002$	(64, 65, 70, 74)
shear modulus stiffening	[-]	$V^{\rm c}_G = 0$, $\vartheta^{\rm c}_G$, $\zeta^{\rm c}_G$	$V^{\rm m}_G = 8$, $\vartheta^{\rm m}_G = 1$, $\zeta^{\rm m}_G = 1.65$	$V^{\rm a}_G = 2$, $\vartheta^{\rm a}_G = 1$, $\zeta^{\rm a}_G = 1.2$	(67)

bulk - shear relaxation times of viscous branches	[s]	$k_1^{\mathrm{c}} = g_1^{\mathrm{c}} = 15$, $k_2^{\mathrm{c}} = g_2^{\mathrm{c}} = 200$	$k_1^{\mathrm{m}} = g_1^{\mathrm{m}} = 15$, $k_2^{\mathrm{m}} = g_2^{\mathrm{m}} = 300$	$k_1^{\mathrm{a}} = g_1^{\mathrm{a}} = 15$, $k_2^{\mathrm{a}} = g_2^{\mathrm{a}} = 300$	(71, 72)
initial tensile yield limit	[MPa]	$\sigma_{\mathrm{t}}^{0\mathrm{c}} = 1000$	$\sigma_{\mathrm{t}}^{0\mathrm{m}} \to \infty$	$\sigma_{\mathrm{t}}^{0\mathrm{a}} \to \infty$	(96)
initial compressive yield limit	[MPa]	$\sigma_{\mathrm{c}}^{0\mathrm{c}} = 1200$	$\sigma_{\mathrm{c}}^{0\mathrm{m}} \to \infty$	$\sigma_{\mathrm{c}}^{0\mathrm{a}} \to \infty$	(96)
tensile hardening parameters	[MPa]	$H_{\mathrm{t}}^{\mathrm{c}} = 1$	$H_{\mathrm{t}}^{\mathrm{m}}$	$H_{\mathrm{t}}^{\mathrm{a}}$	(96)
compressive hardening parameters	[MPa]	$H_{\mathrm{c}}^{\mathrm{c}} = 1.2$	$H_{\mathrm{c}}^{\mathrm{m}}$	$H_{\mathrm{c}}^{\mathrm{a}}$	(96)
yield surface ratio	[-]	$z_0^{\mathrm{c}} = 0.25$, $h_0^{\mathrm{c}} = 0.0001$	z_0^{m}, h_0^{m}	z_0^{a}, h_0^{a}	(97)
kinematic hardening parameters	[MPa]	$H_{\mathrm{k},5}^{\mathrm{c}} = 75000$	$H_{\mathrm{k},j}^{\mathrm{m}}$	$H_{\mathrm{k},j}^{\mathrm{a}}$	(100)
shearing exponent in yield surface	[-]	$\alpha^{\mathrm{c}} = 3.5$	α^{m}	α^{a}	(84)
plastic Poisson's ratio	[-]	$\nu_{\mathrm{p}}^{\mathrm{c}} = 0.26$	$\nu_{\mathrm{p}}^{\mathrm{m}}$	$\nu_{\mathrm{p}}^{\mathrm{a}}$	(94)
initial crystallization-melting temperatures	[K]	$T_{\mathrm{c}0} = 281$, $T_{\mathrm{m}0} = 318$		-	(21, 22)
initial crystallization-melting smoothness parameters	[-]	$w_{\mathrm{c}0} = 8$, $w_{\mathrm{m}0} = 5$		-	(23, 24)
phase transition function constants	[-]	$A_{Tc} = 23$, $A_{Tm} = -2$, $A_{wc} = -4$, $A_{wm} = -4$, $\alpha_{Tc} = 1.8$, $\alpha_{Tm} = 1.8$, $\alpha_{wc} = 3.8$, $\alpha_{wm} = 3.8$		-	(21, 22, 23, 24)

isotropic thermal expansion coefficient	$[\mathrm{K}^{-1}]$	$\alpha_0^{\mathrm{c}} = 0$	$\alpha_0^{\mathrm{m}} = 8 \times 10^{-4}$	$\alpha_0^{\mathrm{a}} = 10^{-5}$	(26)
isotropic strain during phase change	[-]	α_0^{cr}=-0.015, z_0^{cr}=0.1		-	(26, 27)
non-linear thermal spring constants	[-]	$A_{f_K^{\mathrm{vec}}} = 0$, $\alpha_{f_K^{\mathrm{vec}}}$, $A_{f_G^{\mathrm{vec}}} = 0$, $\alpha_{f_G^{\mathrm{vec}}}$	$A_{f_K^{\mathrm{vem}}} = 0$, $\alpha_{f_K^{\mathrm{vem}}}$, $A_{f_G^{\mathrm{vem}}} = 0.3$, $\alpha_{f_G^{\mathrm{vem}}} = 0.02$	$A_{f_K^{\mathrm{vea}}} = 0$, $\alpha_{f_K^{\mathrm{vea}}}$, $A_{f_G^{\mathrm{vea}}} = 0$, $\alpha_{f_G^{\mathrm{vea}}}$	(68-69)
heat conductivity tensor	$[\mathrm{W} \cdot \mathrm{m}^{-1} \cdot \mathrm{K}^{-1}]$	$k^{\mathrm{c}} = 0.22$	$k^{\mathrm{m}} = 0.22$	$k^{\mathrm{a}} = 0.22$	(101)
heat capacity	$[\mathrm{J} \cdot \mathrm{m}^{-3} \cdot \mathrm{K}^{-1}]$	$c_p^{\mathrm{c}} = 2020\rho_0$	$c_p^{\mathrm{m}} = 2020\rho_0$	$c_p^{\mathrm{a}} = 2020\rho_0$	(59)
density	$[\mathrm{kg} \cdot \mathrm{m}^{-3}]$	$\rho_0 = 1200$			-
latent energy	$[\mathrm{m}^2 \cdot \mathrm{s}^{-2} \cdot \mathrm{K}^{-1}]$	$\Delta H^{\mathrm{g\text{-}r}}$		-	(62)
fraction of the plastic dissipation converted to heat	-	β_{TQ}	β_{TQ}	β_{TQ}	(48, 104)

The developed model needs some parameters to be input by the user. The required parameters are listed in Table 1 with reference to the related equations. The values reported for the parameters either are identified from the experimental campaign reported in this paper or were measured on the same PCL76-4MAL/FUR 3 wt%CNT material, processed following the same methodology, in previous publications of the authors, as detailed in Section 6.

5. Incremental formulation and numerical implementation of the model

In this section, the model presented in Sections 2 - 4 is fomulated in an incremental form in order to achieve its numerical implementation. Subscript "n" is used to refer to the fields evaluated at the previous configuration.

5.1. Evaluation of the volume fraction of the crystallized phase, z^c

The crystallinity evolution described Section 2.3 is now formulated for a finite time increment. In its incremental form, the evolution of the volume fraction of the crystallized phase (17), z^{c}, is obtained as:

$$z^{\mathrm{c}} = z_n^{\mathrm{c}} + \Delta z^{\mathrm{c}}\,, \text{ with } z^{\mathrm{c}} \in [0, 1]\,, \tag{107}$$

where z_n^{c} is the value in the previous configuration, Δz^{c} is the increment between the previous and current configurations. In order to evaluate Δz^{c}, the rate function has to be normalized in order to ensure that $z^{\mathrm{c}} \in [0,1]$. If the density function were only a function of T, it would be obtained that $z^{\mathrm{c}} = \int_{T_i}^{T_f} f\, dT = 1$ and $\Delta z^{\mathrm{c}} = \int_{T_n}^{T} f(T)\, \mathrm{d}T = \frac{f(T)+f(T_n)}{2}\Delta T$, where the trapezoidal integration scheme was used for the approximation of Δz^{c}, T_i is the initial temperature and T_f is the final temperature, T_n is the previous temperature and T is the current temperature. But, because of the dependency of the density function on $|\mathbf{E}^{\mathrm{vem}}|$, z^{c} is also a function of $|\mathbf{E}^{\mathrm{vem}}|$, although the crystallinity (z^{c}) changes only if there is a temperature difference, ΔT. Therefore, to overcome this problem, Δz^{c} is normalized at each step and for this purpose a weight is defined as :

$$w_g\left(|\mathbf{E}^{\mathrm{vem}}|\right) = \begin{cases} \dfrac{1 - z_n^{\mathrm{c}}}{1 - z_{\mathrm{tmp}}^{\mathrm{c}}\left(|\mathbf{E}^{\mathrm{vem}}|\right)} & \text{if} \quad \Delta T < 0\,; \\ \dfrac{z_n^{\mathrm{c}}}{z_{\mathrm{tmp}}^{\mathrm{c}}\left(|\mathbf{E}^{\mathrm{vem}}|\right)} & \text{if} \quad \Delta T > 0\,; \end{cases} \tag{108}$$

where

$$z_{\mathrm{tmp}}^{\mathrm{c}}\left(|\mathbf{E}^{\mathrm{vem}}|\right) = 1 - \int_{T_i}^{T_n} f\left(T',\, |\mathbf{E}^{\mathrm{vem}}|\right)\, dT' = 1 - \frac{1 + \mathrm{erf}\left(\frac{T_n - T_{\mathrm{t}}(|\mathbf{E}_n^{\mathrm{vem}}|)}{\sqrt{2} w_{\mathrm{t}}(|\mathbf{E}_n^{\mathrm{vem}}|)}\right)}{2}\,, \tag{109}$$

represents the crystallinity that would be reached at the previous step if the current $T_{\mathrm{t}}\left(T,\, |\mathbf{E}^{\mathrm{vem}}|\right)$ and $w_{\mathrm{t}}\left(T,\, |\mathbf{E}^{\mathrm{vem}}|\right)$, i.e. evaluated at the current $(T,\, |\mathbf{E}^{\mathrm{vem}}|)$, were used. Eventually, Δz^{c} is calculated as:

$$\Delta z^{\mathrm{c}} = -w_g\left(|\mathbf{E}_n^{\mathrm{vem}}|\right) \frac{f\left(T,\, |\mathbf{E}_n^{\mathrm{vem}}|\right) + f(T_n,\, |\mathbf{E}_n^{\mathrm{vem}}|)}{2} \Delta T\,, \tag{110}$$

in which we use the strain measure $|\mathbf{E}_n^{\mathrm{vem}}|$ at the previous configuration to evaluate the transition temperature $T_{\mathrm{t}}\left(|\mathbf{E}_n^{\mathrm{vem}}|\right)$ and the smoothness $w_{\mathrm{t}}\left(|\mathbf{E}_n^{\mathrm{vem}}|\right)$ of the transition as an approximation in order to ease the equations resolutions. It is important to note that the amplitude of ΔT should be limited in order to ensure the accuracy of the integration.

It is then assumed that, depending on the value of z^{c}, the crystalline phase can be in the fully melted, fully crystallized or mixed phase:

$$\begin{cases} \textit{melted} & \text{if} \quad z^{\mathrm{c}} \leqslant 0.001\,; \\ \textit{mixed} & \text{if} \quad 0.001 < z^{\mathrm{c}} < 0.999\,; \\ \textit{crystallized} & \text{if} \quad z^{\mathrm{c}} \geqslant 0.999\,. \end{cases} \tag{111}$$

5.2. Evaluation of the thermal deformation gradient, F^{th}

The evaluation of the thermal deformation gradient developed in Section 2.4, is now presented in its incremental form. The isotropic thermal deformation gradient (25) is calculated as:

$$\mathbf{F}^{\mathrm{th}} = \boldsymbol{\lambda}^{\mathrm{th}} \cdot \mathbf{F}_n^{\mathrm{th}}\,, \tag{112}$$

where $\mathbf{F}_n^{\mathrm{th}}$ is the thermal deformation gradient in the previous step and where the incremental tensor for the isotropic thermal deformation, $\boldsymbol{\lambda}^{\mathrm{th}}$, is considered as:

$$\begin{aligned} \boldsymbol{\lambda}^{\mathrm{th}} = \exp\big[&(1 - z^{\mathrm{a}})\, z_{av}^{\mathrm{c}} \alpha_0^{\mathrm{c}} \Delta T + (1 - z^{\mathrm{a}})\,(1 - z_{av}^{\mathrm{c}})\, \alpha_0^{\mathrm{m}} \Delta T + z^{\mathrm{a}} \alpha_0^{\mathrm{a}} \Delta T + \\ &(1 - z^{\mathrm{a}})\, \Delta z^{\mathrm{c}} \left[\alpha_0^{\mathrm{tr}} + \alpha^{\mathrm{cr}}\left(z_{av}^{\mathrm{c}}\right)\right]\big]\, \mathbf{I}\,, \end{aligned} \tag{113}$$

where $\Delta T = T - T_n$ is the temperature difference between the current and the previous configuration, $z^{\mathrm{c}}_{av} = 1/2(z^{\mathrm{c}} + z^{\mathrm{c}}_n)$, and $\Delta z^{\mathrm{c}} = z^{\mathrm{c}} - z^{\mathrm{c}}_n$.

5.3. Internal state evaluation summary

The evaluation of the internal variables following the model ingredients of Section 2 is summarized in Table 2. The fields T_n, $\mathbf{F}_n$, and internal state $\mathbf{F}^{\mathrm{th}}_n$, $\mathbf{F}^{\mathrm{fc}}_n$, $\mathbf{F}^{\mathrm{pc}}_n$, $\mathbf{F}^{fm}_n$, $\mathbf{F}^{pr}_n$, $\mathbf{F}^{\mathrm{pa}}_n$, $T^{\mathrm{c}}_{\mathrm{Ref}_n}$, $T^{\mathrm{m}}_{\mathrm{Ref}_n}$ and $T^{\mathrm{a}}_{\mathrm{Ref}_n}$ in the previous configuration and the driving kinematic fields, $\mathbf{F}$ and T, in the current configuration are assumed to be known. In order to derive the current time solution, three cases from Eq. (111) are distinguished according to the current value of z^{c}. For each case, updated values are calculated by the ad hoc evolution equations.

5.4. Integration of the viscoelastic-plastic model

The incremental formulation of the viscoelastic-plastic model presented in Section 4.1, is now summarized while the details of the calculations are provided in Appendix B, in which the equations provided by Nguyen et al. (2016) are adapted to account for the non-linear material constants (66-67).

The same viscoelasto-plastic model is considered for all phases: c, m, a. Plastic deformation in each phase is calculated according to the return mapping algorithm, and sample iteration process is given in Table 3. In an elastic trial step, at first, the plastic deformation gradient is predicted to be equal to its value at the previous time step, t_n. Then, the predictors of $\mathbf{F}^{\mathrm{vei}}$, $\widetilde{\boldsymbol{\tau}}^{\mathrm{vei}}$ are calculated. If the plastic yielding condition is met according to Eq. (84), a plastic corrector step follows. Incremental plastic flow Γ^i is calculated iteratively until enough approximation is achieved. Then, $\mathbf{F}^{\mathrm{p}i}$ is updated with an exponential Euler method.

6. Test Campaign and Numerical Results

A test campaign was carried out in the project to investigate the SM behavior of a semi-crystalline polymer. The considered polymer, PCL764MAL/FUR 3 wt%CNT, was a thermo-reversible network synthesized starting from star-shaped PCL (poly-e-caprolactone)-based precursors bearing MAL (maleimide) or FUR (furan) end-groups according to a Diels-Alder (DA) process. Both precursors were coprecipitated with multi-walled carbon nanotubes (MWCNTs) with 3% weight as detailed by Houbben et al. (2023).

The crystallinity ratio of the 3% weight reinforced PCL764MAL/FUR was measured in a differential scanning calorimetry test using a DSC Q500 (TA Instruments) calibrated with indium on the unloaded samples with heating and cooling ramps at $\pm 10°\mathrm{C}\cdot\mathrm{min}^{-1}$ between -40 °C and 80 °C. The DSC curve, reported in Fig. 4, shows that the SMP melting peak temperature is around $T_{\mathrm{m}} = 43°\mathrm{C}$. During cooling, the peak crystallization temperature is at around $T_{\mathrm{c}} = 27°\mathrm{C}$. The degree of crystallinity has been evaluated by comparing the value of the melting enthalpy to the one reported for a PCL presenting

Table 2: Evolution of internal state

Given kinematic variables at previous and current configurations: T_n, T, $\mathbf{F}_n$, $\mathbf{F}$; *Given previous internal variables and previous thermal deformation gradient*: $\mathbf{F}_n^{\mathrm{th}}$, $\mathbf{F}_n^{\mathrm{fc}}$, $\mathbf{F}_n^{\mathrm{pc}}$, $\mathbf{F}_n^{\mathrm{fm}}$, $\mathbf{F}_n^{\mathrm{pm}}$, $\mathbf{F}_n^{\mathrm{pa}}$, $T^{\mathrm{c}}_{\mathrm{Ref}_n}$, $T^{\mathrm{m}}_{\mathrm{Ref}_n}$ and $T^{\mathrm{a}}_{\mathrm{Ref}_n}$;

- *Compute:* $\mathbf{E}_n^{\mathrm{vem}}$, $|\mathbf{E}_n^{\mathrm{vem}}|$, Eq. (7);
- *Compute:* $T_{\mathrm{c}}\left(|\mathbf{E}_n^{\mathrm{vem}}|\right)$, $T_{\mathrm{m}}\left(|\mathbf{E}_n^{\mathrm{vem}}|\right)$, $w_{\mathrm{c}}\left(|\mathbf{E}_n^{\mathrm{vem}}|\right)$, $w_{\mathrm{m}}\left(|\mathbf{E}_n^{\mathrm{vem}}|\right)$, Eqs. (21-24);
- *Compute:* $z^{\mathrm{c}}\left(T, T_n, |\mathbf{E}_n^{\mathrm{vem}}|\right)$, $T_{\mathrm{t}}\left(T, T_n, |\mathbf{E}_n^{\mathrm{vem}}|\right)$, $w_{\mathrm{t}}\left(T, T_n, |\mathbf{E}_n^{\mathrm{vem}}|\right)$, Eqs. (20-107);
- *Compute:* α^{cr}, Eq. (27); α_0^{tr}, Eqs. (28-29);
- *Compute:* $\boldsymbol{\lambda}^{\mathrm{th}}$, $\mathbf{F}^{\mathrm{th}}$, Eqs. (112-113);
- *Compute:* $\mathbf{F}^{\mathrm{m}}$ through Eq. (12);
  - **IF** $z^{\mathrm{c}} \leqslant 0.001$

    Compute:

    $\mathbf{F}^{\mathrm{fm}} = \mathbf{F}_n^{\mathrm{fm}} = \mathbf{I}$;

    $\mathbf{F}^{\mathrm{pm}}$ and $\mathbf{F}^{\mathrm{pa}}$ through predictor-corrector algorithm of Table 3;

    $\mathbf{F}^{\mathrm{fc}} = \mathbf{F}^{\mathrm{m}}$; $\mathbf{F}^{\mathrm{pc}} = \mathbf{I}$;

    $T^{\mathrm{c}}_{\mathrm{Ref}} = T$; $T^{\mathrm{m}}_{\mathrm{Ref}} = T^{\mathrm{m}}_{\mathrm{Ref}_n}$; $T^{\mathrm{a}}_{\mathrm{Ref}} = T^{\mathrm{a}}_{\mathrm{Ref}_n}$;
  - **ELSE IF** $0.001 < z^{\mathrm{c}} < 0.999$

    Compute:

    $\mathbf{F}^{\mathrm{fc}} = \mathbf{F}_n^{\mathrm{fc}}$;

    $\mathbf{F}^{\mathrm{fm}} = \mathbf{F}_n^{\mathrm{fm}} = \mathbf{I}$;

    $\mathbf{F}^{\mathrm{pc}}$, $\mathbf{F}^{\mathrm{pm}}$ and $\mathbf{F}^{\mathrm{pa}}$ through predictor-corrector algorithm of Table 3;

    $T^{\mathrm{c}}_{\mathrm{Ref}} = T^{\mathrm{c}}_{\mathrm{Ref}_n}$; $T^{\mathrm{m}}_{\mathrm{Ref}} = T^{\mathrm{m}}_{\mathrm{Ref}_n}$; $T^{\mathrm{a}}_{\mathrm{Ref}} = T^{\mathrm{a}}_{\mathrm{Ref}_n}$;
  - **ELSE IF** $0.999 \leqslant z^{\mathrm{c}}$

    Compute:

    $\mathbf{F}^{\mathrm{fc}} = \mathbf{F}_n^{\mathrm{fc}}$;

    $\mathbf{F}^{\mathrm{pc}}$ and $\mathbf{F}^{\mathrm{pa}}$ through predictor-corrector algorithm of Table 3;

    $\mathbf{F}^{\mathrm{fm}} = \mathbf{I}$; $\mathbf{F}^{\mathrm{pm}} = \mathbf{I}$; $\mathbf{F}^{\mathrm{vem}} = \mathbf{F}^{m}$;

    $T^{\mathrm{c}}_{\mathrm{Ref}} = T^{\mathrm{c}}_{\mathrm{Ref}_n}$; $T^{\mathrm{m}}_{\mathrm{Ref}} = T^{\mathrm{m}}$; $T^{\mathrm{a}}_{\mathrm{Ref}} = T^{\mathrm{a}}_{\mathrm{Ref}_n}$;
  - **END IF**

100% of crystallinity, i.e. 139.5 $\mathrm{J{\cdot}g^{-1}}$ according to the literature (Yang et al., 2010). The detailed description of the processing operation is provided by Pereira Sanchez et al.

Table 3: Sample elastic predictor-plastic corrector algorithm in phase $i = \mathrm{c}, \mathrm{m}, \mathrm{a}$

Assume: $\mathbf{F}^{\mathrm{p}i} = \mathbf{F}^{\mathrm{p}i}_n$, $\widetilde{\mathbf{b}}^i = \widetilde{\mathbf{b}}^i_n$;
Calculate: $\mathbf{F}^{\mathrm{ve}i,\mathrm{pr}}$,$\widetilde{\boldsymbol{\tau}}^{\mathrm{ve}i,\mathrm{pr}}$, Eqs. (78-79) in the incremental form of Appendix B.2, and $\widetilde{\boldsymbol{\phi}}^{i,\mathrm{pr}}$, Eq. (83);
Calculate: $h^i\left(z^{\mathrm{c}}_n\right)$, Eq. (97);
Evaluate yield surface: $F^i\left(\widetilde{\boldsymbol{\phi}}^{i,\mathrm{pr}}\right)$, Eq. (84);

- **IF** $F^i\left(\widetilde{\boldsymbol{\phi}}^{i,\mathrm{pr}}\right) \leq 0$

  Predictor is the final state;

- **ELSE**

  Plastic correction:

  - LOOP

    Iterate on plastic multiplier integral Γ^i, Eq. (90);

    Follow Appendix B.3;

  - UNTIL

    $F^i\left(\widetilde{\boldsymbol{\phi}}^i\right) \leq \epsilon_f$;

  - *Resulting quantities:* $\mathbf{F}^{\mathrm{p}i} = \exp\left(\gamma^i \mathbf{N}^i\right) \mathbf{F}^{\mathrm{p}i}_n$, with $\mathbf{N}^i$ following Eq. (91), γ^i following Appendix B.3, the isotropic hardening functions $\sigma^i_{\mathrm{t}}\left(\gamma^i\right)$ and $\sigma^i_{\mathrm{c}}\left(\gamma^i\right)$ following Eq. (96), the back-stress $\widetilde{\mathbf{b}}^i$ following Eq. (98) and $\widetilde{\boldsymbol{\tau}}^{\mathrm{ve}i}$;

- **END IF**

Final state: first Piola Kirchhoff stress tensor $\widetilde{\mathbf{P}}^i$ following Eqs. (41-43), and material operator $\widetilde{\mathbb{C}}^i = \frac{\partial \widetilde{\mathbf{P}}^i}{\partial \mathbf{F}}$ following Appendix B.4.

(17 December 2021, 20 July 2022); Houbben et al. (2023). Following this analysis, the PCL764MAL/FUR 3 wt%CNT, synthesized by Houbben et al. (2023) following the same protocol, has a crystallinity degree of about 31.5%. In the semi-crystalline polymer model we thus assume an amorphous phase of volume fraction $v^{\mathrm{a}} = 68.5\%$, allowing to assume that the crystalline phase of volume fraction $(1 - v^{\mathrm{a}}) = 31.5\%$ reaches 100% crystallinity after crystallization during the identification process.

Density ($\rho_0 = 1200\,\mathrm{kg \cdot m^{-3}}$), heat conduction coefficient ($k^{\mathrm{c}} = k^{\mathrm{m}} = k^{\mathrm{a}} = 0.22\,\mathrm{W \cdot m^{-1} \cdot K^{-1}}$) and heat capacity ($c^{\mathrm{c}}_p = c^{\mathrm{m}}_p = c^{\mathrm{a}}_p = 2,424,000\,\mathrm{kg \cdot m^{-1} \cdot s^{-2} \cdot K^{-1}}$) values were measured by Pereira Sanchez et al. (17 December 2021) on the PCL764MAL/FUR 3 wt%CNT samples, synthesized by Houbben et al. (2023) following the same protocol, and are here assumed to be the same for all phases.

Uni-axial-stress thermo-mechanical cycles were studied with a dynamic mechanical analysis test machine, DMA Q800 (TA Instruments) on samples of around $10 \times 5 \times$

0.54 mm^3. Because a DMA test machine was used, it is assumed that the temperature and deformation were uniform on the specimen and the numerical analysis was done for a material point. In the following, measurements obtained with this process are referred to as "DMA samples".

In order to measure the transverse strain, 1W-SM and 2W-SM tests were repeated following the method described by Pereira Sanchez et al. (20 July 2022) on PCL76-4MAL/FUR 3 wt%CNT samples, synthesized by Houbben et al. (2023) following the same protocol, on an in-house test bench with $40 \times 8 \times 0.5$ mm^3 samples. Temperature was controlled by applying an electrical current and measured with a thermal infrared (IR) camera (COX CX320). An S-beam load cell from Applied Measurements (DBBSMM-2 kg) was connected to a strain gauge amplifier (Applied Measurements, SGA/A). In order to measure the force, the strain gauge amplifier was connected to a data acquisition system (DAQ NI, USB-6341). A high-speed camera (Basler, acA2040-120 μm with Edmund Optics 8.5 mm C series lens) was used to record the visible surface of the speckled sample, feeding a digital image correlation (DIC) open access software (ncorr). In the following, measurements obtained with this process are referred to as "Bench samples".

6.1. Cyclic Uni-axial Tensile Test at 65°C

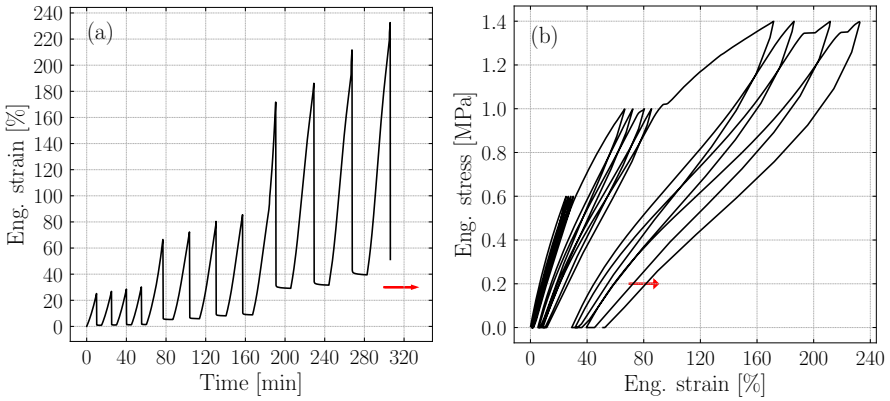

Figure 7: Experimental cyclic uni-axial tensile test measured at 65°C on the DMA samples: (a) Time-strain; and (b) Strain-stress curves

A cyclic uni-axial tensile test was carried out on the DMA-samples to determine the material properties of the material at high temperature (65°C), Figure 7. The test was load-controlled with three different stress levels: 0.6 MPa, 1.0 MPa, 1.4 MPa. At first, the specimen was heated to 65°C and kept there for 10 min to stabilize, then the strain was reset to get rid of the thermal expansion at the start. The test procedure was: $\rightarrow$ load at a rate of 0.06 MPa·min^{-1} to 0.6 MPa $\rightarrow$ sudden release $\rightarrow$ isotherm at 65°C for 5 min, Fig. 7(a). This procedure was repeated 4 times for each load level. The waiting time at the end of the sudden load release at isotherm condition was 10 min for 1.0 MPa and 15 min for 1.4 MPa. For the higher stress level, some slips of the grips can be seen in Fig. 7(b). It can also be seen that the material stiffness reduces even for the same load level, which is the indication of the damage in the material.

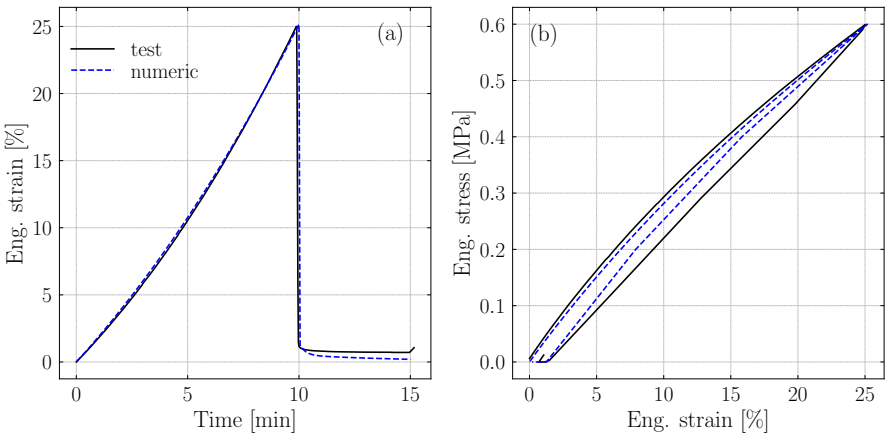

Figure 8: Experimental cyclic uni-axial tensile test vs. numerical results from our model obtained at 65°C on the DMA samples for the 1st cycle: (a) Time-strain; and (b) Strain-stress curves.

In the current model, damage evolution is not considered. Therefore, the material properties were calibrated with respect to the first cycle of the test to get rid of the stiffness reduction, Fig. 8. It can be seen that close results were obtained with the test. A weak viscoelasticity can be seen from the figure where the specimen was released suddenly. The first cycle was used for the calibration and it can be seen from Fig. 7(a) that the first cycle shows an excessive permanent deformation which disappears in next cycles of 0.6 MPa load. This is the adaptation of the specimen to load and it is usual for polymers. Therefore, the plastic deformation in the model was neglected in the melted and amorphous branches.

The calibrated viscoelastic material parameters of both the melted and amorphous phases considering 2 Maxwell branches and the stiffening terms (i.e. $\bar{K}^{\mathrm{m}}_{\infty}$, K^{m}_{i}, $\bar{K}^{\mathrm{a}}_{\infty}$, K^{a}_{i}, V^{m}_{K}, $\vartheta^{\mathrm{m}}_{K}$, ζ^{m}_{K}, V^{a}_{K}, $\vartheta^{\mathrm{a}}_{K}$, ζ^{a}_{K}, $\bar{G}^{\mathrm{m}}_{\infty}$, G^{m}_{i}, $\bar{G}^{\mathrm{a}}_{\infty}$, G^{a}_{i}, V^{m}_{G}, $\vartheta^{\mathrm{m}}_{G}$, ζ^{m}_{G}, V^{a}_{G}, $\vartheta^{\mathrm{a}}_{G}$, ζ^{a}_{G}, k^{m}_{i}, g^{m}_{i}, k^{a}_{i}, and g^{a}_{i}) are reported in Table 1. In order to carry this identification, the Poisson's ratios $v^{\mathrm{m}}_{\infty} = v^{\mathrm{a}}_{\infty}$ were assumed to be 0.26 as reported by Pereira Sanchez et al. (20 July 2022). It was also assumed that the volumetric contributions were not significant in the viscoelastic dashpot branches.

6.2. Cyclic Uni-axial Tensile Test at 0°C

Another cyclic uni-axial tensile test was carried out on the DMA-samples to determine the material properties of the material at low temperature (0°C), Fig. 9. The test was load-controlled with three different levels; 0.6 MPa, 1.0 MPa, 1.4 MPa. At first, the specimen was cooled down to 0°C and kept there for 20 min to stabilize, then the strain was reset to get rid of the thermal expansion at the start. The test procedure was: → load at a rate of 0.06 MPa·min^{-1} to 0.6 MPa → sudden release → isothermal at 0°C for 15 min, Fig. 9. This procedure was repeated 4 times for each load level. The stiffness of crystallized phase is much larger than for the melted phase and it can be seen that there is still a viscous effect during the load cycles. There is a very small permanent deformation during the test. Therefore, the plastic deformation in the crystallized phase was ignored for the isothermal loading.

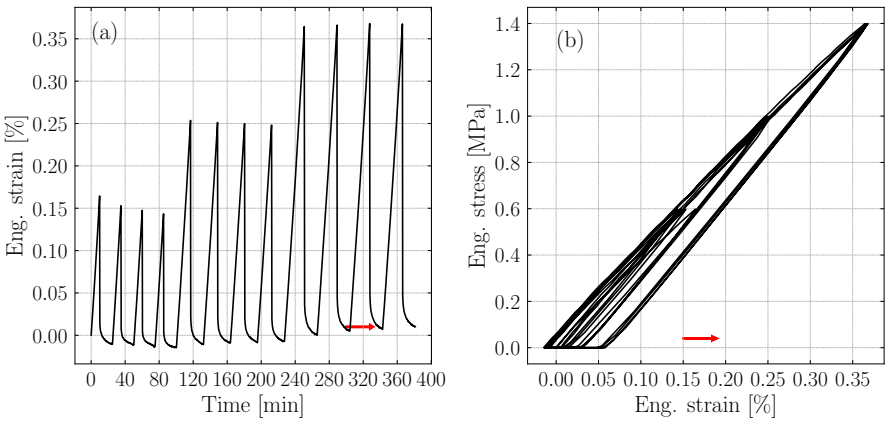

Figure 9: Experimental cyclic uniaxial tensile test measured at 0°C on the DMA samples: (a) Time-strain; and (b) Strain-stress curves.

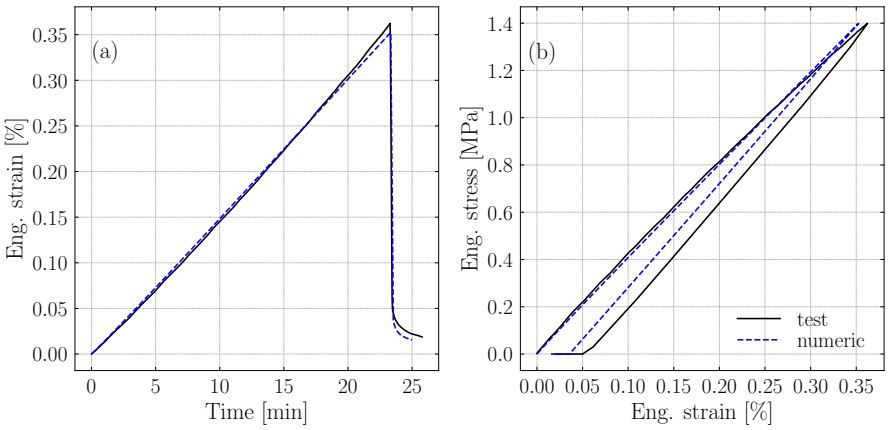

Figure 10: Experimental cyclic uniaxial tensile test vs. numerical result from our model obtained at 0°C on the DMA samples for the 1st cycle: (a) Time-strain; and (b) Strain-stress curves.

The comparison of the experimental test and the numerical model results for the first cycle of the highest stress level is shown in Fig. 10. The negative strain in the test because of the pre-test treatment viscous effect was ignored for the numerical result, Fig. 10(a). The viscoelastic and hysteresis behavior is reproduced as it can be seen from Fig. 10(b).

The material parameters for the crsystallized phase from cyclic tensile test at 0°C were identified with this test. In contrast to the 65°C cyclic test, no stiffening is observed with respect to the strain and the material stiffness is constant so that both V_K^{c} and V_G^{m} are set to zero. The calibrated material parameters ($\bar{K}_\infty^{\mathrm{c}}$, K_i^{c}, $\bar{G}_\infty^{\mathrm{c}}$, G_i^{c}, k_i^{c}, and g_i^{c}) are reported in Table 1.

Although the plastic deformation in the crystallized phase was ignored for the isothermal loading, it will be further calibrated during the phase transition.

6.3. Cyclic Temperature Test

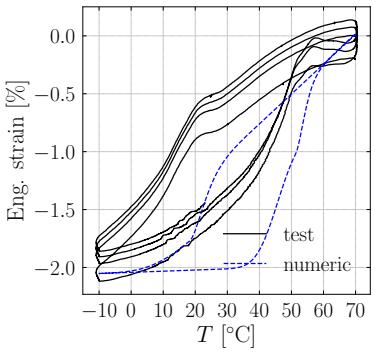

Figure 11: Experimental cyclic temperature test on the DMA-samples vs. numerical results from our model.

A cyclic temperature test was done on the DMA-samples to determine the thermal parameters of the SMP in unloaded state, Fig. 11. A very small load, 0.001 N, was applied to maintain the straightness of the specimen. The test procedure was: → isothermal at 70.0°C → cool down at a rate of 3.0°C·min^{-1} to -10.0°C → isothermal for 5.0 min → heat at a rate of 3.0°C·min^{-1} to 70.0°C → isothermal for 5.0 min; repeat the process for three times. It can be observed that, there is a shift in the test result with each temperature cycle, especially after the first one. However, the corresponding strain values are very small and it can be neglected. Besides the coefficient of thermal expansion was measured by Pereira Sanchez et al. (20 July 2022) on the "Bench samples" and found to be of the order of 0.1 $\times 10^{-3}$K^{-1} below the transition temperature and around 0.4 $\times 10^{-3}$K^{-1} beyond the transition temperature.

The model result was tuned with respect to the first cycle of the DMA samples and using the values reported for the bench samples yielding the predictions of Fig. 11. The material parameters extracted in the tensile tests were used in this test and the following parameters are obtained: T_{c0}, T_{m0}, w_{c0}, w_{m0}, α_0^c, α_0^m, α_0^a, α_0^{cr} and z_0^{cr} , Table 1. The phase transition is smooth during both crystallization and melting, $w_{c0} > 0$, $w_{m0} > 0$. We observe that the model reproduces the loop amplitude, although it is shifted to the right as compared to the experimental curves.

6.4. Two-Way Shape Memory Test Under Thermo-Mechanical Loading

Fig. 12 shows the two-way shape memory behavior of the considered DMA samples under a thermo-mechanical loading cycle. The test was load controlled with three different levels: 0.623 MPa, 0.973 MPa and 1.723 MPa corresponding to 25%, 50%, 100% strain levels, respectively. Because of the damage in the material as seen in the cyclic test at high temperature, different specimens were used for each test to get rid of the softening. At first, the specimen was heated up to 60°C and kept there for 10 min to stabilize, then the strain was reset to get rid of the thermal expansion at the start. The test procedure was: → load at a rate of 0.06 MPa·min^{-1} to the targeted stress level → cool down to -10°C at a rate of 3°C·min^{-1} → sudden release of load→ isothermal at

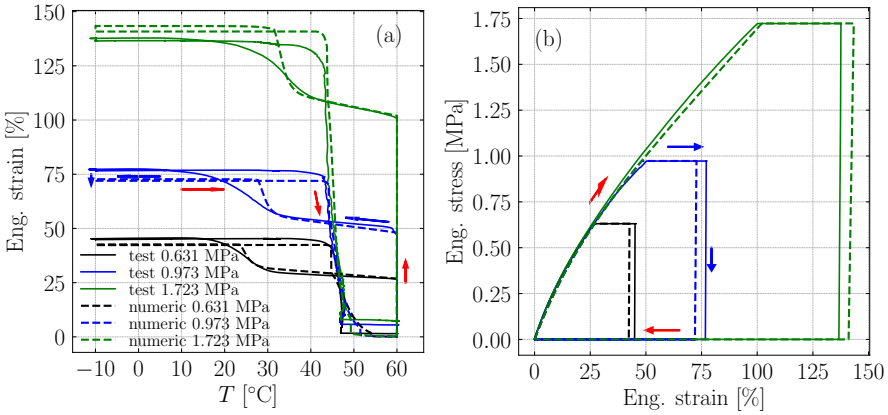

Figure 12: Two-Way Shape Memory test on DMA samples vs. numerical results under thermo-mechanical loading: (a) Temperature-strain; and (b) Strain-stress curves

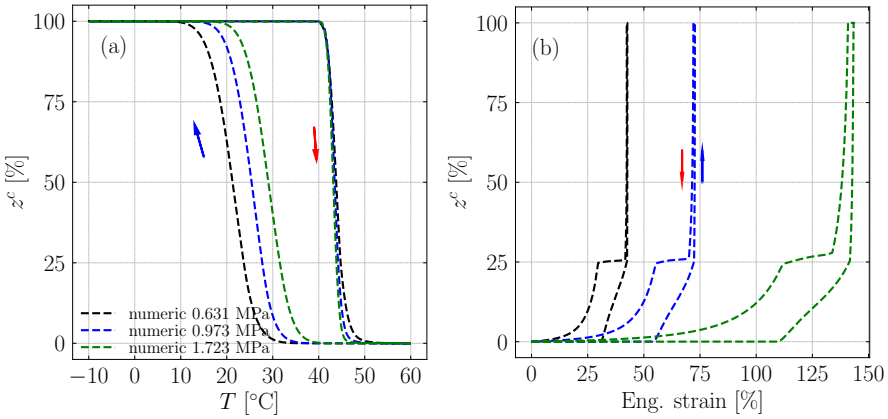

Figure 13: Two-Way Shape Memory numerical results under thermo-mechanical loading: (a) Temperature-crystallinity degree of crystalline phase; and (b) Strain-crystallinity degree of crystalline phase curves

-10°C for 10 min → heat up to 60°C at a rate of 3°C·min^{-1} → isothermal at 60°C for 15 min. The evolution of the crystallinity degree of the crystalline phase predicted by the model during the thermo-mechanical cycle is illustrated in Fig. 13. Accordingly to Figs. 2 and 5, the model captures the fact that the melting temperature T_m is higher than the crystallization temperature T_c, with this temperature gap decreasing with the straining of the material.

Fig. 12 illustrates the apparent negative thermal expansion coefficient of the polymer during the cooling at high temperature before crystallization occurs. In order to characterize further this behavior, the bench samples were submitted to a 2W-SM cycle, during which both transverse and longitudinal strain evolutions were measured by Pereira Sanchez et al. (20 July 2022). To this end, the sample was strain controlled in order to reach two constant stress levels during the full cycles: 0. MPa and 0.6 MPa. The test procedure was: → heat up to 60°C at a rate of 10°C·min^{-1} and kept there for

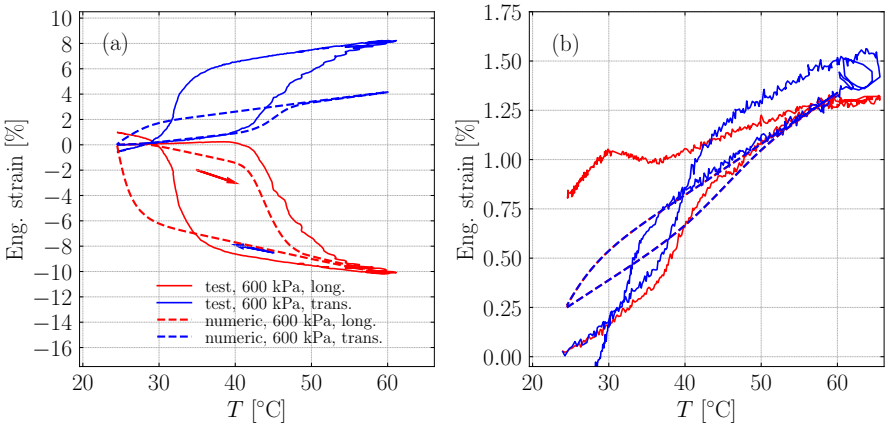

Figure 14: Two-Way Shape Memory test on bench samples vs. numerical results under thermal loading at constant stress level of: (a) 600 kPa; and (b) 0 kPa (red and blue dotted lines superpose). Displayed are the longitudinal strain along the loading direction and the transverse strain evolutions.

5 min to stabilize; → load at a strain rate of 5×10^{-4} s^{-1} to the targeted stress level → cool down to 24.5°C at a rate of 10°C·min^{-1} and kept there for 10 min to stabilize → heat up to 60°C at a rate of 10°C·min^{-1} and kept there for 5 min to stabilize → cool down to 24.5°C at a rate of 10°C·min^{-1}. Fig. 14 reports the last heating-cooling cycle for both stress level. Since the temperature did not go below 24.5°, the thermal cycle is affected and so the crystallinity, and eventually the 2W-SM cycle as reported by Chung et al. (2008). This explains why the crystallization-melting loop exhibited in the temperature-strain curve is smaller in terms of strain in Fig. 14(a) than in Fig. 12 for the 600 kPa stress level. Fig. 14(a) also shows that if the polymer exhibits an apparent negative thermal expansion coefficient during the cooling at high temperature along the loading direction, the transverse direction exhibits the expected positive thermal expansion coefficient. Besides, in the case in which the applied load vanishes, both longitudinal and transverse direction recover a positive thermal expansion coefficient, see Fig. 14(b).

In the numerical analysis, the material parameters calibrated in the previous tests were used. The observed anisotropic thermal expansion coefficient varying with the stress amplitude is captured by the shear component of non-linear thermal spring of the melted phase (i.e. parameters $A_{f_G^{\text{vem}}}$, and $\alpha_{f_G^{\text{vem}}}$). The variation of the crystallization-melting loop exhibited in the temperature-strain curve with respect to the applied loading is captured, on the one hand by the plastic flow in the crystallized phase (i.e. parameters $\sigma_{\text{t}}^{0\text{c}}$, H_{t}^{c}, z_0^{c}, h_0^{c}, and $H_{\text{k},j}^{\text{c}}$, as well as α^{c} and $\nu_{\text{p}}^{\text{c}}$), which controls the strain variation amplitude, and on the other hand by the phase transition function constants (i.e. parameters A_{Tc}, A_{Tm}, A_{wc}, A_{wm}, α_{Tc}, α_{Tm}, α_{wc}, and α_{wm}, which control the transition temperature variation with the respect to the strain level. Table 1 reports the different parameter values.

From Fig. 12 and Fig. 14, it appears that the observed behavior is qualitatively captured and that, at the exception of the amplitude of the transverse positive thermal dilation coefficient which is underestimated, the model captures quantitatively the complex 2W-SM effect. In particular the fact that crystallization-melting loop exhibited in

the temperature-strain curve is smaller for an incomplete thermal cycle is reproduced by the model, Fig. 14(a).

6.5. One-Way Shape Memory Test Under Thermo-Mechanical Loading

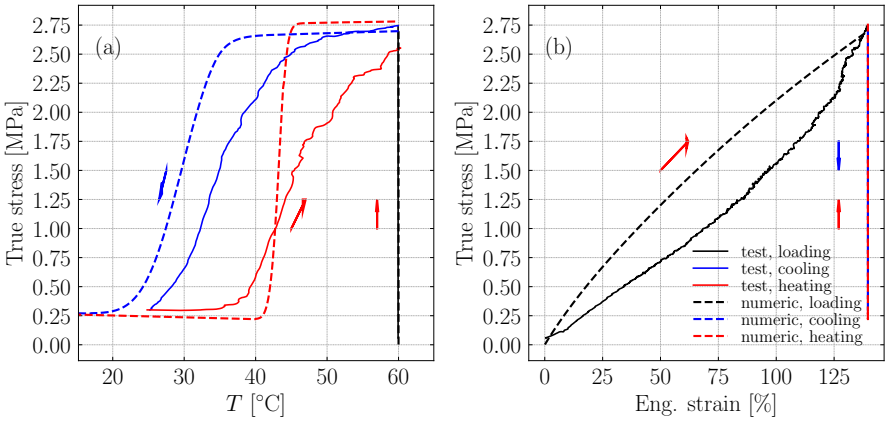

Figure 15: One-Way Shape Memory test on bench samples vs. numerical results under thermal loading at constant strain level.

In order to study the 1W-SM effect, a benched sample loaded at high temperature is further cooled down and reheated at constant 140% engineering strain. The test procedure was: $\rightarrow$ heat up to 60°C at a rate of 10°C·min^{-1} and kept there for 5 min to stabilize; $\rightarrow$ load at a strain rate of 1×10^{-3} s^{-1} to the targeted strain level $\rightarrow$ cool down to 25°C at a rate of 10°C·min^{-1} under constant strain and kept there for 5 min to stabilize $\rightarrow$ heat up to 60°C at a rate of 10°C·min^{-1} under constant strain and kept there for 5 min to stabilize. Fig. 15 illustrates the 1W-SM effect with an imperfect fixity, which is captured by the numerical model, Fig. 15(a), although the latter had to consider lower temperature to reach complete crystallization. We note that the experimental loading curve with the bench sample, Fig. 15(b), is less accurately captured than for the DMA samples, 12(b). The reason is that the 1W-SM effect was studied by Pereira Sanchez et al. (20 July 2022) after performing two loading cycles at 60°C and that the material exhibits some kind of damage during those as discussed in Section 7.

7. Conclusions

A finite strain constitutive model has been developed to simulate the thermo-mechanical behavior of the SMPs. SMPs have been thought to be composed of three different phases: crystallized, melted and amorphous. By considering an additional deformation measure, the shape fixity during cooling has been captured. Viscoelasticity has been used to simulate the rate dependent properties of the SMPs, while stiffening of the polymer in the melted regime is captured by considering non-linear elasticity constants.

The capabilities of the numerical model have been validated within a test campaign. During the tests on SMPs, it has been observed that the thermal expansion coefficients turn out to be negative along the loading direction and anisotropic under deformation,

with a strong dependency on the deformation amplitude. These phenomena have been considered in the developed numerical model by temperature dependent non-linear shear constants. The additional deformation observed during the phase change of the SMPs has been accounted by assuming that the crystallizing phase undergoes a plastic flow during the crystallization and melting, reproducing an anisotropic behavior dependent on the deformation level.

The model is thus able to reproduce the stress-strain response at different isothermal conditions, but also both 1W-SM and 2W-SM effects, with results in good agreement with the experimental tests while reproducing the observed behavior such as: anisotropic, and negative along the loading direction, thermal expansion, strain dependent crystallization-melting loop exhibited in the temperature-strain curve during the SM-effect, imperfect shape fixity.

During cyclic tensile tests at high temperature, damage evolution was observed for the considered polymer even for the same load level. Therefore, the damage initiation and evolution under cyclic load would be an extension to the current model, partly explaining the discrepancy between the model and experimental tests.

Acknowledgments

This research was funded through the "Actions de recherche concertées 2017-Synthesis, Characterization, and Multiscale Model of Smart Composite Materials (S3CM3) 17/21-07", financed by the "Direction Générale de l'Enseignement non obligatoire de la Recherche scientifique, Direction de la Recherche scientifique, Communauté Française de Belgique et octroyées par l'Académie Universitaire Wallonie-Europe".

Data availabilities

The raw/processed data required to reproduce these findings are available under the Creative Commons Attribution 4.0 International (CC BY 4.0) licence (Gülaşik et al., 2023).

Appendix A. Clausius-Duhem Inequality

The term $\dot{\Psi}$ can be obtained from Eq. (39), and it involves the rate of the volume fraction of the crystallized phase $z^{\mathrm{c}}\left(T,\,|\mathbf{E}^{\mathrm{vem}}|\right)$, which can be written in all generality $\dot{z}^{\mathrm{c}}\left(T,\,|\mathbf{E}^{\mathrm{vem}}|\right) = \frac{\partial z^{\mathrm{c}}}{\partial T}\big|_{\mathbf{E}^{\mathrm{vem}}}\dot{T} + \frac{\partial z^{\mathrm{c}}}{\partial \mathbf{E}^{\mathrm{vem}}}\big|_{T}\dot{\mathbf{E}}^{\mathrm{vem}}$. Following Eq. (17), a modification of the strain at constant temperature does not involve a variation of the volume fraction of the crystallized phase and one thus has, using Eqs. (1-3):

$$\dot{v}^{\mathrm{c}}\left(T,\,|\mathbf{E}^{\mathrm{vem}}|\right) = \left.\frac{\partial v^{\mathrm{c}}}{\partial T}\right|_{\mathbf{E}^{\mathrm{vem}}}\dot{T} = \left(1-v^{\mathrm{a}}\right)\left.\frac{\partial z^{\mathrm{c}}}{\partial T}\right|_{\mathbf{E}^{\mathrm{vem}}}\dot{T}\,; \tag{A.1}$$

$$\dot{v}^{\mathrm{m}}\left(T,\,|\mathbf{E}^{\mathrm{vem}}|\right) = \left.\frac{\partial v^{\mathrm{m}}}{\partial T}\right|_{\mathbf{E}^{\mathrm{vem}}}\dot{T} = -\left(1-v^{\mathrm{a}}\right)\left.\frac{\partial z^{\mathrm{c}}}{\partial T}\right|_{\mathbf{E}^{\mathrm{vem}}}\dot{T}\,; \quad \text{and} \tag{A.2}$$

$$\dot{v}^{\mathrm{a}} = 0\,. \tag{A.3}$$

Therefore, using Eqs. (39) and (A.1-A.3), $\dot{\Psi}$ can be written as:

$$\begin{aligned}\dot{\Psi} = &\left[\frac{\partial v^{\mathrm{c}}}{\partial T}\dot{T}\right]\left[\widetilde{\Psi}^{\mathrm{vec}} + \widetilde{\Psi}^{\mathrm{pc}}\right] + \left[\frac{\partial v^{\mathrm{m}}}{\partial T}\dot{T}\right]\left[\widetilde{\Psi}^{\mathrm{vem}} + \widetilde{\Psi}^{\mathrm{pm}}\right] + \frac{\partial \Psi^{\mathrm{th}}}{\partial T}\dot{T} + \frac{\partial \Psi^{\mathrm{th}}}{\partial z^{\mathrm{c}}}\frac{\partial z^{\mathrm{c}}}{\partial T}\dot{T} + \\ & v^{\mathrm{c}}\left[\frac{\partial \widetilde{\Psi}^{\mathrm{vec}}}{\partial \mathbf{C}^{\mathrm{vec}}} : \dot{\mathbf{C}}^{\mathrm{vec}} + \sum_{j}^{N}\frac{\partial \widetilde{\Psi}^{\mathrm{vec}}}{\partial \widetilde{\mathbf{q}}_j^{\mathrm{c}}} : \dot{\widetilde{\mathbf{q}}}_j^{\mathrm{c}} + \frac{\partial \widetilde{\Psi}^{\mathrm{vec}}}{\partial T}\dot{T} + \sum_{i}^{M}\frac{\partial \widetilde{\Psi}^{\mathrm{pc}}}{\partial \xi_i^{\mathrm{pc}}}\dot{\xi}_i^{\mathrm{pc}}\right] + \\ & v^{\mathrm{m}}\left[\frac{\partial \widetilde{\Psi}^{\mathrm{vem}}}{\partial \mathbf{C}^{\mathrm{vem}}} : \dot{\mathbf{C}}^{\mathrm{vem}} + \sum_{j}^{N}\frac{\partial \widetilde{\Psi}^{\mathrm{vem}}}{\partial \widetilde{\mathbf{q}}_j^{\mathrm{m}}} : \dot{\widetilde{\mathbf{q}}}_j^{\mathrm{m}} + \frac{\partial \widetilde{\Psi}^{\mathrm{vem}}}{\partial T}\dot{T} + \sum_{i}^{M}\frac{\partial \widetilde{\Psi}^{\mathrm{pm}}}{\partial \xi_i^{\mathrm{pm}}}\dot{\xi}_i^{\mathrm{pm}}\right] + \\ & v^{\mathrm{a}}\left[\frac{\partial \widetilde{\Psi}^{\mathrm{vea}}}{\partial \mathbf{C}^{\mathrm{vea}}} : \dot{\mathbf{C}}^{\mathrm{vea}} + \sum_{j}^{N}\frac{\partial \widetilde{\Psi}^{\mathrm{vea}}}{\partial \widetilde{\mathbf{q}}_j^{\mathrm{a}}} : \dot{\widetilde{\mathbf{q}}}_j^{\mathrm{a}} + \frac{\partial \widetilde{\Psi}^{\mathrm{vea}}}{\partial T}\dot{T} + \sum_{i}^{M}\frac{\partial \widetilde{\Psi}^{\mathrm{pa}}}{\partial \xi_i^{\mathrm{pa}}}\dot{\xi}_i^{\mathrm{pa}}\right] .\end{aligned} \tag{A.4}$$

By using the deformation gradient decomposition in Section 2.2, $\dot{\mathbf{F}}$ can be expanded as:

$$\begin{aligned}\dot{\mathbf{F}} = &\dot{\mathbf{F}}^{\mathrm{vec}}\cdot\mathbf{F}^{\mathrm{pc}}\cdot\mathbf{F}^{\mathrm{fc}}\cdot\mathbf{F}^{\mathrm{th}} + \mathbf{F}^{\mathrm{vec}}\cdot\mathbf{L}^{\mathrm{pc}}\cdot\mathbf{F}^{\mathrm{pc}}\cdot\mathbf{F}^{\mathrm{fc}}\cdot\mathbf{F}^{\mathrm{th}} + \\ & \mathbf{F}^{\mathrm{vec}}\cdot\mathbf{F}^{\mathrm{pc}}\cdot\mathbf{L}^{\mathrm{fc}}\cdot\mathbf{F}^{\mathrm{fc}}\cdot\mathbf{F}^{\mathrm{th}} + \mathbf{F}^{\mathrm{vec}}\cdot\mathbf{F}^{\mathrm{pc}}\cdot\mathbf{F}^{\mathrm{fc}}\cdot\dot{\mathbf{F}}^{\mathrm{th}} ,\end{aligned} \tag{A.5}$$

where $\mathbf{L}^{\mathrm{pc}} = \dot{\mathbf{F}}^{\mathrm{pc}}\cdot\mathbf{F}^{\mathrm{pc}^{-1}}$ is the plastic velocity gradient and $\mathbf{L}^{\mathrm{fc}} = \dot{\mathbf{F}}^{\mathrm{fc}}\cdot\mathbf{F}^{\mathrm{fc}^{-1}}$ is the frozen velocity gradient for the crystallized phase, as

$$\begin{aligned}\dot{\mathbf{F}} = &\dot{\mathbf{F}}^{\mathrm{vem}}\cdot\mathbf{F}^{\mathrm{pm}}\cdot\mathbf{F}^{\mathrm{fm}}\cdot\mathbf{F}^{\mathrm{th}} + \mathbf{F}^{\mathrm{vem}}\cdot\mathbf{L}^{\mathrm{pm}}\cdot\mathbf{F}^{\mathrm{pm}}\cdot\mathbf{F}^{\mathrm{fm}}\cdot\mathbf{F}^{\mathrm{th}} + \\ & \mathbf{F}^{\mathrm{vem}}\cdot\mathbf{F}^{\mathrm{pm}}\cdot\mathbf{L}^{\mathrm{fm}}\cdot\mathbf{F}^{\mathrm{fm}}\cdot\mathbf{F}^{\mathrm{th}} + \mathbf{F}^{\mathrm{vem}}\cdot\mathbf{F}^{\mathrm{pm}}\cdot\mathbf{F}^{\mathrm{fm}}\cdot\dot{\mathbf{F}}^{\mathrm{th}} ,\end{aligned} \tag{A.6}$$

where $\mathbf{L}^{\mathrm{pm}} = \dot{\mathbf{F}}^{\mathrm{pm}}\cdot\mathbf{F}^{\mathrm{pm}^{-1}}$ is the plastic velocity gradient and $\mathbf{L}^{\mathrm{fm}} = \dot{\mathbf{F}}^{\mathrm{fm}}\cdot\mathbf{F}^{\mathrm{fm}^{-1}}$ is the frozen velocity gradient for the melted phase, and as

$$\dot{\mathbf{F}} = \dot{\mathbf{F}}^{\mathrm{vea}}\cdot\mathbf{F}^{\mathrm{pa}}\cdot\mathbf{F}^{\mathrm{th}} + \mathbf{F}^{\mathrm{vea}}\cdot\mathbf{L}^{\mathrm{pa}}\cdot\mathbf{F}^{\mathrm{pa}}\cdot\mathbf{F}^{\mathrm{th}} + \mathbf{F}^{\mathrm{vea}}\cdot\mathbf{F}^{\mathrm{pa}}\cdot\dot{\mathbf{F}}^{\mathrm{th}} , \tag{A.7}$$

where $\mathbf{L}^{\mathrm{pa}} = \dot{\mathbf{F}}^{\mathrm{pa}}\cdot\mathbf{F}^{\mathrm{pa}^{-1}}$ is the plastic velocity gradient for the amorphous phase. Therefore, by using Eqs. (41-43), these decompositions yield:

$$\begin{aligned}\mathbf{P}^{\mathrm{c}} : \dot{\mathbf{F}} = &v^{\mathrm{c}}\frac{1}{2}\widetilde{\mathbf{S}}^{\mathrm{vec}} : \dot{\mathbf{C}}^{\mathrm{vec}} + v^{\mathrm{c}}\,\widetilde{\mathbf{M}}^{\mathrm{vec}} : \mathbf{L}^{\mathrm{pc}} + v^{\mathrm{c}}\,\widetilde{\mathbf{M}}^{\mathrm{vec}} : \left(\mathbf{F}^{\mathrm{pc}}\cdot\mathbf{L}^{\mathrm{fc}}\cdot\mathbf{F}^{\mathrm{pc}^{-1}}\right) + \\ & v^{\mathrm{c}}\,\widetilde{\mathbf{M}}^{\mathrm{vec}} : \left(\mathbf{F}^{\mathrm{pc}}\cdot\mathbf{F}^{\mathrm{fc}}\cdot\dot{\mathbf{F}}^{\mathrm{th}}\cdot\mathbf{F}^{\mathrm{th}^{-1}}\cdot\mathbf{F}^{\mathrm{fc}^{-1}}\cdot\mathbf{F}^{\mathrm{pc}^{-1}}\right) ,\end{aligned} \tag{A.8}$$

for the crystallized phase,

$$\begin{aligned}\mathbf{P}^{\mathrm{m}} : \dot{\mathbf{F}} = &v^{\mathrm{m}}\frac{1}{2}\widetilde{\mathbf{S}}^{\mathrm{vem}} : \dot{\mathbf{C}}^{\mathrm{vem}} + v^{\mathrm{m}}\,\widetilde{\mathbf{M}}^{\mathrm{vem}} : \mathbf{L}^{\mathrm{pm}} + v^{\mathrm{m}}\,\widetilde{\mathbf{M}}^{\mathrm{vem}} : \left(\mathbf{F}^{\mathrm{pm}}\cdot\mathbf{L}^{\mathrm{fm}}\cdot\mathbf{F}^{\mathrm{pm}^{-1}}\right) + \\ & v^{\mathrm{m}}\,\widetilde{\mathbf{M}}^{\mathrm{vem}} : \left(\mathbf{F}^{\mathrm{pm}}\cdot\mathbf{F}^{\mathrm{fm}}\cdot\dot{\mathbf{F}}^{\mathrm{th}}\cdot\mathbf{F}^{\mathrm{th}^{-1}}\cdot\mathbf{F}^{\mathrm{fm}^{-1}}\cdot\mathbf{F}^{\mathrm{pm}^{-1}}\right) ,\end{aligned} \tag{A.9}$$

for the melted phase, and

$$\mathbf{P}^{\mathrm{a}} : \dot{\mathbf{F}} = v^{\mathrm{a}}\frac{1}{2}\widetilde{\mathbf{S}}^{\mathrm{vea}} : \dot{\mathbf{C}}^{\mathrm{vea}} + v^{\mathrm{a}}\,\widetilde{\mathbf{M}}^{\mathrm{vea}} : \mathbf{L}^{\mathrm{pa}} + v^{\mathrm{a}}\,\widetilde{\mathbf{M}}^{\mathrm{vea}} : \left(\mathbf{F}^{\mathrm{pa}}\cdot\dot{\mathbf{F}}^{\mathrm{th}}\cdot\mathbf{F}^{\mathrm{th}^{-1}}\cdot\mathbf{F}^{\mathrm{pa}^{-1}}\right) , \tag{A.10}$$

for the amorphous phase.

The deformation gradient $\mathbf{F}^{\mathrm{fc}}$ is calculated in the complete melted temperature region in which $v^{\mathrm{c}} = 0$ and stays constant during transition and lower temperatures. Similarly, the deformation gradient $\mathbf{F}^{\mathrm{fm}}$ is calculated in the complete crystallized temperature region in which $v^{\mathrm{m}} = 0$ and stays constant during transition and higher temperatures. Therefore, in Eqs. (A.8) and (A.9), it can be considered that:

$$v^{\mathrm{c}}\widetilde{\mathbf{M}}^{\mathrm{vec}} : \left(\mathbf{F}^{\mathrm{pc}} \cdot \mathbf{L}^{\mathrm{fc}} \cdot \mathbf{F}^{\mathrm{pc}^{-1}}\right) = 0\,; \text{ and } v^{\mathrm{m}}\widetilde{\mathbf{M}}^{\mathrm{vem}} : \left(\mathbf{F}^{\mathrm{pm}} \cdot \mathbf{L}^{\mathrm{fm}} \cdot \mathbf{F}^{\mathrm{pm}^{-1}}\right) = 0\,. \tag{A.11}$$

By considering Eq. (25), $\dot{\mathbf{F}}^{\mathrm{th}}$ can be written as:

$$\begin{aligned}\dot{\mathbf{F}}^{\mathrm{th}} &= \dot{\lambda}^{\mathrm{th}}\mathbf{F}^{\mathrm{th}} = \left.\frac{\partial \lambda^{\mathrm{th}}}{\partial \mathbf{C}^{\mathrm{vem}}}\right|_{T} : \dot{\mathbf{C}}^{\mathrm{vem}}\ \mathbf{F}^{\mathrm{th}} + \left.\frac{\partial \lambda^{\mathrm{th}}}{\partial T}\right|_{\mathbf{C}^{\mathrm{vem}}} : \dot{T}\ \mathbf{F}^{\mathrm{th}} \\ &= \left.\frac{\partial \lambda^{\mathrm{th}}}{\partial T}\right|_{\mathbf{C}^{\mathrm{vem}}} : \dot{T}\ \mathbf{F}^{\mathrm{th}} = \left.\frac{\partial \mathbf{F}^{\mathrm{th}}}{\partial T}\right|_{\mathbf{C}^{\mathrm{vem}}} \dot{T}\,,\end{aligned} \tag{A.12}$$

since $\dot{\lambda}^{\mathrm{th}}$ depends on $\dot{T}$ only, see Eq. (26).

Then, by using the derived equations above in Eq. (45), the Clausius-Duhem inequality can be rewritten as[6]:

$$\begin{aligned}
&v^{\mathrm{c}}\left[\frac{1}{2}\widetilde{\mathbf{S}}^{\mathrm{vec}} - \frac{\partial \widetilde{\Psi}^{\mathrm{vec}}}{\partial \mathbf{C}^{\mathrm{vec}}}\right] : \dot{\mathbf{C}}^{\mathrm{vec}} + v^{\mathrm{m}}\left[\frac{1}{2}\widetilde{\mathbf{S}}^{\mathrm{vem}} - \frac{\partial \widetilde{\Psi}^{\mathrm{vem}}}{\partial \mathbf{C}^{\mathrm{vem}}}\right] : \dot{\mathbf{C}}^{\mathrm{vem}} + v^{\mathrm{a}}\left[\frac{1}{2}\widetilde{\mathbf{S}}^{\mathrm{vea}} - \frac{\partial \widetilde{\Psi}^{\mathrm{vea}}}{\partial \mathbf{C}^{\mathrm{vea}}}\right] : \dot{\mathbf{C}}^{\mathrm{vea}} - \\
&v^{\mathrm{c}}\sum_{j}^{N}\frac{\partial \widetilde{\Psi}^{\mathrm{vec}}}{\partial \widetilde{\mathbf{q}}_j^{\mathrm{c}}} : \dot{\widetilde{\mathbf{q}}}_j^{\mathrm{c}} - v^{\mathrm{m}}\sum_{j}^{N}\frac{\partial \widetilde{\Psi}^{\mathrm{vem}}}{\partial \widetilde{\mathbf{q}}_j^{\mathrm{m}}} : \dot{\widetilde{\mathbf{q}}}_j^{\mathrm{m}} - v^{\mathrm{a}}\sum_{j}^{N}\frac{\partial \widetilde{\Psi}^{\mathrm{vea}}}{\partial \widetilde{\mathbf{q}}_j^{\mathrm{a}}} : \dot{\widetilde{\mathbf{q}}}_j^{\mathrm{a}} - \\
&v^{\mathrm{c}}\sum_{i}^{M}\frac{\partial \widetilde{\Psi}^{\mathrm{pc}}}{\partial \xi_i^{\mathrm{pc}}} : \dot{\xi}_i^{\mathrm{pc}} - v^{\mathrm{m}}\sum_{i}^{M}\frac{\partial \widetilde{\Psi}^{\mathrm{pm}}}{\partial \xi_i^{\mathrm{pm}}} : \dot{\xi}_i^{\mathrm{pm}} - v^{\mathrm{a}}\sum_{i}^{M}\frac{\partial \widetilde{\Psi}^{\mathrm{pa}}}{\partial \xi_i^{\mathrm{pa}}} : \dot{\xi}_i^{\mathrm{a}} + \\
&v^{\mathrm{c}}\widetilde{\mathbf{M}}^{\mathrm{vec}} : \mathbf{L}^{\mathrm{pc}} + v^{\mathrm{m}}\widetilde{\mathbf{M}}^{\mathrm{vem}} : \mathbf{L}^{\mathrm{pm}} + v^{\mathrm{a}}\widetilde{\mathbf{M}}^{\mathrm{vea}} : \mathbf{L}^{\mathrm{pa}} + \mathbf{M}^{\mathrm{m}} : \left(\left.\frac{\partial \mathbf{F}^{\mathrm{th}}}{\partial T}\right|_{\mathbf{C}^{\mathrm{vem}}} \cdot \mathbf{F}^{\mathrm{th}^{-1}}\right)\dot{T} - \\
&\left[\frac{\partial \Psi^{\mathrm{th}}}{\partial T} + \frac{\partial \Psi^{\mathrm{th}}}{\partial z^{\mathrm{c}}}\frac{\partial z^{\mathrm{c}}}{\partial T}\right]\dot{T} - \eta\dot{T} - \left[v^{\mathrm{c}}\frac{\partial \widetilde{\Psi}^{\mathrm{vec}}}{\partial T} + v^{\mathrm{m}}\frac{\partial \widetilde{\Psi}^{\mathrm{vem}}}{\partial T} + v^{\mathrm{a}}\frac{\partial \widetilde{\Psi}^{\mathrm{vea}}}{\partial T}\right]\dot{T} - \\
&\left[(1-v^{\mathrm{a}})\left(\widetilde{\Psi}^{\mathrm{vec}} + \widetilde{\Psi}^{\mathrm{pc}}\right) - (1-v^{\mathrm{a}})\left(\widetilde{\Psi}^{\mathrm{vem}} + \widetilde{\Psi}^{\mathrm{pm}}\right)\right]\frac{\partial z^{\mathrm{c}}}{\partial T}\dot{T} - \frac{1}{T}\mathbf{Q} \cdot \mathrm{Grad}\ T \geq 0\,,
\end{aligned} \tag{A.13}$$

where

$$\begin{aligned}
\mathbf{M}^{\mathrm{m}} =& v^{\mathrm{c}}\mathbf{F}^{\mathrm{fc}^{\mathrm{T}}} \cdot \mathbf{F}^{\mathrm{pc}^{\mathrm{T}}} \cdot \widetilde{\mathbf{M}}^{\mathrm{vec}} \cdot \mathbf{F}^{\mathrm{pc}^{-\mathrm{T}}} \cdot \mathbf{F}^{\mathrm{fc}^{-\mathrm{T}}} + v^{\mathrm{m}}\mathbf{F}^{\mathrm{fm}^{\mathrm{T}}} \cdot \mathbf{F}^{\mathrm{pm}^{\mathrm{T}}} \cdot \widetilde{\mathbf{M}}^{\mathrm{vem}} \cdot \mathbf{F}^{\mathrm{pm}^{-\mathrm{T}}} \cdot \mathbf{F}^{\mathrm{fm}^{-\mathrm{T}}} + \\
& v^{\mathrm{a}}\left(\mathbf{F}^{\mathrm{pa}^{\mathrm{T}}} \cdot \widetilde{\mathbf{M}}^{\mathrm{vea}} \cdot \mathbf{F}^{\mathrm{pa}^{-\mathrm{T}}}\right)\,.
\end{aligned} \tag{A.14}$$

[6] We note that from Eq. (25), $\mathbf{F}^{\mathrm{th}}$ is a diagonal tensor that permutes with its inverse and so its derivative.

In Eq. (A.13), the total dissipation $\mathfrak{D}$ per unit reference volume is defined by:

$$\mathfrak{D} = \mathfrak{D}_{\text{loc}} + \mathfrak{D}_{\text{conv}} \geq 0\,, \tag{A.15}$$

where the local dissipation $\mathfrak{D}_{\text{loc}}$ and the nonlocal convective dissipation $\mathfrak{D}_{\text{conv}}$ are given as:

$$\begin{aligned}\mathfrak{D}_{\text{loc}} = {} & v^{\text{c}}\widetilde{\mathbf{M}}^{\text{vec}} : \mathbf{L}^{\text{pc}} + v^{\text{m}}\widetilde{\mathbf{M}}^{\text{vem}} : \mathbf{L}^{\text{pm}} + v^{\text{a}}\widetilde{\mathbf{M}}^{\text{vea}} : \mathbf{L}^{\text{pa}} - \\ & v^{\text{c}} \sum_{j}^{N} \frac{\partial \widetilde{\Psi}^{\text{vec}}}{\partial \widetilde{\mathbf{q}}_j^{\text{vec}}} : \dot{\widetilde{\mathbf{q}}}_j^{\text{vec}} - v^{\text{vem}} \sum_{j}^{N} \frac{\partial \widetilde{\Psi}^{\text{vem}}}{\partial \widetilde{\mathbf{q}}_j^{\text{vem}}} : \dot{\widetilde{\mathbf{q}}}_j^{\text{vem}} - v^{\text{a}} \sum_{j}^{N} \frac{\partial \widetilde{\Psi}^{\text{vea}}}{\partial \widetilde{\mathbf{q}}_j^{\text{a}}} : \dot{\widetilde{\mathbf{q}}}_j^{\text{a}} - \\ & v^{\text{c}} \sum_{i}^{M} \frac{\partial \widetilde{\Psi}^{\text{pc}}}{\partial \xi_i^{\text{pc}}} : \dot{\xi}_j^{\text{pc}} - v^{\text{m}} \sum_{i}^{M} \frac{\partial \widetilde{\Psi}^{\text{pm}}}{\partial \xi_i^{\text{pm}}} : \dot{\xi}_i^{\text{pm}} - v^{\text{a}} \sum_{i}^{M} \frac{\partial \widetilde{\Psi}^{\text{pa}}}{\partial \xi_i^{\text{pa}}} : \dot{\xi}_i^{\text{pa}} \geq 0\,; \text{ and}\end{aligned} \tag{A.16}$$

$$\mathfrak{D}_{\text{conv}} = -\frac{1}{T}\,\mathbf{Q} \cdot \text{Grad}\, T \geq 0\,, \tag{A.17}$$

where the positive sign should arise when defining the constitutive laws. The local dissipation $\mathfrak{D}_{\text{loc}}$ can be decomposed into a viscous part $\mathfrak{D}_{\text{loc}}^{\text{ve}} \geq 0$ and a plastic part $\mathfrak{D}_{\text{loc}}^{\text{p}} \geq 0$ following

$$\mathfrak{D}_{\text{loc}} = \mathfrak{D}_{\text{loc}}^{\text{ve}} + \mathfrak{D}_{\text{loc}}^{\text{p}}\,, \tag{A.18}$$

with

$$\mathfrak{D}_{\text{loc}}^{\text{ve}} = -v^{\text{c}} \sum_{j}^{N} \frac{\partial \widetilde{\Psi}^{\text{vec}}}{\partial \widetilde{\mathbf{q}}_j^{\text{vec}}} : \dot{\widetilde{\mathbf{q}}}_j^{\text{vec}} - v^{\text{vem}} \sum_{j}^{N} \frac{\partial \widetilde{\Psi}^{\text{vem}}}{\partial \widetilde{\mathbf{q}}_j^{\text{vem}}} : \dot{\widetilde{\mathbf{q}}}_j^{\text{vem}} - v^{\text{a}} \sum_{j}^{N} \frac{\partial \widetilde{\Psi}^{\text{vea}}}{\partial \widetilde{\mathbf{q}}_j^{\text{a}}} : \dot{\widetilde{\mathbf{q}}}_j^{\text{a}} \geq 0\,, \tag{A.19}$$

and

$$\begin{aligned}\mathfrak{D}_{\text{loc}}^{\text{p}} &= v^{\text{c}}\widetilde{\mathbf{M}}^{\text{vec}} : \mathbf{L}^{\text{pc}} + v^{\text{m}}\widetilde{\mathbf{M}}^{\text{vem}} : \mathbf{L}^{\text{pm}} + v^{\text{a}}\widetilde{\mathbf{M}}^{\text{vea}} : \mathbf{L}^{\text{pa}} - \\ &\qquad v^{\text{c}} \sum_{i}^{M} \frac{\partial \widetilde{\Psi}^{\text{pc}}}{\partial \xi_i^{\text{pc}}} : \dot{\xi}_j^{\text{pc}} - v^{\text{m}} \sum_{i}^{M} \frac{\partial \widetilde{\Psi}^{\text{pm}}}{\partial \xi_i^{\text{pm}}} : \dot{\xi}_i^{\text{pm}} - v^{\text{a}} \sum_{i}^{M} \frac{\partial \widetilde{\Psi}^{\text{pa}}}{\partial \xi_i^{\text{pa}}} : \dot{\xi}_i^{\text{pa}} \\ &\simeq \beta_{\text{TQ}} \left[v^{\text{c}}\widetilde{\mathbf{M}}^{\text{vec}} : \mathbf{L}^{\text{pc}} + v^{\text{m}}\widetilde{\mathbf{M}}^{\text{vem}} : \mathbf{L}^{\text{pm}} + v^{\text{a}}\widetilde{\mathbf{M}}^{\text{vea}} : \mathbf{L}^{\text{pa}} \right] \geq 0\,,\end{aligned} \tag{A.20}$$

where we consider the Taylor-Quinney coefficient β_{TQ}.

Eq. (A.13) thus becomes

$$\begin{aligned}0 \leq {} & \mathfrak{D}_{\text{loc}} + \mathfrak{D}_{\text{conv}} + v^{\text{c}} \left[\frac{1}{2}\widetilde{\mathbf{S}}^{\text{vec}} - \frac{\partial \widetilde{\Psi}^{\text{vec}}}{\partial \mathbf{C}^{\text{vec}}} \right] : \dot{\mathbf{C}}^{\text{vec}} + v^{\text{m}} \left[\frac{1}{2}\widetilde{\mathbf{S}}^{\text{vem}} - \frac{\partial \widetilde{\Psi}^{\text{vem}}}{\partial \mathbf{C}^{\text{vem}}} \right] : \dot{\mathbf{C}}^{\text{vem}} + \\ & v^{\text{a}} \left[\frac{1}{2}\widetilde{\mathbf{S}}^{\text{vea}} - \frac{\partial \widetilde{\Psi}^{\text{vea}}}{\partial \mathbf{C}^{\text{vea}}} \right] : \dot{\mathbf{C}}^{\text{vea}} + \mathbf{M}^{\text{m}} : \left(\left. \frac{\partial \mathbf{F}^{\text{th}}}{\partial T} \right|_{\mathbf{C}^{\text{vem}}} \cdot \mathbf{F}^{\text{th}^{-1}} \right) \dot{T} - \eta \dot{T} - \\ & \left[v^{\text{c}} \frac{\partial \widetilde{\Psi}^{\text{vec}}}{\partial T} + v^{\text{m}} \frac{\partial \widetilde{\Psi}^{\text{vem}}}{\partial T} + v^{\text{a}} \frac{\partial \widetilde{\Psi}^{\text{vea}}}{\partial T} \right] \dot{T} - \\ & \left[(1 - v^{\text{a}}) \left(\widetilde{\Psi}^{\text{vec}} + \widetilde{\Psi}^{\text{pc}} \right) - (1 - v^{\text{a}}) \left(\widetilde{\Psi}^{\text{vem}} + \widetilde{\Psi}^{\text{pm}} \right) \right] \frac{\partial z^{\text{c}}}{\partial T} \dot{T} - \left[\frac{\partial \Psi^{\text{th}}}{\partial T} + \frac{\partial \Psi^{\text{th}}}{\partial z^{\text{c}}} \frac{\partial z^{\text{c}}}{\partial T} \right] \dot{T}\,.\end{aligned} \tag{A.21}$$

Appendix B. Viscoelasto-plasticity

Appendix B.1. Viscoelasticity in incremental form

In this appendix, for conciseness, the superscript related to the branch c, m or a is omitted. Unless stated otherwise, the terms are expressed at configuration t_{n+1}, with $\Delta t_n = t - t_n$.

Appendix B.1.1. Internal variables $\widetilde{\mathbf{q}}_j$ in the incremental form

Following (Nguyen et al., 2016), the term dev $\widetilde{\mathbf{q}}_j$ can be found by integrating Eq. (73) up to the current time t_{n+1}, yielding

$$\text{dev}\ \widetilde{\mathbf{q}}_j \quad = \quad 2G_j\ \text{dev}\ \mathbf{E}^{\text{ve}} - \mathbf{A}_{j,n+1}\,, \tag{B.1}$$

where

$$\mathbf{A}_{j,n+1} = \mathbf{A}_{j,n}\text{exp}\left(-\frac{\Delta t_n}{g_j}\right) + 2G_j\ \text{exp}\left(-\frac{\Delta t_n}{2g_j}\right)(\text{dev}\ \mathbf{E}^{\text{ve}} - \text{dev}\ \mathbf{E}^{\text{ve}}_n)\ . \tag{B.2}$$

Following a similar procedure, $\widetilde{p}_{\text{q}j}$ can be found by integrating Eq. (74) up to the current time t_{n+1} , yielding

$$\widetilde{p}_{\text{q}j} = \frac{1}{3}\text{tr}\ \widetilde{\mathbf{q}}_j \quad = \quad K_j\ \text{tr}\ \mathbf{E}^{\text{ve}} - \text{B}_{j,n+1}\,, \tag{B.3}$$

where

$$\text{B}_{j,n+1} = \text{B}_{j,n}\text{exp}\left(-\frac{\Delta t_n}{k_j}\right) + K_j\ \text{exp}\left(-\frac{\Delta t_n}{2k_j}\right)(\text{tr}\ \mathbf{E}^{\text{ve}} - \text{tr}\ \mathbf{E}^{\text{ve}}_n)\ . \tag{B.4}$$

Appendix B.1.2. Corotational stress $\widetilde{\boldsymbol{\tau}}^{ve}$ in the incremental form

The terms dev $\widetilde{\boldsymbol{\tau}}^{\text{ve}}$ and $\widetilde{p}^{\text{ve}}$ can be found by integrating Eq. (78) and Eq. (79), respectively, following the same procedure as here above. Using the definitions of $f_K\,(\text{tr}\ \mathbf{E}^{\text{ve}})$ and $f_G\,(\text{dev}\ \mathbf{E}^{\text{ve}})$ in respectively Eqs. (66) and (67), these terms are respectively rewritten

$$\text{dev}\ \widetilde{\boldsymbol{\tau}}^{\text{ve}} = \underbrace{2\hat{G}_\infty\,(T;\,T_{\text{Ref}})\ \ \text{dev}\ \mathbf{E}^{\text{ve}} + \sum_{j=1}^{N}\mathbf{A}_{j,n+1}}_{\text{dev}\ \widetilde{\boldsymbol{\tau}}^{\text{ve}}_{\text{o}}} + \underbrace{2\hat{G}_\infty\,(T;\,T_{\text{Ref}})\ \ f_G\,(\text{dev}\ \mathbf{E}^{\text{ve}})\ \ \text{dev}\ \mathbf{E}^{\text{ve}}}_{\text{dev}\ \widetilde{\boldsymbol{\tau}}^{\text{ve}}_{\text{c}}}, \tag{B.5}$$

where dev $\widetilde{\boldsymbol{\tau}}^{\text{ve}}_{\text{o}}$ is the term that can be found in (Nguyen et al., 2016) while dev $\widetilde{\boldsymbol{\tau}}^{\text{ve}}_{\text{c}}$ is the deviatoric enhancement, and

$$\widetilde{p}^{\text{ve}} = \frac{1}{3}\text{tr}\ \widetilde{\boldsymbol{\tau}}^{\text{ve}} = \underbrace{\hat{K}_\infty\,(T;\,T_{\text{Ref}})\ \ \text{tr}\ \mathbf{E}^{\text{ve}} + \sum_{j=1}^{N}\text{B}_{j,n+1}}_{\widetilde{p}^{\text{ve}}_{\text{o}}} + \underbrace{\hat{K}_\infty\,(T;\,T_{\text{Ref}})\ \ f_K\,(\text{tr}\ \mathbf{E}^{\text{ve}})\ \ \text{tr}\ \mathbf{E}^{\text{ve}}}_{\widetilde{p}^{\text{ve}}_{\text{c}}}, \tag{B.6}$$

where $\widetilde{p}^{\text{ve}}_{\text{o}}$ is the term that can be found in (Nguyen et al., 2016) while $\widetilde{p}^{\text{ve}}_{\text{c}}$ is the pressure enhancement.

Appendix B.2. Viscoelastic predictor

At the start of a time step, the plastic deformation gradient is predicted to be equal to its value at the previous time step, t_n, yielding the predictor

$$\mathbf{F}^{\mathrm{ve,pr}} = \mathbf{F} \cdot \mathbf{F}^{\mathrm{th}^{-1}} \cdot \mathbf{F}^{\mathrm{f}^{-1}} \cdot \mathbf{F}_n^{\mathrm{p}^{-1}} , \tag{B.7}$$

with $\mathbf{F}^{\mathrm{f}} = \mathbf{I}$ for the amorphous phase. The predictor of the elastic right Cauchy-Green tensor and logarithmic strain tensor follow as

$$\mathbf{C}^{\mathrm{ve,pr}} = \mathbf{F}_n^{\mathrm{p}^{-\mathrm{T}}} \cdot \mathbf{F}^{\mathrm{f}^{-\mathrm{T}}} \cdot \mathbf{F}^{\mathrm{th}^{-\mathrm{T}}} \cdot \mathbf{C} \cdot \mathbf{F}^{\mathrm{th}^{-1}} \cdot \mathbf{F}^{\mathrm{f}^{-1}} \cdot \mathbf{F}_n^{\mathrm{p}^{-1}} \; ; \text{ and } \mathbf{E}^{\mathrm{ve,pr}} = \frac{1}{2} \ln \mathbf{C}^{\mathrm{ve,pr}} . \tag{B.8}$$

The predictor of the corotational Kirchhoff stress, $\widetilde{\boldsymbol{\tau}}^{\mathrm{ve,pr}}$, can be decomposed using Eqs. (B.5) and (B.6) as:

$$\widetilde{\boldsymbol{\tau}}^{\mathrm{ve,pr}} = \mathrm{dev}\, \widetilde{\boldsymbol{\tau}}^{\mathrm{ve,pr}} + \widetilde{p}^{\mathrm{ve,pr}} \mathbf{I} = \mathrm{dev}\, \widetilde{\boldsymbol{\tau}}_{\mathrm{o}}^{\mathrm{ve,pr}} + \widetilde{p}_{\mathrm{o}}^{\mathrm{ve,pr}} \mathbf{I} + \mathrm{dev}\, \widetilde{\boldsymbol{\tau}}_{\mathrm{c}}^{\mathrm{ve,pr}} + \widetilde{p}_{\mathrm{c}}^{\mathrm{ve,pr}} \mathbf{I} , \tag{B.9}$$

where

$$\begin{aligned} \mathrm{dev}\, \widetilde{\boldsymbol{\tau}}_{\mathrm{o}}^{\mathrm{ve,pr}} &= 2G_e\, \mathrm{dev}\, \mathbf{E}^{\mathrm{ve,pr}} - 2\left(G_e - \hat{G}_\infty\left(T; T_{\mathrm{Ref}}\right)\right)\, \mathrm{dev}\, \mathbf{E}_n^{\mathrm{ve}} + \\ &\quad \sum_{j=1}^{N} \mathbf{A}_{jn} \exp\left(-\frac{\Delta t_n}{g_j}\right) \end{aligned} \tag{B.10}$$

$$\mathrm{dev}\, \widetilde{\boldsymbol{\tau}}_{\mathrm{c}}^{\mathrm{ve,pr}} = 2\hat{G}_\infty\left(T; T_{\mathrm{Ref}}\right)\; f_G\left(\mathrm{dev}\, \mathbf{E}^{\mathrm{ve,pr}}\right)\; \mathrm{dev}\, \mathbf{E}^{\mathrm{ve,pr}} , \tag{B.11}$$

and

$$\widetilde{p}_{\mathrm{o}}^{\mathrm{ve,pr}} = K_e\, \mathrm{tr}\, \mathbf{E}^{\mathrm{ve,pr}} - \left(K_e - \hat{K}_\infty\left(T; T_{\mathrm{Ref}}\right)\right)\, \mathrm{tr}\, \mathbf{E}_n^{\mathrm{ve}} + \sum_{j=1}^{N} \mathrm{B}_{jn} \exp\left(-\frac{\Delta t_n}{k_j}\right) \tag{B.12}$$

$$\widetilde{p}_{\mathrm{c}}^{\mathrm{ve,pr}} = \hat{K}_\infty\left(T; T_{\mathrm{Ref}}\right)\; f_K\left(\mathrm{tr}\, \mathbf{E}^{\mathrm{ve,pr}}\right)\; \mathrm{tr}\, \mathbf{E}^{\mathrm{ve,pr}} , \tag{B.13}$$

with

$$G_e = \hat{G}_\infty\left(T; T_{\mathrm{Ref}}\right) + \sum_{j=1}^{N} G_j \exp\left(-\frac{\Delta t_n}{2g_j}\right) , \tag{B.14}$$

$$K_e = \hat{K}_\infty\left(T; T_{\mathrm{Ref}}\right) + \sum_{j=1}^{N} K_j \exp\left(-\frac{\Delta t_n}{2k_j}\right) . \tag{B.15}$$

The predictor of the combined stress tensor (83) is then written as:

$$\widetilde{\boldsymbol{\phi}}^{\mathrm{pr}} = \mathrm{dev}\, \widetilde{\boldsymbol{\phi}}_{\mathrm{o}}^{\mathrm{pr}} + \widetilde{\phi}_{\mathrm{v,o}}^{\mathrm{pr}} \mathbf{I} + \mathrm{dev}\, \widetilde{\boldsymbol{\phi}}_{\mathrm{c}}^{\mathrm{pr}} + \widetilde{\phi}_{\mathrm{v,c}}^{\mathrm{pr}} \mathbf{I} = \mathrm{dev}\, \widetilde{\boldsymbol{\phi}}^{\mathrm{pr}} + \widetilde{\phi}_{\mathrm{v}}^{\mathrm{pr}}\, \mathbf{I} , \tag{B.16}$$

where

$$\mathrm{dev}\, \widetilde{\boldsymbol{\phi}}_{\mathrm{o}}^{\mathrm{pr}} = \mathrm{dev}\, \widetilde{\boldsymbol{\tau}}_{\mathrm{o}}^{\mathrm{ve,pr}} - \mathrm{dev}\, \widetilde{\mathbf{b}}_n , \text{ and } \mathrm{dev}\, \widetilde{\boldsymbol{\phi}}_{\mathrm{c}}^{\mathrm{pr}} = \mathrm{dev}\, \widetilde{\boldsymbol{\tau}}_{\mathrm{c}}^{\mathrm{ve,pr}} ; \tag{B.17}$$

and

$$\widetilde{\phi}^{\mathrm{pr}}_{\mathrm{v,o}} = \widetilde{p}^{\mathrm{ve,pr}}_{\mathrm{o}} - \frac{1}{3}\ \mathrm{tr}\ \widetilde{\mathbf{b}}_n\ ,\ \text{and}\ \widetilde{\phi}^{\mathrm{pr}}_{\mathrm{v,c}} = \widetilde{p}^{\mathrm{ve,pr}}_{\mathrm{c}}\ . \tag{B.18}$$

Since the viscoelastic region is limited by the pressure-sensitive yield function $F\left(\widetilde{\boldsymbol{\phi}}\right)$ (84) expressed in terms of the corotational Kirchhoff stress $\widetilde{\boldsymbol{\phi}}$, if $F\left(\widetilde{\boldsymbol{\phi}}^{\mathrm{pr}}\right) \leq 0$ is not satisfied, a correction follows.

Appendix B.3. Plastic corrector

Using the radial return mapping algorithm applied on Eq. (90), the plastic deformation gradient reads:

$$\mathbf{F}^{\mathrm{p}} = \exp\left(\Gamma\mathbf{N}\right)\mathbf{F}^{\mathrm{p}}_n\,, \tag{B.19}$$

where the normal $\mathbf{N}$ follows from Eq. (91). This allows correcting the viscoelastic deformation gradient and the right Cauchy tensor following

$$\mathbf{F}^{\mathrm{ve}} = \mathbf{F}\cdot\ \mathbf{F}^{\mathrm{th}^{-1}}\cdot\mathbf{F}^{\mathrm{f}^{-1}}\cdot\mathbf{F}^{\mathrm{p}^{-1}} = \mathbf{F}\cdot\ \mathbf{F}^{\mathrm{th}^{-1}}\cdot\mathbf{F}^{\mathrm{f}^{-1}}\cdot\mathbf{F}^{\mathrm{p}-1}_n\cdot\left[\exp\left(\Gamma\mathbf{N}\right)\right]^{-1}\ ,\ \text{and} \tag{B.20}$$

$$\mathbf{C}^{\mathrm{ve}} = \left[\exp(\Gamma\mathbf{N})\right]^{-T}\cdot\mathbf{C}^{\mathrm{ve,pr}}\cdot\left[\exp(\Gamma\mathbf{N})\right]^{-1}, \tag{B.21}$$

where we assume that $\widetilde{\boldsymbol{\tau}}^{\mathrm{ve}}$ and $\mathbf{C}^{\mathrm{ve}}$ permute, see previous discussion in Section 4.1.1. Therefore, it comes

$$\mathbf{E}^{\mathrm{ve}} = \mathbf{E}^{\mathrm{ve,pr}} - \Gamma\mathbf{N}\,. \tag{B.22}$$

Finally, using the definitions of $f_K\left(\mathrm{tr}\ \mathbf{E}^{\mathrm{ve}}\right)$ and $f_G\left(\mathrm{dev}\ \mathbf{E}^{\mathrm{ve}}\right)$, the stress contributions (B.5) and (B.6) are respectively rewritten:

$$\mathrm{dev}\ \widetilde{\boldsymbol{\tau}}^{\mathrm{ve}} = \mathrm{dev}\ \widetilde{\boldsymbol{\tau}}^{\mathrm{ve}}_{\mathrm{o}} + \mathrm{dev}\ \widetilde{\boldsymbol{\tau}}^{\mathrm{ve}}_{\mathrm{c}}\ ,\ \text{and} \tag{B.23}$$

$$\widetilde{p}^{\mathrm{ve}} = \widetilde{p}^{\mathrm{ve}}_{\mathrm{o}} + \widetilde{p}^{\mathrm{ve}}_{\mathrm{c}}\,, \tag{B.24}$$

with, using Eqs. (B.10-B.13),

$$\begin{aligned}
\mathrm{dev}\ \widetilde{\boldsymbol{\tau}}^{\mathrm{ve}}_{\mathrm{o}} &= 2G_e\ \mathrm{dev}\ \left(\mathbf{E}^{\mathrm{ve,pr}} - \Gamma\mathbf{N}\right) - 2\left(G_e - \hat{G}_\infty\left(T;\,T_{\mathrm{Ref}}\right)\right)\ \mathrm{dev}\ \mathbf{E}^{\mathrm{ve}}_n + \\
&\quad \sum_{j=1}^{N}\mathbf{A}_{jn}\exp\left(-\frac{\Delta t_n}{g_j}\right) = \mathrm{dev}\ \widetilde{\boldsymbol{\tau}}^{\mathrm{ve,pr}}_{\mathrm{o}} - 2G_e\Gamma\ \mathrm{dev}\ \mathbf{N}\,,\ \text{and} \qquad \text{(B.25)}\\
\mathrm{dev}\ \widetilde{\boldsymbol{\tau}}^{\mathrm{ve}}_{\mathrm{c}} &= 2\hat{G}_\infty\left(T;\,T_{\mathrm{Ref}}\right)\ f_G\left(\mathrm{dev}\ \mathbf{E}^{\mathrm{ve,pr}} - \Gamma\ \mathrm{dev}\ \mathbf{N}\right)\ \mathrm{dev}\ \left(\mathbf{E}^{\mathrm{ve,pr}} - \Gamma\mathbf{N}\right)\,, \qquad \text{(B.26)}
\end{aligned}$$

and

$$\begin{aligned}
\widetilde{p}^{\mathrm{ve}}_{\mathrm{o}} &= K_e\ \mathrm{tr}\ \left(\mathbf{E}^{\mathrm{ve,pr}} - \Gamma\mathbf{N}\right) - \left(K_e - \hat{K}_\infty\left(T;\,T_{\mathrm{Ref}}\right)\right)\ \mathrm{tr}\ \mathbf{E}^{\mathrm{ve}}_n + \\
&\quad \sum_{j=1}^{N}\mathrm{B}_{jn}\exp\left(-\frac{\Delta t_n}{k_j}\right) = \widetilde{p}^{\mathrm{ve,pr}}_{\mathrm{o}} - K_e\Gamma\ \mathrm{tr}\ \mathbf{N}\,,\ \text{and} \qquad \text{(B.27)}\\
\widetilde{p}^{\mathrm{ve}}_{\mathrm{c}} &= \hat{K}_\infty\left(T;\,T_{\mathrm{Ref}}\right)\ f_K\left(\mathrm{tr}\ \mathbf{E}^{\mathrm{ve,pr}} - \Gamma\ \mathrm{tr}\ \mathbf{N}\right)\ \mathrm{tr}\ \left(\mathbf{E}^{\mathrm{ve,pr}} - \Gamma\mathbf{N}\right)\,, \qquad \text{(B.28)}
\end{aligned}$$

Therefore, Eq. (B.23) is rewritten:

$$\begin{aligned} \text{dev}\,\widetilde{\boldsymbol{\tau}}^{\text{ve}} &= \text{dev}\,\widetilde{\boldsymbol{\tau}}_{\text{c}}^{\text{ve}} + \text{dev}\,\widetilde{\boldsymbol{\tau}}^{\text{ve,pr}} - \text{dev}\,\widetilde{\boldsymbol{\tau}}_{\text{c}}^{\text{ve,pr}} - 2G_e\Gamma\text{dev}\,\mathbf{N} \\ &= \Delta\text{dev}\,\widetilde{\boldsymbol{\tau}}_{\text{c}}^{\text{ve}} + \text{dev}\,\widetilde{\boldsymbol{\tau}}^{\text{ve,pr}} - 2G_e\Gamma\text{dev}\,\mathbf{N}\,, \end{aligned} \tag{B.29}$$

where $\text{dev}\,\widetilde{\boldsymbol{\tau}}_{\text{c}}^{\text{ve}}$ is written in terms of its corrector term $\Delta\text{dev}\,\widetilde{\boldsymbol{\tau}}_{\text{c}}^{\text{ve}}$ as:

$$\text{dev}\,\widetilde{\boldsymbol{\tau}}_{\text{c}}^{\text{ve}} = \text{dev}\,\widetilde{\boldsymbol{\tau}}_{\text{c}}^{\text{ve,pr}} + \Delta\text{dev}\,\widetilde{\boldsymbol{\tau}}_{\text{c}}^{\text{ve}}\,. \tag{B.30}$$

The interagtion of Eq. (98) yields:

$$\widetilde{\mathbf{b}} = \widetilde{\mathbf{b}}_n + kH_{\text{k}}\Gamma\mathbf{N}\,, \tag{B.31}$$

so that, using Eq. (B.16), it comes

$$\text{dev}\,\widetilde{\boldsymbol{\phi}} = \text{dev}\,\widetilde{\boldsymbol{\tau}}^{\text{ve}} - \widetilde{\mathbf{b}} = \Delta\text{dev}\,\widetilde{\boldsymbol{\tau}}_{\text{c}}^{\text{ve}} + \text{dev}\,\widetilde{\boldsymbol{\phi}}^{\text{pr}} - 2G_e\Gamma\text{dev}\,\mathbf{N} - kH_{\text{k}}\Gamma\text{dev}\,\mathbf{N}\,, \tag{B.32}$$

Using Eq. (91) restated as

$$\mathbf{N} = 3\ \text{dev}\,\widetilde{\boldsymbol{\phi}} + \frac{2\beta}{3}\widetilde{\phi}_{\text{v}}\,\mathbf{I}\,, \tag{B.33}$$

Eq. (B.32) becomes

$$\text{dev}\,\widetilde{\boldsymbol{\phi}} = \frac{\text{dev}\,\widetilde{\boldsymbol{\phi}}^{\text{pr}} + \Delta\text{dev}\,\widetilde{\boldsymbol{\tau}}_{\text{c}}^{\text{ve}}}{u}\,, \tag{B.34}$$

where $u = 1 + 6\tilde{G}_e\Gamma$ with $\tilde{G}_e = G_e + \frac{kH_{\text{k}}}{2}$.

Similarly, Eq. (B.24) is rewritten:

$$\begin{aligned} \widetilde{p}^{\text{ve}} &= \widetilde{p}_{\text{c}}^{\text{ve}} + \widetilde{p}^{\text{ve,pr}} - \widetilde{p}_{\text{c}}^{\text{ve,pr}} - K_e\Gamma\ \text{tr}\,\mathbf{N} \\ &= \Delta\widetilde{p}_{\text{c}}^{\text{ve}} + \widetilde{p}^{\text{ve,pr}} - K_e\Gamma\ \text{tr}\,\mathbf{N}\,, \end{aligned} \tag{B.35}$$

where $\widetilde{p}_{\text{c}}^{\text{ve}}$ is defined using its correction $\Delta\widetilde{p}_{\text{c}}^{\text{ve}}$ as:

$$\widetilde{p}_{\text{c}}^{\text{ve}} = \widetilde{p}_{\text{c}}^{\text{ve,pr}} + \Delta\widetilde{p}_{\text{c}}^{\text{ve}}\,. \tag{B.36}$$

Using Eqs. (B.31) and (B.16), it comes

$$\widetilde{\phi}_{\text{v}} = \frac{1}{3}\text{tr}\,\widetilde{\boldsymbol{\phi}} = \widetilde{p}^{\text{ve}} - \frac{1}{3}\text{tr}\,\widetilde{\mathbf{b}} = \Delta\,\widetilde{p}_{\text{c}}^{\text{ve}} + \widetilde{\phi}_{\text{v}}^{\text{pr}} - K_e\Gamma\text{tr}\,\mathbf{N} - \frac{kH_{\text{k}}\Gamma}{3}\text{tr}\,\mathbf{N}\,. \tag{B.37}$$

Making use of the definition of $\mathbf{N}$ (B.33), it is possible to rewrite Eq. (B.37) as:

$$\widetilde{\phi}_{\text{v}} = \frac{\widetilde{\phi}_{\text{v}}^{\text{pr}} + \Delta\widetilde{p}_{\text{c}}^{\text{ve}}}{v}\,, \tag{B.38}$$

where $v = 1 + 2\beta\tilde{K}_e\Gamma$ with $\tilde{K}_e = K_e + \frac{kH_{\text{k}}}{3}$.

Using Eqs. (B.34) and (B.38), the normal $\mathbf{N}$ (B.33) rewrites:

$$\mathbf{N} = \frac{3(\text{dev}\,\widetilde{\boldsymbol{\phi}}^{\text{pr}} + \Delta\text{dev}\,\widetilde{\boldsymbol{\tau}}_{\text{c}}^{\text{ve}})}{u} + \frac{2\beta}{3}\frac{\widetilde{\phi}_{\text{v}}^{\text{pr}} + \Delta\widetilde{p}_{\text{c}}^{\text{ve}}}{v}\mathbf{I}\,. \tag{B.39}$$

The equivalent plastic deformation γ can be now computed, by integration of Eq. (92), yielding

$$\Delta\gamma = k\Gamma\sqrt{\mathbf{N}:\mathbf{N}} = k\Gamma \underbrace{\sqrt{6\widetilde{\phi}_{\mathrm{e}}^2 + \frac{4}{3}\beta^2\widetilde{\phi}_{\mathrm{v}}^2}}_{A}\,, \tag{B.40}$$

with using Eq. (B.39):

$$A = \sqrt{6\left(\frac{\left(\mathrm{dev}\,\widetilde{\boldsymbol{\phi}}^{\mathrm{pr}} + \Delta\mathrm{dev}\,\widetilde{\boldsymbol{\tau}}_{\mathrm{c}}^{\mathrm{ve}}\right)_{\mathrm{e}}}{u}\right)^2 + \frac{4}{3}\beta^2\left(\frac{\widetilde{\phi}_{\mathrm{v}}^{\mathrm{pr}} + \Delta\widetilde{p}_{\mathrm{c}}^{\mathrm{ve}}}{v}\right)^2}\,. \tag{B.41}$$

The corrected extended yield condition $F\left(\widetilde{\boldsymbol{\tau}}^{\mathrm{ve}}\right)$ (84) thus writes:

$$F = a_2\left(\frac{\left(\mathrm{dev}\,\widetilde{\boldsymbol{\phi}}^{\mathrm{pr}} + \Delta\mathrm{dev}\,\widetilde{\boldsymbol{\tau}}_{\mathrm{c}}^{\mathrm{ve}}\right)_{\mathrm{e}}}{u}\right)^{\alpha} - a_1\frac{\widetilde{\phi}_{\mathrm{v}}^{\mathrm{pr}} + \Delta\widetilde{p}_{\mathrm{c}}^{\mathrm{ve}}}{v} - a_0 = 0\,. \tag{B.42}$$

Using Eq. (B.40), we find that:

$$\Gamma = \frac{\Delta\gamma}{k\sqrt{6\left(\widetilde{\phi}_{\mathrm{e}}\right)^2 + \frac{4}{3}\beta^2\left(\widetilde{\phi}_{\mathrm{v}}\right)^2}} = \frac{\Delta\gamma}{kA}\,. \tag{B.43}$$

In order to solve for Γ, which is therefore the only unknown, a Newton-Raphson algorithm is used. To that end, we need to compute:

$$\frac{\mathrm{d}F}{\mathrm{d}\Gamma} = \frac{\partial F}{\partial\Delta\gamma}\frac{\partial\Delta\gamma}{\partial\Gamma} + \frac{\partial F}{\partial\Gamma}\,, \tag{B.44}$$

with the following derivatives

- The derivative $\frac{\partial F}{\partial\Delta\gamma}$ follows from

$$\frac{\partial F}{\partial\Delta\gamma} = H_2\left(\frac{\left(\mathrm{dev}\,\widetilde{\boldsymbol{\phi}}^{\mathrm{pr}} + \Delta\mathrm{dev}\,\widetilde{\boldsymbol{\tau}}_{\mathrm{c}}^{\mathrm{ve}}\right)_{\mathrm{e}}}{u}\right)^{\alpha} - H_1\frac{\widetilde{\phi}_{\mathrm{v}}^{\mathrm{pr}} + \Delta\widetilde{p}_{\mathrm{c}}^{\mathrm{ve}}}{v} - H_0\,, \tag{B.45}$$

  where, using Eqs. (88-96):

$$H_2 = \frac{\partial a_2}{\partial\Delta\gamma} = -\frac{\alpha}{\sigma_{\mathrm{c}}^{\alpha+1}}hH_{\mathrm{c}}\,, \tag{B.46}$$

$$H_1 = \frac{\partial a_1}{\partial\Delta\gamma} = \frac{3h}{\sigma_{\mathrm{c}}}\left[\frac{\alpha m^{\alpha-1}}{m+1} - \frac{m^{\alpha}-1}{(m+1)^2}\right]\frac{H_{\mathrm{t}}\sigma_{\mathrm{c}} - H_{\mathrm{c}}\sigma_{\mathrm{t}}}{\sigma_{\mathrm{c}}^2} - 3h\frac{m^{\alpha}-1}{m+1}\frac{H_{\mathrm{c}}}{\sigma_{\mathrm{c}}^2}\,,\ \text{and} \tag{B.47}$$

$$H_0 = \frac{\partial a_0}{\partial\Delta\gamma} = \frac{\left(\alpha m^{\alpha-1}+1\right)(m+1) - m^{\alpha} - m}{(m+1)^2}h\frac{H_{\mathrm{t}}\sigma_{\mathrm{c}} - H_{\mathrm{c}}\sigma_{\mathrm{t}}}{\sigma_{\mathrm{c}}^2}\,. \tag{B.48}$$

- The derivative $\frac{\partial \Delta\gamma}{\partial \Gamma}$ follows from Eqs. (B.40-B.41) rewritten as:

$$\Delta\gamma = k\Gamma A = k\Gamma \sqrt{\underbrace{6\left(\frac{\left(\text{dev}\,\widetilde{\boldsymbol{\phi}}^{\text{pr}} + \Delta\text{dev}\,\widetilde{\boldsymbol{\tau}}_{\text{c}}^{\text{ve}}\right)_{\text{e}}}{u}\right)^2 + \frac{4}{3}\beta^2\left(\frac{\widetilde{\phi}_{\text{v}}^{\text{pr}} + \Delta\widetilde{p}_{\text{c}}^{\text{ve}}}{v}\right)^2}_{\mathcal{Z}}}\,. \tag{B.49}$$

The partial derivative with respect to Γ is then written as:

$$\frac{\partial \Delta\gamma}{\partial \Gamma} = k\left(A + \Gamma\frac{\partial A}{\partial \Gamma}\right)\,,\ \text{where}\ \frac{\partial A}{\partial \Gamma} = \frac{1}{2A}\frac{\partial}{\partial \Gamma}\mathcal{Z}\,. \tag{B.50}$$

The derivative $\frac{\partial}{\partial \Gamma}(\mathcal{Z})$ writes:

$$\begin{aligned}\frac{\partial \mathcal{Z}}{\partial \Gamma} \quad = \quad & -\frac{72\tilde{G}_e\left[\left(\text{dev}\,\widetilde{\boldsymbol{\phi}}^{\text{pr}} + \Delta\text{dev}\,\widetilde{\boldsymbol{\tau}}_{\text{c}}^{\text{ve}}\right)_{\text{e}}\right]^2}{u^3} + \\ & \frac{18}{u^2}\left(\text{dev}\,\widetilde{\boldsymbol{\phi}}^{\text{pr}} + \Delta\text{dev}\,\widetilde{\boldsymbol{\tau}}_{\text{c}}^{\text{ve}}\right) : \frac{\partial \text{dev}\,\widetilde{\boldsymbol{\tau}}_{\text{c}}^{\text{ve}}}{\partial \Gamma} - \\ & \frac{16\beta^3\tilde{K}_e\left(\widetilde{\phi}_{\text{v}}^{\text{pr}} + \Delta\widetilde{p}_{\text{c}}^{\text{ve}}\right)^2}{3v^3} + \frac{8\beta^2\left(\widetilde{\phi}_{\text{v}}^{\text{pr}} + \Delta\widetilde{p}_{\text{c}}^{\text{ve}}\right)}{3v^2}\frac{\partial \widetilde{p}_{\text{c}}^{\text{ve}}}{\partial \Gamma}\,,\end{aligned} \tag{B.51}$$

where $\frac{\partial \text{dev}\,\widetilde{\boldsymbol{\tau}}_{\text{c}}^{\text{ve}}}{\partial \Gamma}$ and $\frac{\partial \widetilde{p}_{\text{c}}^{\text{ve}}}{\partial \Gamma}$ are given in Appendix B.5.1.

- The derivative $\frac{\partial F}{\partial \Gamma}$ follows from

$$\frac{\partial F}{\partial \Gamma} = \frac{\partial}{\partial \Gamma}\left[a_2\left(\frac{\left(\text{dev}\,\widetilde{\boldsymbol{\phi}}^{\text{pr}} + \Delta\text{dev}\,\widetilde{\boldsymbol{\tau}}_{\text{c}}^{\text{ve}}\right)_{\text{e}}}{u}\right)^{\alpha} - a_1\frac{\widetilde{\phi}_{\text{v}}^{\text{pr}} + \Delta\widetilde{p}_{\text{c}}^{\text{ve}}}{v} - a_0\right]\,. \tag{B.52}$$

The first derivative reads:

$$\begin{aligned}&\frac{\partial}{\partial \Gamma}\left[a_2\left(\frac{\left(\text{dev}\,\widetilde{\boldsymbol{\phi}}^{\text{pr}} + \Delta\text{dev}\,\widetilde{\boldsymbol{\tau}}_{\text{c}}^{\text{ve}}\right)_{\text{e}}}{u}\right)^{\alpha}\right] = \\ &\frac{3a_2\alpha}{2u^2}\left(\frac{\left(\text{dev}\,\widetilde{\boldsymbol{\phi}}^{\text{pr}} + \Delta\text{dev}\,\widetilde{\boldsymbol{\tau}}_{\text{c}}^{\text{ve}}\right)_{\text{e}}}{u}\right)^{\alpha-2}\left(\text{dev}\,\widetilde{\boldsymbol{\phi}}^{\text{pr}} + \Delta\text{dev}\,\widetilde{\boldsymbol{\tau}}_{\text{c}}^{\text{ve}}\right) : \frac{\partial \text{dev}\,\widetilde{\boldsymbol{\tau}}_{\text{c}}^{\text{ve}}}{\partial \Gamma} \\ &-a_2\left(\frac{\left(\text{dev}\,\widetilde{\boldsymbol{\phi}}^{\text{pr}} + \Delta\text{dev}\,\widetilde{\boldsymbol{\tau}}_{\text{c}}^{\text{ve}}\right)_{\text{e}}}{u}\right)^{\alpha}\frac{6\alpha\tilde{G}_e}{u}\,,\end{aligned} \tag{B.53}$$

the second derivative reads:

$$\frac{\partial}{\partial \Gamma}\left[-a_1\frac{\widetilde{\phi}_{\text{v}}^{\text{pr}} + \Delta\widetilde{p}_{\text{c}}^{\text{ve}}}{v}\right] = a_1\left(\frac{\widetilde{\phi}_{\text{v}}^{\text{pr}} + \Delta\widetilde{p}_{\text{c}}^{\text{ve}}}{v}\right)\frac{2\beta\tilde{K}_e}{v} - \frac{a_1}{v}\frac{\partial \widetilde{p}_{\text{c}}^{\text{ve}}}{\partial \Gamma}\,, \tag{B.54}$$

where $\frac{\partial \text{dev } \widetilde{\boldsymbol{\tau}}_{\text{c}}^{\text{ve}}}{\partial \Gamma}$ and $\frac{\partial \widetilde{p}_{\text{c}}^{\text{ve}}}{\partial \Gamma}$ are given in Appendix B.5.1, and the third derivative reads $\frac{\partial a_0}{\partial \Gamma} = 0$.

Eq. (B.42) can now be solved in terms of Γ, using the derivative (B.44). This is achieved using a Newton-Raphson loop, in which the stress values are updated at each iteration with the new value of Γ. Following Eq. (B.28), these updates, which include the updated value of $\widetilde{p}_{\text{c}}^{\text{ve}}$, depend on the corrected logarithmic strain measure $(\mathbf{E}^{\text{ve,pr}} - \Gamma \mathbf{N})$, which due to its dependency on the normal $\mathbf{N}$, directly depends on the value of $\widetilde{p}_{\text{c}}^{\text{ve}}$. Therefore, the value of $\widetilde{p}_{\text{c}}^{\text{ve}}$ is obtained using a secondary Newton Raphson iterative process at fixed Γ. To that end, let us define a new function J_{v}:

$$0 = J_{\text{v}} = \hat{K}_\infty \left(T; T_{\text{Ref}}\right) \; f_K \left(\text{tr } \mathbf{E}^{\text{ve,pr}} - \Gamma \text{ tr } \mathbf{N}\right) \; \text{tr } \left(\mathbf{E}^{\text{ve,pr}} - \Gamma \mathbf{N}\right) - \widetilde{p}_{\text{c}}^{\text{ve}} \,, \tag{B.55}$$

with, following Eqs. (B.33) and (B.38),

$$\text{tr } \left(\mathbf{N}\right) = 2\beta \frac{\widetilde{\phi}_{\text{v}}^{\text{pr}} + \Delta \widetilde{p}_{\text{c}}^{\text{ve}}}{v} \,. \tag{B.56}$$

Noting that, at fixed Γ, $\left.\frac{\partial \text{tr} \mathbf{N}}{\partial \widetilde{p}_{\text{c}}^{\text{ve}}}\right|_\Gamma = \frac{2\beta}{v}$, and the Jacobian of Eq. (B.55) reads:

$$\left.\frac{\partial J_{\text{v}}}{\partial \widetilde{p}_{\text{c}}^{\text{ve}}}\right|_\Gamma = -\frac{2\beta\Gamma}{v} \hat{K}_\infty \left(T; T_{\text{Ref}}\right) \left[\text{tr } \left(\mathbf{E}^{\text{ve,pr}} - \Gamma \mathbf{N}\right) \; f_K' + f_K\right] - 1 \,, \tag{B.57}$$

with, using the definition of f_K in Eq. (66),

$$f_K' \left(\text{tr } \mathbf{E}^{\text{ve}}\right) = \frac{\partial f_K}{\partial \text{tr } \mathbf{E}^{\text{ve}}} = \frac{2 V_K \vartheta_K}{3} \left[1 - \tanh^2 \left(\frac{\vartheta_K}{3} \left(\text{tr } \mathbf{E}^{\text{ve}}\right)^2 - \zeta_K\right)\right] \text{ tr } \mathbf{E}^{\text{ve}} \,. \tag{B.58}$$

Similarly, following Eq. (B.26), the secondary Newton-Raphson loop related to the deviatoric part of the correcting terms aims at solving the equation

$$0 = \mathbf{J}_{\text{dev}} = 2\hat{G}_\infty \left(T; T_{\text{Ref}}\right) \; f_G \left(\text{dev } \mathbf{E}^{\text{ve,pr}} - \Gamma \text{ dev } \mathbf{N}\right) \text{ dev } \left(\mathbf{E}^{\text{ve,pr}} - \Gamma \mathbf{N}\right) - \text{dev } \widetilde{\boldsymbol{\tau}}_{\text{c}}^{\text{ve}} \,, \tag{B.59}$$

with following Eqs. (B.33) and (B.34),

$$\text{dev } \mathbf{N} = 3 \frac{\text{dev } \widetilde{\boldsymbol{\phi}}^{\text{pr}} + \Delta \text{dev } \widetilde{\boldsymbol{\tau}}_{\text{c}}^{\text{ve}}}{u} \,, \text{ and } \left.\frac{\partial \text{dev } \mathbf{N}}{\partial \text{dev } \widetilde{\boldsymbol{\tau}}_{\text{c}}^{\text{ve}}}\right|_\Gamma = \frac{3}{u} \left(\mathcal{I} - \frac{1}{3} \mathbf{I} \otimes \mathbf{I}\right) \,. \tag{B.60}$$

Therefore, the Jacobian of Eq. (B.59) reads:

$$\begin{aligned} \left.\frac{\partial \mathbf{J}_{\text{dev}}}{\partial \text{dev } \widetilde{\boldsymbol{\tau}}_{\text{c}}^{\text{ve}}}\right|_\Gamma = & -\frac{6\Gamma}{u} \hat{G}_\infty \left(T; T_{\text{Ref}}\right) \left[\text{dev } \left(\mathbf{E}^{\text{ve,pr}} - \Gamma \mathbf{N}\right) \otimes \mathbf{f}_G' + f_G \left(\mathcal{I} - \frac{1}{3} \mathbf{I} \otimes \mathbf{I}\right)\right] \\ & - \left(\mathcal{I} - \frac{1}{3} \mathbf{I} \otimes \mathbf{I}\right) \,, \end{aligned} \tag{B.61}$$

where, using the definition of f_G in Eq. (67),

$$\begin{aligned} \mathbf{f}_G' \left(\text{dev } \mathbf{E}^{\text{ve}}\right) = \frac{\partial f_G}{\partial \text{dev } \mathbf{E}^{\text{ve}}} = & \; 2 V_G \vartheta_G \left[1 - \tanh^2 \left(\vartheta_G \text{dev } \mathbf{E}^{\text{ve}} : \text{dev } \mathbf{E}^{\text{ve}} - \zeta_G\right)\right] \\ & \text{dev } \mathbf{E}^{\text{ve}} \,. \end{aligned} \tag{B.62}$$

Appendix B.4. Material operator

Let us define the deformation gradient tensor

$$\mathbf{F}^{\text{ve-p}} = \mathbf{F} \cdot \mathbf{F}^{\text{th}^{-1}} \cdot \mathbf{F}^{\text{f}^{-1}} , \tag{B.63}$$

as the deformation gradient acting as an input of the viscoelastic-plastic constitutive law, with $\mathbf{F}^{\text{f}} = \mathbf{I}$ for the amorphous phase. Similarly, using Eqs. (41-43), we define the first Piola Kirchhoff stress tensor

$$\widetilde{\mathbf{P}}^{\text{ve-p}} = \widetilde{\mathbf{P}} \cdot \mathbf{F}^{\text{th}^{\text{T}}} \cdot \mathbf{F}^{\text{f}^{\text{T}}} = \mathbf{F}^{\text{ve}} \cdot \widetilde{\mathbf{S}}^{\text{ve}} \cdot \mathbf{F}^{\text{p}^{-\text{T}}} , \tag{B.64}$$

as the output of the viscoelastic-plastic constitutive law. Finally, the corresponding tangent operator $\widetilde{\mathbb{C}}^{\text{ve-p}}$ can be obtained as:

$$\begin{aligned} \widetilde{\mathbb{C}}^{\text{ve-p}} = \frac{\partial \widetilde{\mathbf{P}}^{\text{ve-p}}}{\partial \mathbf{F}^{\text{ve-p}}} \quad = \quad & \frac{\partial \mathbf{F}^{\text{ve}}}{\partial \mathbf{F}^{\text{ve-p}}}^{2} \cdot \left(\widetilde{\mathbf{S}}^{\text{ve}} \cdot \mathbf{F}^{\text{p}^{-\text{T}}} \right) + \\ & \mathbf{F}^{\text{ve}} \cdot^{1} \frac{\partial \widetilde{\mathbf{S}}^{\text{ve}}}{\partial \mathbf{F}^{\text{ve-p}}}^{2} \cdot \mathbf{F}^{\text{p}^{-\text{T}}} + \left(\mathbf{F}^{\text{ve}} \cdot \widetilde{\mathbf{S}}^{\text{ve}} \right) \cdot \frac{\partial \mathbf{F}^{\text{p}^{-\text{T}}}}{\partial \mathbf{F}^{\text{ve-p}}} , \end{aligned} \tag{B.65}$$

where $^{i}\cdot$ ($\cdot^{i}$) is the i^{th} left (right) dot product operator of two tensors considering i^{th} index of the left (right) tensor.

The relation $\mathbf{F}^{\text{ve}} = \mathbf{F}^{\text{ve-p}} \cdot \mathbf{F}^{\text{p}^{-1}}$ allows writing:

$$\frac{\partial \mathbf{F}^{\text{ve}}}{\partial \mathbf{F}^{\text{ve-p}}} = (\mathbf{I} \otimes \mathbf{I})^{2} \cdot \mathbf{F}^{\text{p}^{-1}} + \mathbf{F}^{\text{ve-p}} \cdot \frac{\partial \mathbf{F}^{\text{p}^{-1}}}{\partial \mathbf{F}^{\text{ve-p}}} . \tag{B.66}$$

In order to compute the tangent operator $\widetilde{\mathbb{C}}^{\text{ve-p}}$ (B.65), the terms $\frac{\partial \widetilde{\mathbf{S}}^{\text{ve}}}{\partial \mathbf{F}^{\text{ve-p}}}$ and $\frac{\partial \mathbf{F}^{\text{p}}}{\partial \mathbf{F}^{\text{ve-p}}}$ need to be computed. The definition of the right Cauchy strain tensor $\mathbf{C}^{\text{ve-p}} = \mathbf{F}^{\text{ve-p}^{\text{T}}} \cdot \mathbf{F}^{\text{ve-p}}$ yields:

$$\frac{\partial \bullet}{\partial \mathbf{F}^{\text{ve-p}}} = \frac{\partial \bullet}{\partial \mathbf{C}^{\text{ve-p}}} : \frac{\partial \mathbf{C}^{\text{ve-p}}}{\partial \mathbf{F}^{\text{ve-p}}} = 2 \frac{\partial \bullet}{\partial \mathbf{C}^{\text{ve-p}}}^{4} \cdot \mathbf{F}^{\text{ve-p}^{\text{T}}} , \tag{B.67}$$

since $\mathbf{C}^{\text{ve-p}}$ is symmetrical and where $\bullet$ represents an arbitrary tensor field. Using Eqs. (B.7-B.8) leads to:

$$\frac{\partial \bullet}{\partial \mathbf{C}^{\text{ve-p}}} \quad = \quad \mathbf{F}_{n}^{\text{p}^{-1}} \cdot^{3} \frac{\partial \bullet}{\partial \mathbf{C}^{\text{ve,pr}}}^{4} \cdot \mathbf{F}_{n}^{\text{p}^{-\text{T}}} . \tag{B.68}$$

The remaining derivatives with respect to $\mathbf{C}^{\text{ve,pr}}$ can be found in Appendix B.5.2.

Finally, using the definition of $\widetilde{\mathbf{P}}^{\text{ve-p}}$ in Eq. (B.64), the complete material operator

can be obtained using Eq. (B.63) as

$$\begin{aligned}
\widetilde{\mathbb{C}} &= \frac{\partial \widetilde{\mathbf{P}}}{\partial \mathbf{F}} = \frac{\partial \widetilde{\mathbf{P}}^{\text{ve-p}}}{\partial \mathbf{F}}\,^{2}\cdot \mathbf{F}^{\text{f}^{-\text{T}}}\cdot \mathbf{F}^{\text{th}^{-\text{T}}} + \widetilde{\mathbf{P}}^{\text{ve-p}}\cdot \frac{\partial \mathbf{F}^{\text{f}^{-\text{T}}}}{\partial \mathbf{F}}\,^{2}\cdot \mathbf{F}^{\text{th}^{-\text{T}}} + \widetilde{\mathbf{P}}^{\text{ve-p}}\cdot \mathbf{F}^{\text{f}^{-\text{T}}}\cdot \frac{\partial \mathbf{F}^{\text{th}^{-\text{T}}}}{\partial \mathbf{F}} \\
&= \left[\widetilde{\mathbb{C}}^{\text{ve-p}} :^{1,3} \left(\mathbf{I}\otimes\left(\mathbf{F}^{\text{f}^{-\text{T}}}\cdot \mathbf{F}^{\text{th}^{-\text{T}}}\right)\right)\right]^{2}\cdot \mathbf{F}^{\text{f}^{-\text{T}}}\cdot \mathbf{F}^{\text{th}^{-\text{T}}} + \\
&\quad \left[\widetilde{\mathbb{C}}^{\text{ve-p}} : \left[\mathbf{F}\cdot \frac{\partial \mathbf{F}^{\text{th}^{-1}}}{\partial \mathbf{F}}\,^{2}\cdot \mathbf{F}^{\text{f}^{-1}}\right]\right]^{2}\cdot \mathbf{F}^{\text{f}^{-\text{T}}}\cdot \mathbf{F}^{\text{th}^{-\text{T}}} + \\
&\quad \left[\widetilde{\mathbb{C}}^{\text{ve-p}} : \left[\mathbf{F}\cdot \mathbf{F}^{\text{th}^{-1}}\cdot \frac{\partial \mathbf{F}^{\text{f}^{-1}}}{\partial \mathbf{F}}\right]\right]^{2}\cdot \mathbf{F}^{\text{f}^{-\text{T}}}\cdot \mathbf{F}^{\text{th}^{-\text{T}}} + \\
&\quad \widetilde{\mathbf{P}}^{\text{ve-p}}\cdot \frac{\partial \mathbf{F}^{\text{f}^{-\text{T}}}}{\partial \mathbf{F}}\,^{2}\cdot \mathbf{F}^{\text{th}^{-\text{T}}} + \widetilde{\mathbf{P}}^{\text{ve-p}}\cdot \mathbf{F}^{\text{f}^{-\text{T}}}\cdot \frac{\partial \mathbf{F}^{\text{th}^{-\text{T}}}}{\partial \mathbf{F}}\,,
\end{aligned} \tag{B.69}$$

with the corresponding tangent operator $\widetilde{\mathbb{C}}^{\text{ve-p}}$ obtained in (B.65).

The derivation with respect to the temperature follows a similar procedure.

Appendix B.5. Derivative of correctors terms

Appendix B.5.1. Derivatives with respect to the plastic multiplier integral Γ

Starting from Eq. (B.26), and noting that $\mathbf{N}$ depends on Γ as well, the derivative of dev $\widetilde{\boldsymbol{\tau}}_{\text{c}}^{\text{ve}}$ writes:

$$\begin{aligned}
\frac{\partial \text{dev}\ \widetilde{\boldsymbol{\tau}}_{\text{c}}^{\text{ve}}}{\partial \Gamma} &= 2\hat{G}_{\infty}\left(T;T_{\text{Ref}}\right)\ \mathbf{f}'_{G}\left(\text{dev}\ \mathbf{E}^{\text{ve,pr}} - \Gamma\ \text{dev}\ \mathbf{N}\right) : \frac{\partial \text{dev}\ \mathbf{E}^{\text{ve}}}{\partial \Gamma}\ \text{dev}\ \left(\mathbf{E}^{\text{ve,pr}} - \Gamma\mathbf{N}\right) + \\
&\quad 2\hat{G}_{\infty}\left(T;T_{\text{Ref}}\right)\ f_{G}\left(\text{dev}\ \mathbf{E}^{\text{ve,pr}} - \Gamma\ \text{dev}\ \mathbf{N}\right)\frac{\partial \text{dev}\ \mathbf{E}^{\text{ve}}}{\partial \Gamma}\,,
\end{aligned} \tag{B.70}$$

where $\mathbf{f}'_{G}$ is given in Eq. (B.62). In order to obtain the derivative (B.70), after evaluating $\frac{\partial \text{dev}\ \mathbf{E}^{\text{ve}}}{\partial \Gamma}$, from Eq. (B.39), the system of equations can be written in a compact way

$$\begin{aligned}
&\left[\mathcal{I} + \frac{6\Gamma}{u}\hat{G}_{\infty}\left(T;T_{\text{Ref}}\right)\left[\text{dev}\ \left(\mathbf{E}^{\text{ve,pr}} - \Gamma\mathbf{N}\right)\otimes \mathbf{f}'_{G} + f_{G}\mathcal{I}\right]\right] : \frac{\partial \text{dev}\ \widetilde{\boldsymbol{\tau}}_{\text{c}}^{\text{ve}}}{\partial \Gamma} = \\
&\frac{-6}{u^{2}}\hat{G}_{\infty}\left(T;T_{\text{Ref}}\right)\left[\text{dev}\ \left(\mathbf{E}^{\text{ve,pr}} - \Gamma\mathbf{N}\right)\otimes \mathbf{f}'_{G} + f_{G}\mathcal{I}\right] : \left(\text{dev}\ \widetilde{\boldsymbol{\phi}}^{\text{pr}} + \Delta\text{dev}\ \widetilde{\boldsymbol{\tau}}_{\text{c}}^{\text{ve}}\right)\,,
\end{aligned} \tag{B.71}$$

yielding the solution $\frac{\partial \text{dev}\ \widetilde{\boldsymbol{\tau}}_{\text{c}}^{\text{ve}}}{\partial \Gamma}$.

Similarly, starting from Eq. (B.28), it comes

$$\frac{\partial \widetilde{p}_{\text{c}}^{\text{ve}}}{\partial \Gamma} = -\frac{2\beta\hat{K}_{\infty}\left(T;T_{\text{Ref}}\right)}{v^{2}}\frac{\left(f'_{K}\ \text{tr}\ \left(\mathbf{E}^{\text{ve,pr}} - \Gamma\mathbf{N}\right) + f_{K}\right)\left(\widetilde{\phi}_{\text{v}}^{\text{pr}} + \Delta\widetilde{p}_{\text{c}}^{\text{ve}}\right)}{1 + \frac{2\beta\Gamma}{v}\hat{K}_{\infty}\left(T;T_{\text{Ref}}\right)\left(f_{K} + \text{tr}\ \left(\mathbf{E}^{\text{ve,pr}} - \Gamma\mathbf{N}\right)\ f'_{K}\right)}\,, \tag{B.72}$$

with the expression of f'_{K} provided in Eq. (B.58).

Appendix B.5.2. Derivatives with respect to the predictor strain

Derivative of the corotational Kirchhoff stress predictor. Dividing into its volumetric and deviatoric parts, the derivative of the volumetric predictor of the corotational Kirchhoff stress (B.9) writes:

$$\frac{\partial \widetilde{p}^{\mathrm{ve,pr}}}{\partial \mathbf{C}^{\mathrm{ve,pr}}} = \frac{K_e}{2}\mathbf{I} : \mathcal{L}^{\mathrm{pr}} + \frac{\partial \widetilde{p}_{\mathrm{c}}^{\mathrm{ve,pr}}}{\partial \mathbf{C}^{\mathrm{ve,pr}}}\,, \tag{B.73}$$

where:

$$\mathcal{L}^{\mathrm{pr}} = \left.\frac{\partial \ln \mathbf{C}^{\mathrm{ve}}}{\partial \mathbf{C}^{\mathrm{ve}}}\right|_{\mathbf{C}^{\mathrm{ve,pr}}}\,, \tag{B.74}$$

and where:

$$\frac{\partial \widetilde{p}_{\mathrm{c}}^{\mathrm{ve,pr}}}{\partial \mathbf{C}^{\mathrm{ve,pr}}} = \frac{\hat{K}_\infty\left(T;\, T_{\mathrm{Ref}}\right)}{2}\left[f_K + f_K' \mathrm{tr}\ \mathbf{E}^{\mathrm{ve,pr}}\right]\mathbf{I} : \mathcal{L}^{\mathrm{pr}}\,. \tag{B.75}$$

For the deviatoric part of the predictor Kirchhoff stress (B.9) one has:

$$\frac{\partial \mathrm{dev}\ \widetilde{\boldsymbol{\tau}}^{\mathrm{ve,pr}}}{\partial \mathbf{C}^{\mathrm{ve,pr}}} = G_e\left(\mathcal{I} - \frac{1}{3}\mathbf{I}\otimes\mathbf{I}\right) : \mathcal{L}^{\mathrm{pr}} + \frac{\partial \mathrm{dev}\ \widetilde{\boldsymbol{\tau}}_{\mathrm{c}}^{\mathrm{ve,pr}}}{\partial \mathbf{C}^{\mathrm{ve,pr}}}\,, \tag{B.76}$$

where:

$$\frac{\partial \mathrm{dev}\ \widetilde{\boldsymbol{\tau}}_{\mathrm{c}}^{\mathrm{ve,pr}}}{\partial \mathbf{C}^{\mathrm{ve,pr}}} = \hat{G}_\infty\left(T;\, T_{\mathrm{Ref}}\right)\ \left[f_G\mathcal{I} + \mathrm{dev}\ \mathbf{E}^{\mathrm{ve,pr}} \otimes \mathbf{f}_G'\right] : \left(\mathcal{I} - \frac{1}{3}\mathbf{I}\otimes\mathbf{I}\right) : \mathcal{L}^{\mathrm{pr}}\,. \tag{B.77}$$

Derivative of the yield condition at constant plastic multiplier integral Γ. The derivative of yield condition with respect to the logarithm strain predictor at constant Γ reads:

$$\left.\frac{dF}{d\mathbf{E}^{\mathrm{ve,pr}}}\right|_{\Gamma} = \frac{\partial F}{\partial \Delta\gamma}\frac{\partial \Delta\gamma}{\partial \mathbf{E}^{\mathrm{ve,pr}}} + \frac{\partial F}{\partial \mathbf{E}^{\mathrm{ve,pr}}}\,, \tag{B.78}$$

where the derivative $\frac{\partial F}{\partial \Delta\gamma}$ is given in Eq. (B.45) and where the derivatives $\frac{\partial \Delta\gamma}{\partial \mathbf{E}^{\mathrm{ve\,pr}}}$ and $\frac{\partial F}{\partial \mathbf{E}^{\mathrm{ve\,pr}}}$ are now explicited.

- The derivative $\frac{\partial \Delta\gamma}{\partial \mathbf{E}^{\mathrm{ve,pr}}}$ follows from Eqs. (B.40-B.41)

$$\frac{\partial \Delta\gamma}{\partial \mathbf{E}^{\mathrm{ve,pr}}} = k\Gamma\frac{\partial A}{\partial \mathbf{E}^{\mathrm{ve,pr}}}\,, \tag{B.79}$$

with

$$\begin{aligned}\frac{\partial A}{\partial \mathbf{E}^{\mathrm{ve,pr}}} = &\frac{1}{2A}\frac{\partial}{\partial \mathbf{E}^{\mathrm{ve,pr}}}\left[6\left(\frac{\left(\mathrm{dev}\ \widetilde{\boldsymbol{\phi}}^{\mathrm{pr}} + \Delta\mathrm{dev}\ \widetilde{\boldsymbol{\tau}}_{\mathrm{c}}^{\mathrm{ve}}\right)_{\mathrm{e}}}{u}\right)^2\right] + \\ &\frac{1}{2A}\frac{\partial}{\partial \mathbf{E}^{\mathrm{ve,pr}}}\left[\frac{4}{3}\beta^2\left(\frac{\widetilde{\phi}_{\mathrm{v}}^{\mathrm{pr}} + \Delta\widetilde{p}_{\mathrm{c}}^{\mathrm{ve}}}{v}\right)^2\right]\end{aligned} \tag{B.80}$$

The first derivative reads:

$$\frac{\partial}{\partial \mathbf{E}^{\mathrm{ve,pr}}}\left[6\left(\frac{\left(\operatorname{dev}\widetilde{\boldsymbol{\phi}}^{\mathrm{pr}}+\Delta\operatorname{dev}\widetilde{\boldsymbol{\tau}}_{\mathrm{c}}^{\mathrm{ve}}\right)_{\mathrm{e}}}{u}\right)^{2}\right]=$$
$$\frac{18\left(\operatorname{dev}\widetilde{\boldsymbol{\phi}}^{\mathrm{pr}}+\Delta\operatorname{dev}\widetilde{\boldsymbol{\tau}}_{\mathrm{c}}^{\mathrm{ve}}\right)}{u^{2}}:\left[2G_{e}\left(\mathcal{I}-\frac{1}{3}\mathbf{I}\otimes\mathbf{I}\right)+\frac{\partial\operatorname{dev}\widetilde{\boldsymbol{\tau}}_{\mathrm{c}}^{\mathrm{ve}}}{\partial\mathbf{E}^{\mathrm{ve\,pr}}}\right], \quad \text{(B.81)}$$

and the second derivative reads:

$$\frac{\partial}{\partial \mathbf{E}^{\mathrm{ve,pr}}}\left[\frac{4}{3}\beta^{2}\left(\frac{\widetilde{\phi}_{\mathrm{v}}^{\mathrm{pr}}+\Delta\widetilde{p}_{\mathrm{c}}^{\mathrm{ve}}}{v}\right)^{2}\right]=\frac{8\beta^{2}\left(\widetilde{\phi}_{\mathrm{v}}^{\mathrm{pr}}+\Delta\widetilde{p}_{\mathrm{c}}^{\mathrm{ve}}\right)}{3v^{2}}\left(K_{e}\mathbf{I}+\frac{\partial\widetilde{p}_{\mathrm{c}}^{\mathrm{ve}}}{\partial\mathbf{E}^{\mathrm{ve\,pr}}}\right).$$

- The derivative $\frac{\partial F}{\partial \mathbf{E}^{\mathrm{ve,pr}}}$ follows from Eq. (84):

$$\frac{\partial F}{\partial \mathbf{E}^{\mathrm{ve,pr}}}=\frac{\partial}{\partial \mathbf{E}^{\mathrm{ve,pr}}}\left(a_{2}\left(\frac{\left(\operatorname{dev}\widetilde{\boldsymbol{\phi}}^{\mathrm{pr}}+\Delta\operatorname{dev}\widetilde{\boldsymbol{\tau}}_{\mathrm{c}}^{\mathrm{ve}}\right)_{\mathrm{e}}}{u}\right)^{\alpha}-a_{1}\frac{\widetilde{\phi}_{\mathrm{v}}^{\mathrm{pr}}+\Delta\widetilde{p}_{\mathrm{c}}^{\mathrm{ve}}}{v}-a_{0}\right), \quad \text{(B.82)}$$

where the first derivative reads:

$$\frac{\partial}{\partial \mathbf{E}^{\mathrm{ve,pr}}}\left(a_{2}\left(\frac{\left(\operatorname{dev}\widetilde{\boldsymbol{\phi}}^{\mathrm{pr}}+\Delta\operatorname{dev}\widetilde{\boldsymbol{\tau}}_{\mathrm{c}}^{\mathrm{ve}}\right)_{\mathrm{e}}}{u}\right)^{\alpha}\right)=$$
$$\frac{3a_{2}\alpha\left(\left(\operatorname{dev}\widetilde{\boldsymbol{\phi}}^{\mathrm{pr}}+\Delta\operatorname{dev}\widetilde{\boldsymbol{\tau}}_{\mathrm{c}}^{\mathrm{ve}}\right)_{\mathrm{e}}\right)^{\alpha-2}}{2u^{\alpha}}\left(\operatorname{dev}\widetilde{\boldsymbol{\phi}}^{\mathrm{pr}}+\Delta\operatorname{dev}\widetilde{\boldsymbol{\tau}}_{\mathrm{c}}^{\mathrm{ve}}\right):$$
$$\left[2G_{e}\left(\mathcal{I}-\frac{1}{3}\mathbf{I}\otimes\mathbf{I}\right)+\frac{\partial\operatorname{dev}\widetilde{\boldsymbol{\tau}}_{\mathrm{c}}^{\mathrm{ve}}}{\partial\mathbf{E}^{\mathrm{ve\,pr}}}\right], \quad \text{(B.83)}$$

the second derivative reads:

$$\frac{\partial}{\partial \mathbf{E}^{\mathrm{ve,pr}}}\left(-a_{1}\frac{\widetilde{\phi}_{\mathrm{v}}^{\mathrm{pr}}+\Delta\widetilde{p}_{\mathrm{c}}^{\mathrm{ve}}}{v}\right)=-\frac{a_{1}}{v}\left(K_{e}\mathbf{I}+\frac{\partial\widetilde{p}_{\mathrm{c}}^{\mathrm{ve}}}{\partial\mathbf{E}^{\mathrm{ve\,pr}}}\right), \quad \text{(B.84)}$$

and the third derivative reads

$$\frac{\partial}{\partial \mathbf{E}^{\mathrm{ve,pr}}}(-a_{0})=0\,. \quad \text{(B.85)}$$

- The derivative $\frac{\partial\widetilde{p}_{\mathrm{c}}^{\mathrm{ve}}}{\partial \mathbf{E}^{\mathrm{ve,pr}}}$ follows from (B.28), and using Eq. (B.39) to evaluate $\frac{\partial\operatorname{tr}\mathbf{E}^{\mathrm{ve}}}{\partial \mathbf{E}^{\mathrm{ve,pr}}}$, yielding

$$\frac{\partial\widetilde{p}_{\mathrm{c}}^{\mathrm{ve}}}{\partial \mathbf{E}^{\mathrm{ve,pr}}}=\frac{\hat{K}_{\infty}\left(T;T_{\mathrm{Ref}}\right)\left(1-\frac{2\beta\Gamma K_{e}}{v}\right)\left(f_{K}+f_{K}'\ \operatorname{tr}\ \left(\mathbf{E}^{\mathrm{ve,pr}}-\Gamma\mathbf{N}\right)\right)}{1+\frac{2\beta\Gamma\hat{K}_{\infty}(T;T_{\mathrm{Ref}})}{v}\left(f_{K}+f_{K}'\ \operatorname{tr}\ \left(\mathbf{E}^{\mathrm{ve,pr}}-\Gamma\mathbf{N}\right)\right)}\mathbf{I}\,. \quad \text{(B.86)}$$

- The derivative $\frac{\partial \text{dev } \widetilde{\boldsymbol{\tau}}_{\text{c}}^{\text{ve}}}{\partial \mathbf{E}^{\text{ve,pr}}}$ follows from Eq. (B.26), and using Eq. (B.39) to evaluate $\frac{\partial \text{dev } \mathbf{E}^{\text{ve}}}{\partial \mathbf{E}^{\text{ve,pr}}}$, yielding

$$\mathcal{S} : \frac{\partial \text{dev } \widetilde{\boldsymbol{\tau}}_{\text{c}}^{\text{ve}}}{\partial \mathbf{E}^{\text{ve,pr}}} = 2\hat{G}_{\infty}\left(T; T_{\text{Ref}}\right) \left(1 - \frac{6G_e\Gamma}{u}\right) \left[\text{dev } \left(\mathbf{E}^{\text{ve,pr}} - \Gamma\mathbf{N}\right) \otimes \mathbf{f}'_G : \left(\mathcal{I} - \frac{1}{3}\mathbf{I}\otimes\mathbf{I}\right) + f_G\left(\mathcal{I} - \frac{1}{3}\mathbf{I}\otimes\mathbf{I}\right)\right], \quad \text{(B.87)}$$

with the fourth order tensor

$$\mathcal{S} = \left(1 + \frac{6\Gamma\hat{G}_{\infty}\left(T; T_{\text{Ref}}\right)}{u} f_G\right)\left(\mathcal{I} - \frac{1}{3}\mathbf{I}\otimes\mathbf{I}\right) + \frac{6\Gamma\hat{G}_{\infty}\left(T; T_{\text{Ref}}\right)}{u} \left(\mathbf{E}^{\text{ve,pr}} - \Gamma\mathbf{N}\right) \otimes \mathbf{f}'_G : \left(\mathcal{I} - \frac{1}{3}\mathbf{I}\otimes\mathbf{I}\right). \quad \text{(B.88)}$$

Derivative of the plastic strain increment. The derivative $\frac{d\Delta\gamma}{d\mathbf{E}^{\text{ve pr}}}$ can then be computed as:

$$\frac{d\Delta\gamma}{d\mathbf{E}^{\text{ve pr}}} = \frac{\partial\Delta\gamma}{\partial\Gamma}\frac{\partial\Gamma}{\partial\mathbf{E}^{\text{ve pr}}} + \frac{\partial\Delta\gamma}{\partial\mathbf{E}^{\text{ve pr}}} = k\left(A + \Gamma\frac{\partial A}{\partial\Gamma}\right)\frac{\partial\Gamma}{\partial\mathbf{E}^{\text{ve pr}}} + k\Gamma\frac{\partial A}{\partial\mathbf{E}^{\text{ve pr}}}, \quad \text{(B.89)}$$

where $\frac{\partial A}{\partial \mathbf{E}^{\text{ve,pr}}}$ comes from Eq. (B.80), $\frac{\partial A}{\partial \Gamma}$ from Eq. (B.50) and $\frac{\partial \Gamma}{\partial \mathbf{E}^{\text{ve,pr}}}$ is computed from the consistency condition of the yield condition. This consistency writes $\text{d}F\left(\mathbf{C}^{\text{ve,pr}}, \Delta\gamma, \Gamma\right) = 0$, yielding:

$$\frac{\partial\Gamma}{\partial\mathbf{E}^{\text{ve,pr}}} = -\left(\frac{dF}{d\Gamma}\right)^{-1} \left.\frac{dF}{d\mathbf{E}^{\text{ve,pr}}}\right|_{\Gamma}, \quad \text{(B.90)}$$

where $\frac{dF}{d\Gamma}$ is solved in Eq. (B.44) and $\left.\frac{dF}{d\mathbf{E}^{\text{ve,pr}}}\right|_{\Gamma}$ in Eq. (B.78).

Derivative of the normal. Starting from Eq. (B.39), the derivatives with respect to the logarithmic strain measure of the deviatoric and trace of the normal $\mathbf{N}$ write:

$$\frac{\partial \text{dev } \mathbf{N}}{\partial \mathbf{E}^{\text{ve,pr}}} = \frac{3}{u}\left[2G_e\left(\mathcal{I} - \frac{1}{3}\mathbf{I}\otimes\mathbf{I}\right) + \frac{\partial \text{dev } \widetilde{\boldsymbol{\tau}}_{\text{c}}^{\text{ve}}}{\partial \mathbf{E}^{\text{ve,pr}}}\right] + \left[\frac{3}{u}\frac{\partial \text{dev } \widetilde{\boldsymbol{\tau}}_{\text{c}}^{\text{ve}}}{\partial\Gamma} - \frac{18}{u^2}\tilde{G}_e(\text{dev } \widetilde{\boldsymbol{\phi}}^{\text{pr}} + \Delta\text{dev } \widetilde{\boldsymbol{\tau}}_{\text{c}}^{\text{ve}})\right] \otimes \frac{\partial\Gamma}{\partial\mathbf{E}^{\text{ve,pr}}}. \quad \text{(B.91)}$$

and

$$\frac{\partial \text{tr}\mathbf{N}}{\partial \mathbf{E}^{\text{ve,pr}}} = \frac{2\beta}{v}\left(K_e\mathbf{I} + \frac{\partial \widetilde{p}_{\text{c}}^{\text{ve}}}{\partial \mathbf{E}^{\text{ve,pr}}}\right) + \left[\frac{2\beta}{v}\frac{\partial \widetilde{p}_{\text{c}}^{\text{ve}}}{\partial\Gamma} - \frac{4\beta^2\tilde{K}_e}{v^2}\left(\widetilde{\phi}_{\text{v}}^{\text{pr}} + \Delta\widetilde{p}_{\text{c}}^{\text{ve}}\right)\right]\frac{\partial\Gamma}{\partial\mathbf{E}^{\text{ve,pr}}}. \quad \text{(B.92)}$$

Derivative of the stress tensors. Starting from Eqs. (B.29-B.30), it comes

$$\frac{\partial \text{dev } \widetilde{\boldsymbol{\tau}}^{\text{ve}}}{\partial \mathbf{E}^{\text{ve,pr}}} = \frac{\partial(\text{dev } \widetilde{\boldsymbol{\tau}}^{\text{ve,pr}} - \text{dev } \widetilde{\boldsymbol{\tau}}_{\text{c}}^{\text{ve,pr}})}{\partial \mathbf{E}^{\text{ve,pr}}} + \frac{\partial \text{dev } \widetilde{\boldsymbol{\tau}}_{\text{c}}^{\text{ve}}}{\partial \mathbf{E}^{\text{ve,pr}}} + \frac{\partial \text{dev } \widetilde{\boldsymbol{\tau}}_{\text{c}}^{\text{ve}}}{\partial \Gamma} \otimes \frac{\partial \Gamma}{\partial \mathbf{E}^{\text{ve,pr}}} - 2G_e\Gamma \frac{\partial \text{dev } \mathbf{N}}{\partial \mathbf{E}^{\text{ve,pr}}} - 2G_e \text{dev } \mathbf{N} \otimes \frac{\partial \Gamma}{\partial \mathbf{E}^{\text{ve,pr}}}, \tag{B.93}$$

and starting from Eqs. (B.35-B.36), it comes

$$\frac{\partial \widetilde{p}^{\text{ve}}}{\partial \mathbf{E}^{\text{ve,pr}}} = K_e \mathbf{I} - K_e \Gamma \frac{\partial \, \text{tr } \mathbf{N}}{\partial \mathbf{E}^{\text{ve,pr}}} - K_e \, \text{tr } \mathbf{N} \frac{\partial \Gamma}{\partial \mathbf{E}^{\text{ve,pr}}} + \frac{\partial \widetilde{p}_{\text{c}}^{\text{ve}}}{\partial \Gamma} \frac{\partial \Gamma}{\partial \mathbf{E}^{\text{ve,pr}}} + \frac{\partial \widetilde{p}_{\text{c}}^{\text{ve}}}{\partial \mathbf{E}^{\text{ve,pr}}}. \tag{B.94}$$

Finally one has:

$$\frac{\partial \widetilde{\mathbf{S}}^{\text{ve}}}{\partial \mathbf{C}^{\text{ve,pr}}} = \frac{\partial \mathcal{L}^{\text{ve}}}{\partial \mathbf{C}^{\text{ve,pr}}}^{3,4} : \widetilde{\boldsymbol{\tau}}^{\text{ve}} + \mathcal{L}^{\text{ve}} : \frac{\partial \widetilde{\boldsymbol{\tau}}^{\text{ve}}}{\partial \mathbf{C}^{\text{ve,pr}}}. \tag{B.95}$$

Derivative of the plastic deformation gradient. $\frac{\partial \mathbf{F}^{\text{p}}}{\partial \mathbf{C}^{\text{ve,pr}}}$ have to be estimated. Eq. (B.19) leads to

$$\frac{\partial \mathbf{F}^{\text{p}}}{\partial \mathbf{C}^{\text{ve,pr}}} = \left[\boldsymbol{\mathcal{E}} : \left(\mathbf{N} \otimes \frac{\partial \Gamma}{\partial \mathbf{C}^{\text{ve,pr}}} + \Gamma \frac{\partial \text{dev } \mathbf{N}}{\partial \mathbf{C}^{\text{ve,pr}}} + \frac{\Gamma}{3} \mathbf{I} \otimes \frac{\partial \text{tr } \mathbf{N}}{\partial \mathbf{C}^{\text{ve,pr}}} \right) \right]^{2} \cdot \mathbf{F}_n^{\text{p}}, \tag{B.96}$$

where $\boldsymbol{\mathcal{E}}$ is given by

$$\boldsymbol{\mathcal{E}} = \frac{\partial \exp \mathbf{A}}{\partial \mathbf{A}}\Big|_{\Gamma \mathbf{N}}, \tag{B.97}$$

and where all the other derivatives where given here above.

References

Boatti, E., Scalet, G., Auricchio, F., 2016. A three-dimensional finite-strain phenomenological model for shape-memory polymers: Formulation, numerical simulations, and comparison with experimental data. International Journal of Plasticity 83, 153–177. URL: https://www.sciencedirect.com/science/article/pii/S0749641916300572, doi:https://doi.org/10.1016/j.ijplas.2016.04.008.

Buckley, P., McKinley, G., Wilson, T., Small, W., Benett, W., Bearinger, J., McElfresh, M., Maitland, D., 2006. Inductively heated shape memory polymer for the magnetic actuation of medical devices. IEEE Transactions on Biomedical Engineering 53, 2075–2083. URL: https://pubmed.ncbi.nlm.nih.gov/17019872/, doi:https://doi.org/10.1109/TBME.2006.877113.

Choy, C.L., Chen, F.C., Young, K., 1981. Negative thermal expansion in oriented crystalline polymers. Journal of Polymer Science: Polymer Physics Edition 19, 335–352. URL: https://onlinelibrary.wiley.com/doi/abs/10.1002/pol.1981.180190213, doi:https://doi.org/10.1002/pol.1981.180190213, arXiv:https://onlinelibrary.wiley.com/doi/pdf/10.1002/pol.1981.180190213.

Chung, T., Romo-Uribe, A., Mather, P.T., 2008. Two-way reversible shape memory in a semicrystalline network. Macromolecules 41, 184–192. URL: https://doi.org/10.1021/ma071517z, doi:10.1021/ma071517z, arXiv:https://doi.org/10.1021/ma071517z.

Defize, T., Riva, R., Jérôme, C., Alexandre, M., 2012. Multifunctional poly(ϵ-caprolactone)-forming networks by diels–alder cycloaddition: Effect of the adduct on the shape-memory properties. Macromolecular Chemistry and Physics 213, 187–197.

Diani, J., Gilormini, P., Frédy, C., Rousseau, I., 2012. Predicting thermal shape memory of crosslinked polymer networks from linear viscoelasticity. International Journal of Solids and Structures 49, 793–799. URL: https://www.sciencedirect.com/science/article/pii/S002076831100401X, doi:https://doi.org/10.1016/j.ijsolstr.2011.11.019.

Ge, Q., Luo, X., Rodriguez, E.D., Zhang, X., Mather, P.T., Dunn, M.L., Qi, H.J., 2012. Thermomechanical behavior of shape memory elastomeric composites. Journal of the Mechanics and Physics of Solids 60, 67–83. URL: https://www.sciencedirect.com/science/article/pii/S0022509611001852, doi:https://doi.org/10.1016/j.jmps.2011.09.011.

Gülaşik, H., Houbben, M., Sànchez, C.P., Calleja Vázquez, J.M., Vanderbemden, P., Jérôme, C., Noels, L., 2023. Data of A Thermo-Mechanical, Viscoelasto-Plastic Model for Semi-Crystalline Polymers Exhibiting One-Way and Two-Way Shape Memory Effects Under Phase Change. URL: https://doi.org/10.5281/zenodo.10822690, doi:10.5281/zenodo.10822690.

Guo, X., Liu, L., Zhou, B., Liu, Y., Leng, J., 2016. Constitutive model for shape memory polymer based on the viscoelasticity and phase transition theories. Journal of Intelligent Material Systems and Structures 27, 314–323. URL: https://doi.org/10.1177/1045389X15571380, doi:10.1177/1045389X15571380, arXiv:https://doi.org/10.1177/1045389X15571380.

Houbben, M., Sànchez, C.P., Vanderbemden, P., Noels, L., Jérôme, C., 2023. Mwcnts filled pcl covalent adaptable networks: Towards reprocessable, self-healing and fast electrically-triggered shape-memory composites. Polymer 278, 125992. URL: https://www.sciencedirect.com/science/article/pii/S0032386123003221, doi:https://doi.org/10.1016/j.polymer.2023.125992.

Jones, D., MacKerron, D., Norval, S., 2013. Effect of crystal texture on the anisotropy of thermal expansion in polyethylene naphthalate: measurements and modelling. Plastics, Rubber and Composites 42, 66–74. URL: https://doi.org/10.1179/1743289812Y.0000000034, doi:10.1179/1743289812Y.0000000034, arXiv:https://doi.org/10.1179/1743289812Y.0000000034.

Lee, J.H., Hinchet, R., Kim, S.K., Kim, S., Kim, S.W., 2015. Shape memory polymer-based self-healing triboelectric nanogenerator. Energy Environ. Sci. 8, 3605–3613. URL: http://dx.doi.org/10.1039/C5EE02711J, doi:10.1039/C5EE02711J.

Lendlein, A., Jiang, H., Jünger, O., Langer, R., 2005. Light-induced shape-memory polymers. Nature 434, 879–882. URL: https://doi.org/10.1038/nature03496, doi:10.1038/nature03496.

Li, J., Rodgers, W.R., Xie, T., 2011. Semi-crystalline two-way shape memory elastomer. Polymer 52, 5320–5325. URL: https://www.sciencedirect.com/science/article/pii/S003238611100783X, doi:https://doi.org/10.1016/j.polymer.2011.09.030.

Liu, C., Qin, H., Mather, P.T., 2007. Review of progress in shape-memory polymers. Journal of Materials Chemistry 17, 1543–1558. URL: http://dx.doi.org/10.1039/B615954K, doi:10.1039/B615954K.

Maksimkin, A.V., Kaloshkin, S.D., Zadorozhnyy, M.V., Senatov, F.S., Salimon, A.I., Dayyoub, T., 2018. Artificial muscles based on coiled uhmwpe fibers with shape memory effect. Express Polymer Letters 12, 1072–1080. URL: https://www.proquest.com/scholarly-journals/artificial-muscles-based-on-coiled-uhmwpe-fibers/docview/2131578443/se-2. copyright - © 2018. This work is published under NOCC (the "License"). Notwithstanding the ProQuest Terms and Conditions, you may use this content in accordance with the terms of the License; Dernière mise à jour - 2020-06-09.

Melro, A., Camanho, P., Andrade Pires, F., Pinho, S., 2013. Micromechanical analysis of polymer composites reinforced by unidirectional fibres: Part i – constitutive modelling. International Journal of Solids and Structures 50, 1897–1905. URL: https://www.sciencedirect.com/science/article/pii/S0020768313000747, doi:https://doi.org/10.1016/j.ijsolstr.2013.02.009.

Mu, T., Liu, L., Lan, X., Liu, Y., Leng, J., 2018. Shape memory polymers for composites. Composites Science and Technology 160, 169–198. URL: https://www.sciencedirect.com/science/article/pii/S0266353817310990, doi:https://doi.org/10.1016/j.compscitech.2018.03.018.

Nguyen, T.D., Jerry Qi, H., Castro, F., Long, K.N., 2008. A thermoviscoelastic model for amorphous shape memory polymers: Incorporating structural and stress relaxation. Journal of the Mechanics and Physics of Solids 56, 2792–2814. URL: https://www.sciencedirect.com/science/article/pii/S0022509608000951, doi:https://doi.org/10.1016/j.jmps.2008.04.007.

Nguyen, V.D., Lani, F., Pardoen, T., Morelle, X., Noels, L., 2016. A large strain hyperelastic viscoelastic-viscoplastic-damage constitutive model based on a multi-mechanism non-local damage continuum for amorphous glassy polymers. International Journal of Solids and Structures 96, 192–216. URL: https://www.sciencedirect.com/science/article/pii/S0020768316301238, doi:https://doi.org/10.1016/j.ijsolstr.2016.06.008.

Niyonzima, I., Jiao, Y., Fish, J., 2019. Modeling and simulation of nonlinear electro-thermo-mechanical continua with application to shape memory polymeric medical devices. Computer Methods in Applied Mechanics and Engineering 350, 511–534. URL: https://www.sciencedirect.com/science/article/pii/S004578251930129X, doi:https://doi.org/10.1016/j.cma.2019.03.003.

Pereira Sanchez, C.A., Houbben, M., Fagnard, J.F., Harmeling, P., Jérôme, C., Noels, L., Vanderbemden, P., 20 July 2022. Experimental characterization of the thermo-electro-mechanical properties of a

shape memory composite during electric activation. Smart Materials and Structures 31, 095029. URL: https://iopscience.iop.org/article/10.1088/1361-665X/ac8297, doi:10.1088/1361-665x/ac8297.

Pereira Sanchez, C.A., Houbben, M., Fagnard, J.F., Laurent, P., Jérôme, C., Noels, L., Vanderbemden, P., 17 December 2021. Resistive heating of a shape memory composite: Analytical, numerical and experimental study. Smart Materials and Structures 31, 025003. doi:10.1088/1361-665X/ac3ebd.

Pereira Sanchez, C.A., Jérôme, C., Noels, L., Vanderbemden, P., 02 November 2022. Review of thermoresponsive electroactive and magnetoactive shape memory polymer nanocomposites. ACS Omega 7. URL: https://pubs.acs.org/doi/pdf/10.1021/acsomega.2c05930, doi:10.1021/acsomega.2c05930.

Reese, S., Böl, M., Christ, D., 2010. Finite element-based multi-phase modelling of shape memory polymer stents. Computer Methods in Applied Mechanics and Engineering 199, 1276–1286. URL: https://www.sciencedirect.com/science/article/pii/S004578250900262X, doi:https://doi.org/10.1016/j.cma.2009.08.014. multiscale Models and Mathematical Aspects in Solid and Fluid Mechanics.

Simo, J., 1987. On a fully three-dimensional finite-strain viscoelastic damage model: Formulation and computational aspects. Computer Methods in Applied Mechanics and Engineering 60, 153–173. URL: https://www.sciencedirect.com/science/article/pii/0045782587901071, doi:https://doi.org/10.1016/0045-7825(87)90107-1.

Srivastava, V., Chester, S.A., Anand, L., 2010. Thermally actuated shape-memory polymers: Experiments, theory, and numerical simulations. Journal of the Mechanics and Physics of Solids 58, 1100–1124. URL: https://www.sciencedirect.com/science/article/pii/S0022509610000736, doi:https://doi.org/10.1016/j.jmps.2010.04.004.

Volk, B.L., Lagoudas, D.C., Maitland, D.J., 2011. Characterizing and modeling the free recovery and constrained recovery behavior of a polyurethane shape memory polymer. Smart Materials and Structures 20, 094004. URL: https://dx.doi.org/10.1088/0964-1726/20/9/094004, doi:10.1088/0964-1726/20/9/094004.

Xu, W., Li, G., 2010. Constitutive modeling of shape memory polymer based self-healing syntactic foam. International Journal of Solids and Structures 47, 1306–1316. URL: https://www.sciencedirect.com/science/article/pii/S0020768310000260, doi:https://doi.org/10.1016/j.ijsolstr.2010.01.015.

Yang, Q., Li, G., 2016. Temperature and rate dependent thermomechanical modeling of shape memory polymers with physics based phase evolution law. International Journal of Plasticity 80, 168–186. URL: https://www.sciencedirect.com/science/article/pii/S0749641915001588, doi:https://doi.org/10.1016/j.ijplas.2015.09.005.

Yang, Z., Peng, H., Wang, W., Liu, T., 2010. Crystallization behavior of poly(ecaprolactone)/layered double hydroxide nanocomposites. Journal of Applied Polymer Science 116, 2658–2667. URL: https://onlinelibrary.wiley.com/doi/abs/10.1002/app.31787, doi:https://doi.org/10.1002/app.31787, arXiv:https://onlinelibrary.wiley.com/doi/pdf/10.1002/app.31787.